

REVIEW ARTICLE | JANUARY 29 2024

## Metal anodes meet ionic liquids: An interfacial perspective

Rabia Jamil ; Suraj Loomba ; Mega Kar ; Gavin E. Collis ; Debbie S. Silvester  ;  
Nasir Mahmood 



*Appl. Phys. Rev.* 11, 011307 (2024)

<https://doi.org/10.1063/5.0180923>



### Articles You May Be Interested In

Cluster approach to the prediction of thermodynamic and transport properties of ionic liquids

*J. Chem. Phys.* (February 2018)

Electrochemical cell for neutron reflectometry studies of the structure of ionic liquids at electrified interface

*Rev. Sci. Instrum.* (July 2010)

Solubility of CO<sub>2</sub> in ionic liquids: Predictions based on QSPR study with artificial neural network

*AIP Conf. Proc.* (January 2024)



## Special Topics Open for Submissions

[Learn More](#)

# Metal anodes meet ionic liquids: An interfacial perspective

Cite as: Appl. Phys. Rev. **11**, 011307 (2024); doi: [10.1063/5.0180923](https://doi.org/10.1063/5.0180923)

Submitted: 12 October 2023 · Accepted: 27 December 2023 ·

Published Online: 29 January 2024



View Online



Export Citation



CrossMark

Rabia Jamil,<sup>1</sup> Suraj Loomba,<sup>2</sup> Mega Kar,<sup>3</sup> Gavin E. Collis,<sup>4</sup> Debbie S. Silvester,<sup>1,a)</sup>   
and Nasir Mahmood<sup>2,5,a)</sup>

## AFFILIATIONS

<sup>1</sup>School of Molecular and Life Sciences, Curtin University, GPO Box U1987, Perth 6845, Western Australia, Australia

<sup>2</sup>School of Engineering, RMIT University, Melbourne Victoria 3001, Australia

<sup>3</sup>Institute of Frontier Materials, Deakin University, 221 Burwood Highway, Burwood, Victoria 3125, Australia

<sup>4</sup>CSIRO Manufacturing, Melbourne, Victoria 3169, Australia

<sup>5</sup>School of Science, RMIT University, Melbourne, VIC 3001, Australia

<sup>a)</sup>Authors to whom correspondence should be addressed: [d.silvester-dean@curtin.edu.au](mailto:d.silvester-dean@curtin.edu.au) and [nasir.mahmood@rmit.edu.au](mailto:nasir.mahmood@rmit.edu.au)

## ABSTRACT

Ionic liquids (ILs) are nonvolatile, intrinsically conductive electrolytes with high thermal and electrochemical stability. They represent a fascinating yet-to-be-fully exploited electrolyte class that could be appropriate for metal anode batteries. Through their chemical design and structure modification, ILs are highly tunable electrolytes. Exploring the impact of their different structures on the anode/electrolyte interface allows the tailoring of ILs for post-Li-ion batteries. This comprehensive review gives an overview of the current challenges of different metal anodes, followed by a fundamental understanding of metal anode/electrolyte interface evolution in ILs in a coherent manner, highlighting the potential of ILs to address the specific problems of each type of metal anode. Electrochemical reactions—such as passivating film formation, metal deposition/stripping, dendritic growth—occurring at the metal anodes in IL-based electrolytes are openly debated, and how ILs can help to improve these phenomena is presented. Unanswered scientific questions on the nature of electrode/electrolyte coupling are identified. Finally, conclusions and perspectives are proposed regarding the development, limitations, and opportunities of metal anode/ionic liquid interfaces. This timely review will expose literature gaps and provide novel opportunities to exploit ILs in materials science and technology research.

© 2024 Author(s). All article content, except where otherwise noted, is licensed under a Creative Commons Attribution (CC BY) license (<http://creativecommons.org/licenses/by/4.0/>). <https://doi.org/10.1063/5.0180923>

## TABLE OF CONTENTS

I. INTRODUCTION.....	1	2. Al anode.....	13
II. NEXT-GENERATION METAL ANODES.....	2	3. Mg anode.....	21
A. Reversible metal deposition/dissolution and dendrites.....	2	IV. SUMMARY AND FUTURE PROSPECTS.....	24
B. Unstable solid-electrolyte interphase (SEI): A real challenge.....	3		
III. IONIC LIQUIDS—DESIGNER ELECTROLYTES FOR METAL ANODES.....	4		
A. Design strategies for tuning ILs-based electrolytes.....	5		
1. Chemistry of IL anions and cations.....	5		
2. Role of additives.....	9		
B. Interfacial electrochemistry of metal anodes in IL electrolytes.....	12		
1. Na anode.....	12		

## I. INTRODUCTION

Lithium-ion batteries (LIBs) have taken center stage in the current energy-storage industry, ranging from high-energy portable electronics to electric vehicles and now to battery energy storage systems. Increasing performance requirements, as well as growing concerns about the limited Li (lithium) reserves and other critical element reservoirs, have motivated researchers to look for alternative base metals.<sup>1,2</sup> Furthermore, diversification of materials enables the development of battery technologies tailored to specific applications rather than

deploying LIBs for every situation. Therefore, post-Li chemistries—for example, sodium (Na), potassium (K), aluminum (Al), zinc (Zn), calcium (Ca), magnesium (Mg), and Si (silicon)—are emerging candidates for next-generation secondary batteries because of their low cost, intrinsic safety, and long-term sustainability.<sup>1,3–8</sup> The techno-economic benefits of using Na and K include a natural abundance of these elements and a lower cost compared to Li, as well as the chemical similarity of the alkali metals with Li.<sup>1</sup> Similarly, multivalent metal anode rechargeable batteries (containing Mg, Ca, Al, and Zn) are the subject of intense research due to their superior theoretical volumetric energy densities compared to Li.<sup>9–12</sup>

Batteries are composed of various components that interact via interfaces, the most important of which are the electrodes and electrolytes. The interfaces control the transport of charge and matter between components, and thus are critical in determining the battery's performance, safety, and long-term stability.<sup>13–15</sup> During electrochemical cycling, a solid, passivating layer is formed at the interface of electrode/electrolyte and is recognized as the solid electrolyte interphase (SEI). This layer is initiated from the decomposition of electrolytes and is comprised of organic/inorganic species. Ideally, the electrochemically generated SEI should be stable, self-limiting, and ionically conductive, but electronically insulating.<sup>16,17</sup> As a consequence, parasitic reactions between the electrolyte and the anode are minimized, preserving electrode material, preventing electrolyte consumption and extending battery life. Despite the significant advantages of using earth-abundant metals as anodes for high energy density batteries, “beyond-Li” metal batteries are still in their infancy due to numerous challenges.<sup>2,10,13,18</sup> Key challenges with metal anodes include unstable SEI film or passive film formation, dendrite formation, self-corrosion, and volume expansion, which need to be addressed to enable technologies that can be commercially realized.<sup>19,20</sup> Numerous strategies, including surface modification (*in situ* and *ex situ*), alloying, using different electrolytes and complex mixtures, different additive salts or salt mixtures, and high salt concentrations, continue to be investigated for metal anodes to improve the structure, composition, and evolution of such interphases.<sup>17,21–25</sup> The electrolyte is a highly important component as it connects the cathode and anode, governs the interfacial chemistry, overall battery performance, and lifetime.<sup>26,27</sup> A lack of fundamental knowledge of solution chemistry and the interfacial electrochemistry of electrolytes is a major roadblock to developing new and emerging metal battery technologies.

Ionic liquids (ILs) represent a category of materials that have been investigated and utilized as electrolytes for energy storage systems like supercapacitors and batteries, because of their many desirable properties, including low volatility and high ionic conductivity, thermal and electrochemical stability.<sup>28–31</sup> In contrast to conventional organic solvents, ILs consist of organic anions and cations bound by various inter-ionic interactions, such as electrostatic, hydrogen bonding, and hydrophobic interactions, making them a complicated yet highly tunable electrolyte system. Furthermore, the coexistence of various aromatic and alkyl groups, as well as electrostatic charges in ILs, increases their affinity for both organic and inorganic materials.<sup>32–34</sup> ILs have been proposed as replacement solvents to address the shortcomings of traditional organic electrolytes, such as volatility and flammability for metal batteries.<sup>35</sup> Furthermore, the electrochemical stability of various metal anodes in ILs, as well as the high charge carrier population in ILs, may mitigate the continuous electrolyte depletion during operation and enable more stable metal battery cycling.<sup>1,36</sup>

To date, there are numerous reviews on different battery systems, focusing on advancements in cathode and anode materials or electrolytes.<sup>2,16,26,35,37–41</sup> There are reviews covering ILs as electrolytes for different batteries, highlighting the prospects of ILs in energy storage and conversion systems.<sup>1,32,36,42–45</sup> However, there is a need for a more coherent and comparative understanding of individual metal anode–IL interfacial evolution, characterization, and its limitations. To develop IL-based electrolytes, fundamental chemical and electrochemical characteristics and mechanisms of different metal anodes must be identified and understood. This timely review will provide a thorough knowledge foundation for designing IL-based electrolytes tailored to specific monovalent or multivalent metal anodes.

This review specifically focuses on the interfacial perspective of emerging metal anodes with ILs as electrolytes. The ongoing development of ILs as electrolytes for mono- and multivalent metal batteries is outlined and discussed. An overview of the most substantial approaches used to develop IL-based-electrolyte for emerging metal anode batteries is presented, with an explicit focus on basic characteristics, metal anode–IL interfacial properties, and reaction mechanisms. Answers to certain particular questions related to the potential of ILs as electrolytes for reversible metal electrodeposition/dissolution—including their controversies—are sought through exploring the most significant research work. Finally, particular viewpoints are presented on the future opportunities and directions that are needed toward a more bespoke electrode–electrolyte coupling using computationally aided design and advanced simulation tools. This review aims to stimulate a sense of curiosity and a deeper comprehension of the potential of ILs and encourage the design of new ILs with specific properties as suitable electrolytes for emerging battery technologies.

## II. NEXT-GENERATION METAL ANODES

Metal battery technologies can be grouped as monovalent (e.g., Li, Na) or multivalent (e.g., Zn, Mg etc.) based on the use of metal anode. Metal anode/electrolyte interaction is of particular interest as it directly impacts the two fundamental chemical and electrochemical processes—reversible metal deposition/dissolution and electrolyte decomposition—rendering the use of any pure metal anode.<sup>2</sup> Dendrite formation and thermal runaway are found at different degrees in many metal anodes, particularly in monovalent anodes.<sup>46</sup> For example, a Na-metal or K-metal battery exhibits more severe thermal runaway due to cell short-circuiting than a Li-metal battery, owing to lower melting point and higher chemical reactivity of these metals than Li.<sup>2</sup> In addition to safety risks associated with uncontrolled dendrite formation, continuous electrolyte decomposition on the metal anode is undesirable since it results in reduced coulombic efficiency and, eventually, electrolyte dry-out. Aside from the nature of the metal anode, the severity of these issues is determined by operating circumstances such as electrolyte composition and concentration, temperature, current density, and cycle rates.<sup>47</sup> This section provides a detailed discussion of two fundamental electrochemical phenomenon occurring at metal anode/electrolyte interface: metal deposition/dissolution and electrolyte decomposition.

### A. Reversible metal deposition/dissolution and dendrites

In theory, safe and efficient reversible electrodeposition and metallic dissolution at the metal anode is critical for secondary

batteries (rechargeable batteries) with high power and energy densities. However, in practice, repeated metal deposition and dissolution is complex and complicated by several issues that result in dendrite growth.<sup>48</sup> The five successive processes governing metal electrodeposition are: (1) metal ion movement from the bulk electrolyte to the electrode surface, (2) metal ion desolvation from the electrolyte, (3) adsorption of metal ions on the surface, (4) transfer of charge, and (5) surface diffusion toward the deposition site.<sup>49</sup> Any one of these processes has the potential to dramatically influence the quality and morphology of deposited metal if not designed and engineered effectively. Almost all metal anode design strategies focus on improving one or more of these processes.<sup>2</sup> Non-planar deposition morphology (often referred to as dendrites) between different metal anodes can be rationalized in a variety of ways. In the literature, the variation in surface and/or cohesive energy between monovalent and multivalent metals is typically used to explain the observed discrepancies in dendrite growth across different metal anodes.<sup>2,50</sup> Density functional theory (DFT) calculations predict dendrite-free Mg and Al plating on the basis of having higher surface energy than that of Li.<sup>2,51</sup> Contrary to this explanation, there have been many reports of dendritic Al plating despite the fact that Al's cohesive energy ( $327 \text{ kJ mol}^{-1}$ ) is considerably higher than that of Li ( $158 \text{ kJ mol}^{-1}$ ) and Mg ( $145 \text{ kJ mol}^{-1}$ ).<sup>50,52,53</sup> Furthermore, dendrite growth is observed during Mg deposition from ether-based electrolytes.<sup>54–56</sup> For example, the resistant passivation layer that forms on the Mg anode cannot be completely removed by the glyme/Mg(TFSI)<sub>2</sub> electrolyte, therefore Mg plating only takes place on limited active sites, causing a high local current density and dendritic growth. Hence, plating morphology may not be an inherent characteristic resulting from cohesive and/or surface energy, rather from the operating circumstances of metal anodes. In this regard, the choice of electrolyte, salt additive, current densities and cycle rates of the batteries will have significant impacts on the final morphology of the metal deposits.<sup>57–59</sup>

In contrast to Li metal anodes, which have been shown to suffer from uncontrolled dendrite growth and subsequent internal short-circuiting,<sup>60</sup> Na metal anodes typically suffer from loss of active anode during battery recharging due to the extremely fragile nature of mossy/non-planar Na, as well as electrolyte depletion. During repeated stripping cycles, fragile Na deposits easily break away and are electrically disconnected from the metal electrode. Furthermore, the mechanical susceptibility of Na dendrites is electrolyte-sensitive.<sup>17</sup> Due to the absence of the in-operando visual characterization of the electrolyte/electrode interface, this phenomenon is frequently concluded incorrectly as adverse reactions between the electrolyte and the Na anode.<sup>61</sup> There have been few reports addressing the SEI formation and characteristics on Na metal anode in ambient-temperature cells; nonetheless, there are evident contrasts with lithium regarding SEI composition, metal plating, and dendrite growth mechanisms.<sup>62,63</sup>

The main roadblock to the commercialization of post-Li battery technologies (particularly Al and Mg) is the lack of appropriate electrolytes that allow reversible plating/stripping of these metals with high efficiency at low overpotential.<sup>64</sup> For instance, in aluminum-based batteries, Al metal has been used as an anode in the form of a plate or particles,<sup>19</sup> which are not thermodynamically rechargeable because the discharged product (e.g., aluminum oxide/hydroxide in Al–air batteries) is unable to undergo conversion into metallic aluminum in aqueous electrolytes. Research has been focused toward the advancement of

non-aqueous electrolytes that enable the reversible dissolution/deposition of Al, but the success is limited.<sup>19</sup> Similarly, the stability and durability of Mg metal batteries are limited by substantial capacity deterioration caused by irreversible Mg dissolution/deposition processes.<sup>65</sup> So, the development of ideal electrolytes for magnesium has determined the pace of advancement in the field.

It is clear that selecting an appropriate electrolyte for metal anodes necessitates careful consideration of the numerous distinct contributing properties and features such as non-flammability and non-toxicity, efficient ion transport, wide electrochemical stability window, reversible metal electrodeposition with high coulombic efficiency, good surface-wettability, and good electrode/electrolyte interfacial contact.

## B. Unstable solid-electrolyte interphase (SEI): A real challenge

The real-world application of monovalent metal anodes is hampered by fundamental challenges, such as an unstable SEI layer, uncontrolled dendritic growth, and abrupt volume changes during charging/discharging. Even though chemical reactivity and ionic radius increase down the alkali metal group, SEI formation and properties do not correspond linearly between Li, Na, and K, with the instability of SEI on the Na anode being the most problematic.<sup>2</sup> The irreversible reaction between the Na anode and conventional non-aqueous electrolytes results in the spontaneous development of a non-ideal SEI film on the anode. This *in situ* produced SEI layer is destroyed during electrochemical cycling, either because it dissolves in certain electrolytes or cannot tolerate the significant volume expansion during the Na electrodeposition and migrates into the electrolyte matrix.<sup>2</sup> On the other hand, fissures in the SEI film could become active locations for the Na dendrite growth, reducing the electrochemical performance and safety of sodium metal batteries (SMBs) significantly.<sup>17</sup> Computational simulations of migration of metal ions across SEI have revealed that a greater energy barrier has to be overcome by Na ions to transport in comparison to the Li ions.<sup>66–68</sup> Notably, the SEI undergoes constant breakdown and reformation during the repetitious Na plating/stripping process, which increases the non-uniformity of the SEI layer and hence has a negative impact on Na electrodeposition.<sup>17</sup>

Since K has a larger ionic radius than Li or Na, it is assumed that the solubility of K-based SEIs in the electrolyte will be higher compared to Li or Na-SEIs. However, when K is combined with a large anion (such as perchlorate), it precipitates readily; therefore, non-soluble K-based SEIs are more accessible than Na-based SEIs.<sup>2,69</sup> The difference is due to the size of the K and Na ions—their relative solubility, and the ease with which they precipitate from the electrolyte. The solubility issue of Na SEI can be addressed by employing an electrolyte with a lower dielectric constant (e.g., an ether), however, flammability is still a concern with some organic solvents.<sup>2</sup> As a result, electrolyte solubility is crucial in SEI stability and battery performance.

More intriguing phenomena are observed when shifting right of the alkali metals to other elements and incorporating more than one cation. The formation of an ideal SEI is not as problematic for multivalent cations. The two primary concerns with multivalent SEIs are either the limited diffusion of multivalent cations across SEI film or complete insulating SEI preventing the movement of both electrons and cations.<sup>2,70</sup> For instance, in comparison to Li<sup>+</sup>, Mg<sup>2+</sup> cations have stronger electrostatic interactions and a higher charge density, thereby

resulting in Mg-based electrolytes with low ionic conductivities.<sup>71</sup> Thus, this ultimately reduces the cation mobility, making it problematic for  $\text{Mg}^{2+}$  ions to migrate through the passivating layers at the electrode/electrolyte interface. Therefore, early research into multivalent metal batteries concentrated on developing electrolytes that do not decompose over metal anodes (SEI-free anodes) and exhibit cathodic stability.<sup>2,4,35,36</sup>

Ideally, the electrolyte for Mg batteries should have high reduction stability to circumvent the passivating layer formation. Lewis acid-base pairs or Grignard reagents immersed in ether-type solvents are well-known electrolytes that allow reversible electrodeposition/dissolution of magnesium ions.<sup>32,72</sup> Magnesium has a large negative reduction potential; therefore, plating/stripping of magnesium is only possible in solutions that are aprotic. However, when Mg salts are dissolved in aprotic solvents having high dielectric constants (e.g., acetonitrile, esters, or carbonates), dense passivating layers form that restrict the transfer of magnesium ions and prevent any plating/stripping.<sup>35</sup> Ethers exhibit a low dielectric constant; when used as solvent with magnesium organohaloaluminates or magnesium organoborate, they show successful Mg plating/stripping.<sup>35</sup> However, ether limits the magnesium salts' solubility ( $< 0.5$  M) and reduces their ionic dissociation. Therefore, electrolytes with lower concentrations of electroactive salts have lower charge/discharge rates.

Similarly, the fundamental challenge with Al anodes has been finding a suitable electrolyte that allows efficient ion transport and accommodates the reversible Al plating/stripping without surface passivation. Until now, numerous aqueous and non-aqueous electrolytes, such as water-in-salt electrolytes, inorganic molten salts, organic solvents, deep eutectic solvents (DES), and polymer electrolytes, have been employed.<sup>73</sup> Although aqueous electrolytes have numerous advantages, e.g., excellent ionic conductivity ( $\approx 10^1$ – $10^2$   $\text{mS cm}^{-1}$ ), low cost, non-flammability, and a low environmental impact compared to organic solvents, the formation of aluminum oxide ( $\text{Al}_2\text{O}_3$ )—a true passivating layer—makes aqueous Al systems inherently challenging.<sup>73,74</sup> Given the widespread use of organic solvents in the Al electroplating industry, non-aqueous electrolytes have been the focus of much of the present research in Al-batteries. Although dendrite-free electrodeposition of Al has been reported from organic electrolytes, the operating temperature (usually above room temperature) and safety concerns (highly flammable and volatile) make these electrolytes unsuitable for batteries.<sup>73,75</sup> Therefore, inorganic molten salts, DES, and ILs are emerging electrolytes in Al secondary battery research.<sup>73,76</sup>

Low-cost analogs of ILs are called deep eutectic solvents (DESS). DES is a blend of Brønsted or Lewis based acids comprising diverse cations and/or anions.<sup>77</sup> For Al-battery applications, DESSs are generally composed of Lewis acidic metal salts ( $\text{AlCl}_3$ ) and a Lewis basic ligand or a hydrogen bond donor, e.g., urea, urea derivatives, or acetamide.<sup>78</sup> In Al-batteries, a DES-based electrolyte demonstrated high coulombic efficiencies ( $>95\%$ ) with improved cycling stability.<sup>78–80</sup> However, they suffer from relatively low specific discharge capacities compared to traditional chloroaluminate ILs, due to their high viscosity and low ionic conductivity.<sup>80</sup> Some researchers reported that using urea derivatives (N-ethyl urea and N-methyl urea with  $\text{AlCl}_3$ ) may increase the ionic conductivity of these DESSs.<sup>80</sup>

DESSs may become a viable alternative if their physiochemical properties and specific capacity are improved. In the case of other

metal anodes, such as zinc, DESSs can certainly be considered a cheaper alternative to ionic liquids, especially since a wide reductive stability window is not required to undergo anode reversibility. Moreover, in comparison to aqueous electrolytes, DESSs have also demonstrated dendrite suppression due to the weak interaction between water and  $\text{Zn}^{2+}$  ions.<sup>81</sup> Similar to ILs, the tunability of DESSs also opens the pathway to consider a variety of zinc salts and eutectic mixtures for the SEI layer formation. For example, in the presence of  $\text{Zn}(\text{TFSI})_2$  in acetamide, the decomposition of the TFSI anion prior to zinc deposition leads to the formation of an anion-rich SEI layer comprising  $\text{ZnF}_2$  that enhances zinc's long-term cycling.<sup>82</sup>

For all multivalent metal batteries, a fundamental challenge is the passivation of the surface of electrode because of the electrolyte decomposition and the inhibition of multivalent cation movement through it. Designing an electrolyte that does not decompose over the metal anode and possesses high cathodic stability is an appealing strategy.<sup>83,84</sup> However, issues related to the SEI-free anode, such as elevated costs, inferior anodic stability, and current collector corrosion, complicate multivalent battery research. The nature of the SEI layer that is unique to each metal is explained by numerous factors, including dissimilarities in solvation structure, the diffusion rate of the metal cation through the passivating film, and the dissolution stability of the interfacial film. Based on this understanding and the different properties of metals, it is obvious that metal batteries will necessitate their own bespoke, optimized electrolytes and additives with improved electrochemical stability. These will be critical to creating SEIs that are robust to realize high-performance metal batteries.

### III. IONIC LIQUIDS—DESIGNER ELECTROLYTES FOR METAL ANODES

Room temperature ILs (RTILs) are room temperature liquid organic salts and are comprised of weakly coordinated complex ions. ILs have been intensively researched for use in energy storage devices because of their exceptional properties like non-flammability, high thermal stability, and low vapor pressures.<sup>30,85</sup> In metal batteries, IL-based electrolytes generally comprise of a metal salt and an organic salt. Some common organic cations are pyrrolidinium, imidazolium, piperidinium, quaternary ammonium and phosphonium, while anions are dicyanamide (DCA), sulfonylimide (TFSI and FSI) and halides (for Al-batteries).<sup>86,87</sup> ILs are often called “designer solvents” and are easily customizable for specific applications by employing various cation and anion combinations. The structures of some of the commonly used anions and cations in ILs are summarized in Table I.

Among several choices for next-generation electrolytes, ILs enable the employment of techniques to reduce active electrode material dissolution and the corrosion of current collectors.<sup>1</sup> As opposed to conventional organic solvents, which are composed of neutral molecular species, ILs are entirely composed of ions. Therefore, ILs allow the cycling of negative metal electrodes and show decreased parasitic reactions between the electrolyte and metal anode, which is not typically possible with traditional organic solvent-based electrolytes.<sup>1</sup> ILs have emerged as potential solvents across a range of metal salts to combat the challenges of conventional electrolytes, such as low metal salt solubility, high vapor pressure, and the flammable nature of organic electrolytes.<sup>35</sup> In addition, electrochemical and chemical stability and a high charge carrier population in ILs may alleviate electrolyte decomposition and depletion during operation, resulting in improved energy efficiency and power capacities of metal batteries. A detailed

**TABLE I.** Nomenclature, abbreviations, and structures of some of the commonly used anions and cations of ILs explored for metal anode batteries and discussed in this review.

Cations	Abbreviation	Structure
1-ethyl-3-methylimidazolium	[EMIM] <sup>+</sup>	
1-butyl-3-methylimidazolium	[BMIM] <sup>+</sup>	
N-methyl-N-propylpyrrolidinium	[C <sub>3</sub> mpyr] <sup>+</sup>	
N-butyl-N-methylpyrrolidinium	[C <sub>4</sub> mpyr] <sup>+</sup>	
N-methyl-N-propylpiperidinium	[PP <sub>13</sub> ] <sup>+</sup>	
N-methyl-N-butylpiperidinium	[PP <sub>14</sub> ] <sup>+</sup>	
Trimethyl-iso-butyl phosphonium	[P <sub>111i4</sub> ] <sup>+</sup>	
Methyl-tri-iso-butyl phosphonium	[P <sub>1i4i4i4</sub> ] <sup>+</sup>	
triethyl(tetradecyl)phosphonium	[P <sub>6,6,6,14</sub> ] <sup>+</sup>	
Ammonium	[N <sub>a,b,c,d</sub> ] <sup>+</sup>	

explanation of how ILs can be tailored for different metal anodes, along with the technological possibilities of IL-based electrolytes for different metal anodes, are discussed in Secs. III A and III B.



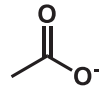
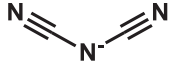
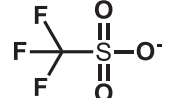
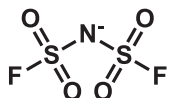
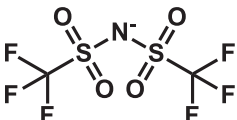
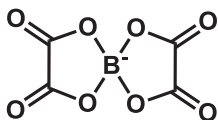
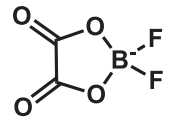
## A. Design strategies for tuning ILs-based electrolytes

### 1. Chemistry of IL anions and cations

*a. Role of the IL anion in stable SEI formation.* Task-specific ILs can be designed by regulating the chemistry of anions or cations of ILs

to modulate the metal anode/IL interfaces. The IL anion effect on the interfacial electrolyte structure and SEI layer formation needs to be appropriately considered. ILs with anions containing sulfonylimide or a nitrile group (such as DCA) are commonly used as electrolytes for metal batteries.<sup>17</sup> More recently, the use of borate anions such as difluoro(oxalato)borate (DFOB) and bis(oxalato)borate (BOB) has been explored in lithium and sodium batteries.<sup>88–91</sup> Different anions contribute to unique interfacial structures and electrochemical stability against certain metal anodes. Fluorinated molecules have been

TABLE I. (Continued.)

Anion	Abbreviation	Structure
Tetrafluoroborate	[BF <sub>4</sub> ] <sup>-</sup>	
Hexafluorophosphate	[PF <sub>6</sub> ] <sup>-</sup>	
Acetate	[OAc] <sup>-</sup>	
Dicyanamide	[DCA] <sup>-</sup>	
Triflate or trifluoromethanesulfonate	[OTf] <sup>-</sup>	
bis(fluorosulfonyl)imide	[FSI] <sup>-</sup>	
bis(trifluoromethylsulfonyl) imide	[TFSI] <sup>-</sup>	
bis(oxalato)borate	[BOB] <sup>-</sup>	
difluoro(oxalato)borate	[DFOB] <sup>-</sup>	

recognized to support stable SEI layers formation for both Li and Na batteries.<sup>92,93</sup> In particular, adding TFSI and FSI anions brings salient features to some electrolyte/metal anode interfaces owing to their high ionic conductivities and low corrosivity to current collectors.<sup>92,94-97</sup> The use of FSI and TFSI anions may prevent the decomposition of cations, however, the cathodic limit of the IL is determined by both anionic and cationic species of the IL.<sup>94,98</sup> In addition, Na<sup>+</sup> cations play a crucial part in increasing the stability of the IL against Na metal, and they also affect the surface film thickness.<sup>94</sup>

In the negative potential region, imidazolium-based ILs are less reductively stable; therefore, pairing an imidazolium cation with a more cathodically stable anion may improve electrolyte stability in Na and Li batteries.<sup>94,98</sup> Imidazolium TFSI ILs are not stable with Na metal even in the presence of Na<sup>+</sup> cations. In contrast, imidazolium FSI mixed ILs are stable because the chemical reactions between Na

and the IL are suppressed. The low reactivity of the FSI anion and the presence of Na<sup>+</sup> cations dramatically improves the stability of imidazolium FSI ILs toward the reactive Na metal and facilitates development of a thin, stable SEI with a small permeability to the IL.<sup>94</sup> In contrast to imidazolium-based ILs, ILs with a more electrochemically stable cation, such as pyrrolidinium, showed stable Na plating/stripping when mixed with both FSI and TFSI-based ILs.<sup>94,99</sup> In contrast, TFSI anions are incompatible with magnesium electrochemistry due to strong interactions between Mg<sup>2+</sup> and the surrounding TFSI.<sup>100,101</sup> The TFSI anion can only be regarded as electrochemically stable enough under certain conditions, such as in completely water-free electrolytes or systems where TFSI is not allowed to participate in direct coordination with magnesium.<sup>70,100</sup> The use of ionic liquid media for calcium electrochemistry is scarce in the literature. Nevertheless recent findings by Gao *et al.*<sup>102</sup> have documented the

utilization of an IL electrolyte comprised of calcium borohydride [ $\text{Ca}(\text{BH}_4)_2$ ] in an alkoxy-ammonium-based ionic liquid, i.e.,  $[\text{N}_{07}][\text{TFSI}]$  (N,N,N-tri-(2-(2-methoxyethoxy)ethyl)-N-(2-methoxyethyl)ammonium bis(trifluoromethylsulfonyl) imide), which demonstrated a reversible capacity of  $244 \text{ mA h g}^{-1}$  and a high initial discharge capacity of  $332 \text{ mA h g}^{-1}$  in a  $\text{Ca}|\text{V}_2\text{O}_5$  cell.  $\text{TFSI}^-$ 's displacement from  $\text{Ca}^{2+}$  ion coordination by the alkoxy-functionalized ammonium cation containing seven ether oxygen atoms is a significant factor for the efficient Ca plating/stripping from this IL-based electrolyte. The authors found that a SEI layer rich in organic and low in inorganic content, with some  $\text{CaH}_2$  degradation product, is beneficial in enabling  $\text{Ca}^{2+}$  ion diffusion.

Although fluorinated anion-based ILs are relatively easy to synthesize and, due to their hydrophobic nature, are widely used as electrolytes, their high cost and high viscosity are the main drawbacks.<sup>103</sup> Doi *et al.* proposed that fluorinated-free electrolytes can offer a stable SEI for Na anodes with minimal interfacial resistance.<sup>104</sup> Na plating/stripping was demonstrated in a DCA-based IL with  $\text{Na}[\text{DCA}]$  salt under a controlled moisture content.<sup>105</sup> In this regard, ILs with anions such as DCA are considered cost-effective solutions to stabilize electrochemistry in both lithium and sodium systems.<sup>103,105</sup> The use of dicyanamide ILs has also been shown to support the facile electrochemical cycling of divalent metals such as Zn.<sup>106–108</sup> Furthermore, cations with superior reductive stability are not essential because of Zn's low reduction potential (i.e.,  $-0.76 \text{ V}$  vs The standard hydrogen electrode, SHE), providing opportunities to consider a large number of cations. Recently, Ghazvini *et al.* demonstrated Zn plating/stripping in the presence of zinc acetate  $[\text{Zn}(\text{OAc})_2]$  ( $>4\text{M}$ ) in  $[\text{EMIM}][\text{OAc}]$ .<sup>109</sup> In another work, Simons *et al.* demonstrated non-dendritic, uniform Zn deposits on the metal anode upon long-term cycling ( $>100$  cycles) of  $\text{Zn}(\text{DCA})_2$  in  $[\text{EMIM}][\text{DCA}]$ .<sup>110</sup> Interestingly enough, when compared to  $[\text{C}_4\text{mpyr}][\text{DCA}]$ , a lower overpotential, i.e.,  $-0.23 \text{ V}$  vs zinc pseudo-reference, was required to commence zinc deposition in the presence of  $[\text{EMIM}][\text{DCA}]$ . Overall, the electrochemical performance of Zn was found to be superior in this IL as well. Molecular dynamics (MD) simulations and atomic force microscopy (AFM) suggest that such drastic differences between the ILs are attributed to the interfacial structure and dynamics.<sup>111</sup> For a Na metal anode, it was discovered that long-term Na plating/stripping with high efficiency in a DCA-based IL is not possible owing to the DCA anion's presumed instability, leading to electrode passivation, and the presence of moisture brings further complications.<sup>103</sup> Similar results have been observed for Mg-batteries where the tendency of the DCA anion-based IL to form crystalline complexes preventing charge transport at the Mg anode interface.<sup>112</sup>

For monovalent battery systems, the instability issue of the DCA anion can be addressed by mixing the metal salt with a different anion to that of the anion of the IL. The use of mixed anions can combat the challenges associated with fluorinated and non-fluorinated anions. Mixing a Na salt with different anions to that of the anion of IL improves ion transport and solvation in the electrolyte, which then positively impacts the electrochemical performance, as demonstrated by the FSI-TFSI mixed anion system in both sodium and lithium battery electrolytes.<sup>103,113–115</sup> Wongittarom *et al.* demonstrated the impact of various Na salts ( $\text{NaBF}_4$ ,  $\text{NaClO}_4$ ,  $\text{Na}[\text{DCA}]$ , and  $\text{NaPF}_6$  with salt concentration of  $1\text{M}$ ) on the charge transfer resistance and ionic conductivity of  $[\text{C}_4\text{mpyr}][\text{TFSI}]$ .<sup>116</sup> Among various Na solutes,

the  $\text{BF}_4^-$ -TFSI mixed anion system showed the best performance in relation to capacity retention and cycle life in a  $\text{Na}/\text{IL}/\text{NaFePO}_4$  cell.<sup>116</sup> However, the authors did not provide data on the dissolution of high concentrations of salts with high lattice energy in ILs to obtain a real understanding of the nature of mixed electrolytes. The electrochemical behavior of Na needs to be explained in terms of the coordination environment and changing ion dynamics. Sodium plating and stripping on a metallic Na anode is specific to every mixed anion system.<sup>117</sup> In  $\text{NaClO}_4$  with the IL  $[\text{C}_4\text{mpyr}][\text{TFSI}]$ , Na plating/stripping is hindered due to an unstable layer formation on the Na metal surface. In the mixed FSI-TFSI IL system, a stable SEI layer is formed when in contact with the Na anode, which is amenable to repeated Na plating/stripping.<sup>117</sup> To account for the overall cell performance and cyclability of the battery, changes that occur both on the cathode and the Na metal anode due to a mixture of anions should be considered.

Using mixed anions can not only improve the ion dynamics but can also impact SEI formation. Recently, Forsyth *et al.* systematically investigated incorporating fluorinated anion Na salts ( $\text{NaFSI}$ ,  $\text{NaTSFI}$ ,  $\text{NaFTSFI}$ ) as SEI-forming species with pyrrolidinium-based DCA IL (Fig. 1).<sup>103</sup> Although fluorinated co-anions addition did not affect the ionic conductivity, oxidative stability of the IL, and oxidation onset potential, they did have a dramatic influence on the cycling profiles, which are associated with the SEI layer and are unique to each system [see Figs. 1(a)–1(f)]. By further increasing the overpotential (polarization potential) for the larger fluorinated anions ( $\text{NaTFSI}$ ,  $\text{NaFTSI}$ ), as shown in Figs. 1(c), 1(d), and 1(f), continuous surface layer passivation was observed. Furthermore, enormous polarization values at the beginning of cycling of  $\text{NaTFSI}$  and  $\text{NaFTSFI}$  [sodium (fluorosulfonyl)(trifluoromethanesulfonyl)imide amide] indicates a highly passive and resistive surface that forms immediately upon contact with the Na anode. In the case of  $\text{NaTFSI}$ , though the thick film was more resistive, it was not completely passivating, and therefore, trapped electrolyte may adopt a tortuous ionic pathway. On the other hand, the  $\text{NaFSI}$  system maintained stable cycling ( $>100$  cycles) with a low overpotential. In the absence of a mixed-anion system, i.e.,  $\text{Na}[\text{DCA}]/[\text{C}_3\text{mpyr}][\text{DCA}]$  allowed limited cycling with increased overpotential [Fig. 1(i)]. Theoretical computational simulations highlighted the role of metal ion solvation in the decomposition process. The coordination environment, changing ion dynamics, and local structuring of ions at the charged electrode have appeared to depend on the IL cation and anion structures [Fig. 1(h)]. Using density distribution functions for charged graphene sheets ( $\pm 1 \sigma$ ), it was found that when the electrolyte is comprised of only DCA anions, the inner most layer only consisted of the  $[\text{C}_3\text{mpyr}]^+$  cation. In contrast, in the presence of mixed anions, e.g., the fluorinated FSI and TFSI anions, along with the  $[\text{C}_3\text{mpyr}]^+$  cation, the anions also remained in the inner most layer. It is postulated that the attraction between the cation and anions highly dominates this layering at the interface, which ultimately guides the breakdown process of anions on the electrode. Electrochemical measurements and advanced surface characterization techniques proved that the ion speciation and interfacial behavior at a charged electrode can be controlled by an appropriate choice of anions in the mixture.<sup>103</sup> Hence, mixed anion systems allow the flexibility to use low-cost ILs while maintaining the desirable SEI features. This concept can be explored with multivalent batteries with a view of improving metal-ion solvation and stabilizing the multivalent anode/electrolyte interface.



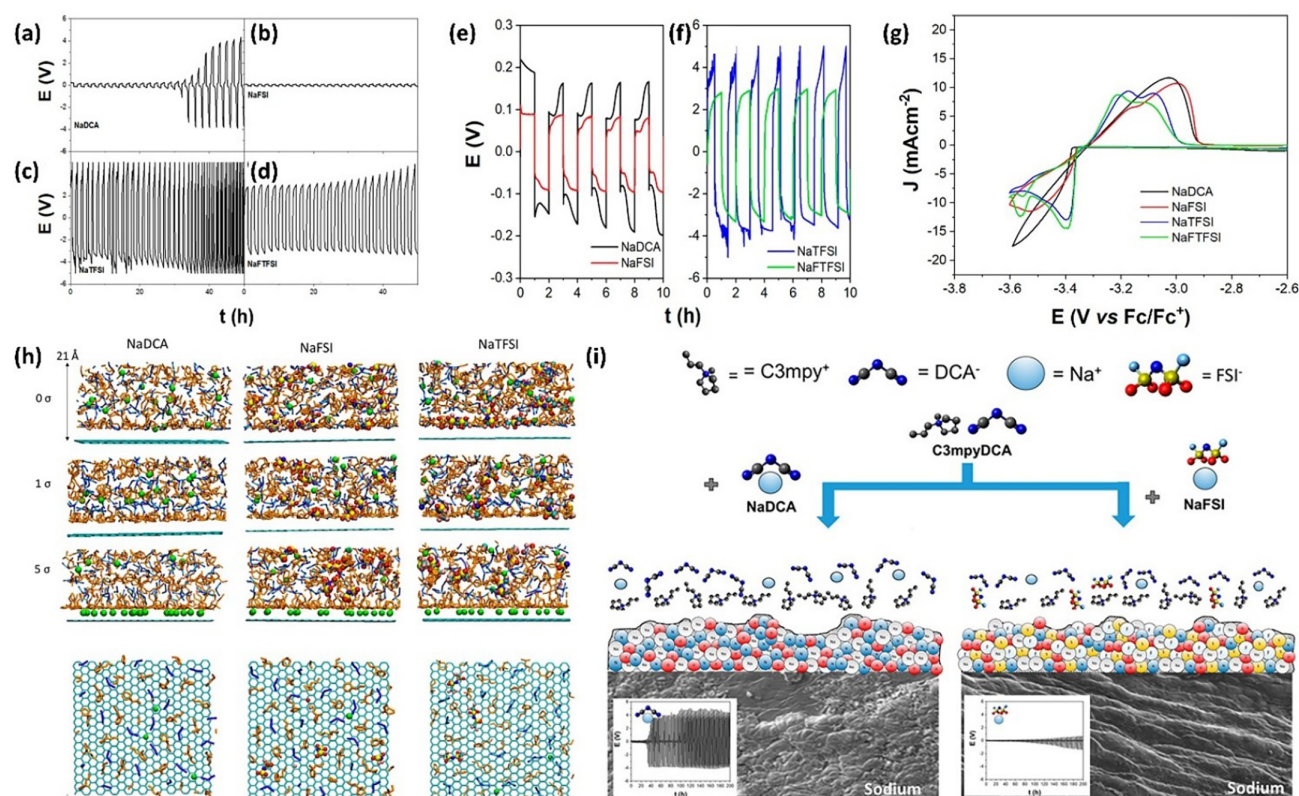


**FIG. 1.** Cycling plot for Na symmetric cell of the solution of  $[C_3\text{mpy}][\text{DCA}]$  ( $50^\circ\text{C}$ ,  $0.1\text{ mAcm}^{-2}$ ; 1 h cycles): (a) Na[DCA]; (b) NaFSI; (c) NaTFSI; (d) NaFTFSI; (e) expanded 10 h for Na[DCA] and NaFSI; (f) expanded 10 cycles for NaTFSI and NaFTFSI; (g) Comparison of cyclic voltammetry (first cycle shown) for  $[C_3\text{mpy}][\text{DCA}]$  based electrolyte linking with each Na[DCA], NaFSI, NaTFSI, and NaFTFSI; (h) Interfacial structures of three IL/salt systems displayed via snapshots. In the yz plane projection, layer within a  $z < 21\text{ \AA}$  is displayed near the graphene surface which is negatively charged and has 0, 1, or 5  $\sigma$  charge. In the xy plane projection, first layer ( $z < 7\text{ \AA}$ ) comprising of the ions on uncharged graphene surface is demonstrated; (i) graphical representation to control the interfacial electrochemistry using a fluorinated anion and providing a SEI in DCA IIs which is more stable, scanning electron microscopy (SEM) images of the cycled Na surfaces: left Na[DCA]; right NaFSI, insets cycling plot of Na symmetric cells showing 100 cycles at  $50^\circ\text{C}$  at  $0.1\text{ mAcm}^{-2}$ : left Na[DCA]; right NaFSI. Reproduced with permission from Forsyth *et al.*, *Appl. Mater. Interfaces* **11**, 43093 (2019). Copyright 2019, American Chemical Society.<sup>103</sup>

*b. Role of the IL cation in stable SEI formation.* By extending the organic moieties, IL cations can be more diverse than their anionic counterparts. Na metal deposition-dissolution is strongly influenced by the cation structure.<sup>94,99,118</sup> Asymmetric cations containing short alkyl chains, e.g.,  $[C_3\text{mpyr}]^+$  and  $[\text{EMIM}]^+$ , are often favored, and pyrrolidinium-based cations are widely employed for high-potential electrochemical device applications due to their greater reductive stability than imidazolium-based cations.<sup>1,119</sup> Pyrrolidinium-based ILs also have a higher chemical stability at Na metal anodes compared to imidazolium-based ILs. As a result, several pyrrolidinium- and phosphonium-based ILs have been studied, incorporating the FSI anion because of its high ionic conductivity and formation of robust and stable SEI.<sup>62</sup> The addition of long alkyl chains or bulky functional groups often decreases melting points, increases viscosity, and decreases ionic conductivity. Small alkylphosphonium FSI-based ILs not only allow solubility of high concentrations of alkali metal salts but also show promising properties for sodium batteries in particular.<sup>29,120</sup> As high NaFSI concentration promotes improved cycling, solubility of metal salt in the IL can be increased by adding oxygen groups into

cationic alkyl chains as coordination sites. Alkoxy-substituted quaternary ammonium ILs have been proven to exhibit intriguing physico-chemical features and to improve the cycling performance of SMBs in this regard.<sup>1,113,114</sup> A comparison of alkyl phosphonium ( $P_{11114}^+$ ,  $P_{1141414}^+$ ) and alkoxy ammonium cations  $[N_{2(2O_2O_1)_3}]^+$  in the form of FSI-based ILs reveals that  $P_{11114}\text{FSI}:\text{NaFSI}$  and  $N_{2(2O_2O_1)_3}\text{FSI}:\text{NaFSI}$  exhibit better cycling performance and rate capability, with  $P_{11114}\text{FSI}:\text{NaFSI}$  exceeding the other ILs in terms of higher conductivity and more stabilized SEI layer formation.<sup>121</sup>

Mg-ion speciation in TFSI-based ILs can be modified by replacing the alkyl-substituted cation ( $[C_4\text{mpyr}]^+$ ) with alkoxy-functionalized cations (alkoxy-pyrrolidinium or alkoxy-ammonium).<sup>100,122–124</sup> However, alkoxy-pyrrolidinium-based ILs show overall inferior electrochemical performance compared to the alkoxy-ammonium-based ILs because of steric hindrance of the pyrrolidinium ring.<sup>100</sup> According to experimental and simulation studies, the alkoxy group of the cation replaces TFSI anions from  $\text{Mg}^{2+}$ 's coordination sphere, thereby facilitating a reversible Mg plating/stripping process.<sup>100,122,123</sup> ILs with higher denticity [such as N,N,N-tri-(2-(2-methoxyethoxy)ethyl)-N-(2-methoxyethyl)ammonium bis

(trifluoromethylsulfonyl) imide,  $[\text{N}_{07}][\text{TFSI}]$  effectively suppress ion agglomeration and show higher Coulombic efficiency than  $[\text{C}_4\text{mpyr}][\text{TFSI}]$ .<sup>122</sup> However, there is disagreement in the literature about the minimum number of ether oxygen atoms necessary in alkoxy-functionalized ILs for the displacement of TFSI anions from  $\text{Mg}^{2+}$ 's coordination sphere.<sup>100,124,125</sup>

The use of ether-based ammonium cations in ionic liquids has also been shown to play an important role in  $\text{Zn}^{2+}$  ion-chelation, thereby improving the long-term electrochemical cycling of Zn.<sup>126,127</sup> The careful modification of the ether chain-length can be crucial in the metal-ion coordination that ultimately determines Zn's electrochemical performance. For example, Kar *et al.* have shown in comparison to shorter-chain oligo-ether chain lengths (i.e.,  $n = 2$ ), the incorporation of long oligo-ether chain lengths ( $n \geq 2$ ) can improve the metal-ion coordination and thereby better facilitate the zinc electrochemistry.<sup>126</sup>

The difference in cation/anion size, structure, solvation, and coordination of ions in the ILs is responsible for the differences in physicochemical characteristics, such as density, ionic conductivity, viscosity, electrochemical stability window, and corrosivity, as well as the overall battery performance and power density.<sup>86,128–130</sup> For an IL to be an efficient electrolyte, its cationic size must be carefully controlled since a larger cation size may result in increased viscosity, decreased ionic conductivity, and overall battery efficiency during charge and discharge cycles.<sup>128</sup> Furthermore, the intermolecular interactions between IL constituents (organic cations and anions) can significantly influence the reversible metal electrodeposition/dissolution. For example, in the case of Al electrodeposition, decreasing the cation-anion interactions leads to more smooth and compact Al deposits as well as increased intercalation and deintercalation of  $\text{AlCl}_4^-$  in graphite cathode.<sup>87,131</sup> Hence, when designing task-specific ILs for metal batteries, the size of IL constituents (particularly cationic size) and intermolecular interaction between ions should be taken into consideration.<sup>132</sup>

## 2. Role of additives

Apart from altering the cations and anions of ILs, the electrochemical properties of ILs can also be enhanced by using additives (organic solvents or metal salts).<sup>131,133,134</sup> The nature and amount of the organic additive [e.g., propylene carbonate (PC), benzene, toluene, dichloromethane, ethylene carbonate (EC)] also has a considerable influence on the electrochemical properties and ionic conductivity of hybrid mixtures of ILs and additives.<sup>133,135</sup> Extensive research on the role of additives in lithium batteries revealed that additives could increase cycle life at higher temperatures, maintain low internal resistance, and extend cycle life.<sup>16</sup> Fluorinated ethylene carbonate (FEC), often used in LIBs when used for sodium batteries, can improve passivation and reduce side reactions at the metal anode/electrolyte interface.<sup>136</sup> Nevertheless, FEC is not economical for large-scale implementation due to its high cost. Furthermore, film-forming additives successfully used in lithium batteries may not necessarily produce beneficial results in sodium batteries due to the dissimilarity in the chemical nature of the two metals.<sup>136</sup> Hence, more efforts are required to achieve future breakthroughs.

Organic additives, in general, raise safety concerns and are harmful to the environment.<sup>73</sup> Recently, a chloroaluminate-based IL [i.e., NaCl-buffered  $\text{AlCl}_3/[\text{EMIM}]\text{Cl}$  (represented as Na-Cl-IL)] was reported to be nonflammable and highly conductive electrolyte for rechargeable Na batteries with the addition of appropriate additives.<sup>135</sup>

Ethylaluminum dichloride ( $\text{EtAlCl}_2$ ) and  $[\text{EMIM}][\text{FSI}]$  were found to be two additives that allow reversible and stable deposition/dissolution of Na metal by stabilizing the SEI. The leading components of the uniform SEI film were NaF,  $\text{Al}_2\text{O}_3$ , and NaCl, with NaF resulting from the decomposition of  $\text{FSI}^-$  anion over Na [Fig. 2(a)]. Furthermore, some other minor substances (such as  $\text{Na}_2\text{O}$ ,  $\text{Na}_2\text{SO}_4$ , and Al) could contribute to the composition of SEI. The Na-Cl-IL electrolyte is safe due to its non-flammable properties. Thermogravimetric analysis revealed that the Na-Cl-IL electrolyte could withstand temperatures as high as 400 °C, whereas 1 M  $\text{NaClO}_4\text{-EC/DEC/FEC}$  ( $V_{\text{EC}}:V_{\text{DEC}} = 1:1$ , DEC:diethyl carbonate; FEC: fluoroethylene carbonate, 5 wt. %) suffer from rapid weight loss at 132 °C and only 15% was retained at 230 °C [Fig. 2(b)]. With these two electrolytes, the cycling performance of SIBs using NVP (sodium vanadium phosphate)/NVPF (sodium vanadium phosphate fluoride) as cathodes showed significant differences. SIBs with IL electrolytes demonstrated coulombic high efficiencies ( $> 95\%$ ) between 50 and 500  $\text{mA g}^{-1}$ , a high capacity retention ratio ( $> 90\%$ ), and a high capacity efficiency ( $\sim 98.5\%$ ) [Figs. 2(c) and 2(d)]. In comparison, after 450 cycles at 150  $\text{mA g}^{-1}$ , SIBs with a 1 M  $\text{NaClO}_4\text{-EC/DEC/FEC}$  as electrolyte only retained 79% specific capacity [Fig. 2(e)]. Both additives contribute to the improved performance in Na-Cl-IL electrolytes, such as  $[\text{EMIM}][\text{FSI}]$ , which stabilizes Na plating/stripping, and  $\text{EtAlCl}_2$ , which promotes SIB cycling stability. The rapid capacity drop at 300  $\text{mA g}^{-1}$  after 200 cycles in the absence of  $\text{EtAlCl}_2$  suggests the role of  $\text{EtAlCl}_2$  in eliminating small amounts of free chloride ions and residual protons in the electrolyte [Fig. 2(f)].<sup>135</sup> Adding Li salt to imidazolium-based  $\text{AlCl}_3$  ILs extended the cycle life of Al-S batteries.<sup>137</sup> The presence of  $\text{Li}^+$  ions in  $[\text{EMIM}][\text{Cl}]-\text{AlCl}_3$  facilitates the soluble polysulfide intermediates' formation, lowering the electrochemical kinetic barrier to reduce or oxidize Al polysulfide.

To combat the instability of IL-based electrolytes (particularly containing TFSI anions) upon interaction with  $\text{Mg}^{2+}$  species in Mg-batteries, additives are chosen based on their ability to reduce any adverse reaction between  $\text{Mg}^{2+}$  and the IL and allow reversible Mg plating/stripping.<sup>138</sup> The stabilization and dissolution/stripping of the Mg anode cannot be explained simply by comparing the physicochemical properties of the different IL/additive mixtures. The effect of different additives including water and organic solvents [toluene, tetrahydrofuran (THF), ethylene glycol (EG)], and dimethyl sulfoxide (DMSO) has been studied for trihexyl(tetradecyl)phosphonium chloride ( $[\text{P}_{6,6,6,14}][\text{Cl}]$ ) IL.<sup>112,139–141</sup> It is evident that protons and/or oxygen-donor groups present in additives play an important role in allowing the Mg anode's stable discharge in Mg-air batteries.<sup>112,140</sup> Additives like THF and toluene reduce the viscosity of the IL, toluene lacks donor atoms, therefore, is unlikely to interact with  $\text{Mg}^{2+}$  ions, while the presence of the ether group in THF may facilitate coordination with magnesium ions and/or binding to the surface of the electrode. DMSO—a polar aprotic solvent—may enhance ion dissociation and increase conductivity of the IL. Ethylene glycol potentially shows similar behavior to water as an additive to  $[\text{P}_{6,6,6,14}]\text{Cl}$ , because during discharge, it caters to active protons and the alkoxide that can potentially react/coordinate with magnesium species, in addition to boosting the transport properties of IL.<sup>140,141</sup> Other additives, such as salts or supporting electrolytes, have also demonstrated enhanced current densities and stable electrochemical cycling of metal ions in ionic liquids.<sup>123</sup> Hence, a better understanding of the additives' role in metal ion speciation and supporting stable and reversible metal plating/

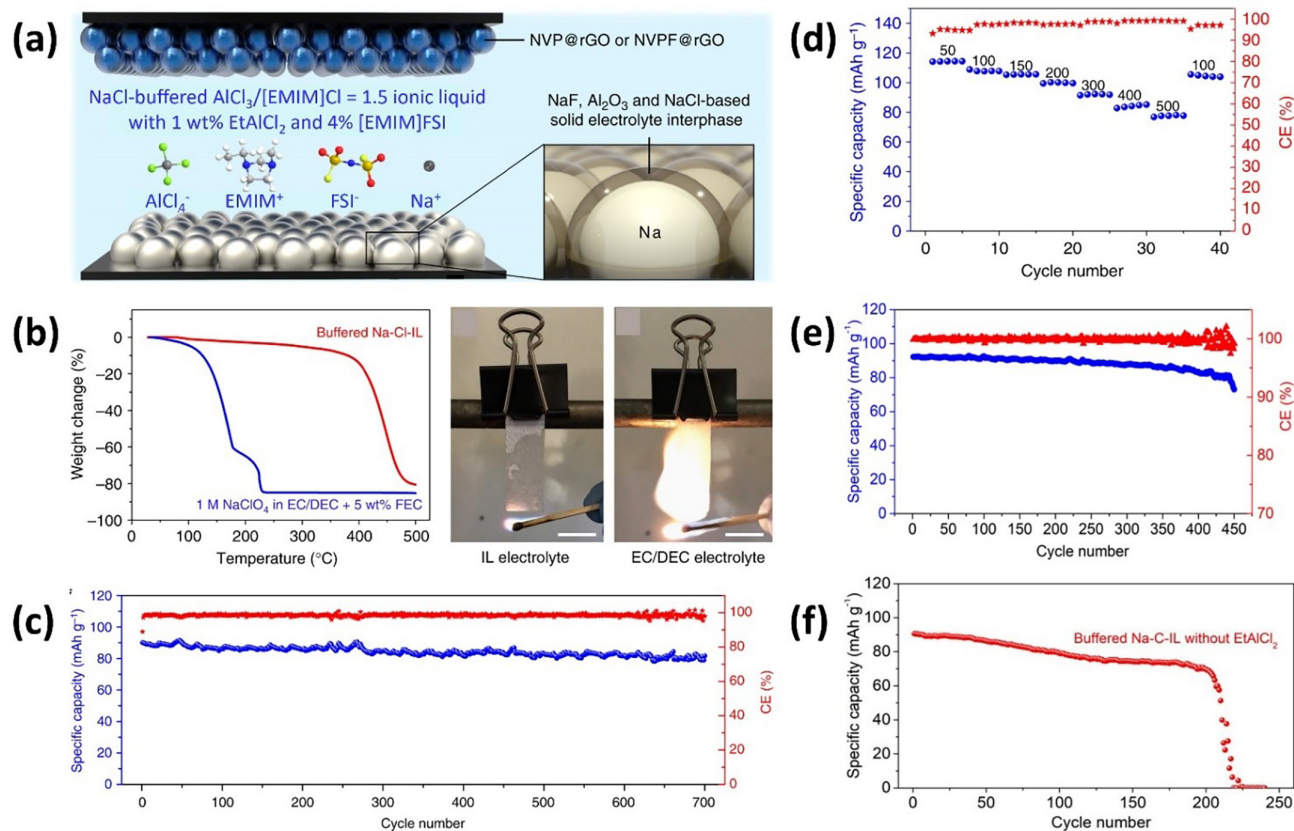


**FIG. 2.** (a) Schematic illustration of the composition of buffered Na-Cl-IL electrolyte and battery configuration (Na anode and NVPF@rGO cathode) (b) Flammability tests and thermogravimetric analysis (TGA) on the Na-Cl-IL and  $\text{NaClO}_4$ -EC/DEC/FEC electrolytes showing the nonflammable nature and thermal stability of Na-Cl-IL, (c) SIBs cyclic stability with Na-Cl-IL electrolyte, Na anode, and NVPF@rGO cathode at  $300 \text{ mA g}^{-1}$ , (d) changes in Coulombic efficiency and specific capacity of SIBs with Na-Cl-IL electrolyte under current densities (50–500  $\text{mA g}^{-1}$ ) (e) SIBs cyclic stability with  $\text{NaClO}_4$ -EC/DEC/FEC electrolyte, Na anode, and NVPF@rGO cathode at  $150 \text{ mA g}^{-1}$ , and (f) SIBs cyclic stability with Na-Cl-IL electrolyte without  $\text{EtAlCl}_2$  additive at  $150 \text{ mA g}^{-1}$ . Reproduced with permission from Sun *et al.*, Nat. Commun. **10**, 3302 (2019). Copyright 2019, Nature.<sup>135</sup>

stripping will help to identify the generic features in designing high-performance IL-based hybrid electrolytes for metal batteries. Understanding the structure-effect relationship and battery performance can aid in the design of novel IL electrolytes for this application.

*a. Water—An inexpensive additive for metal anodes.* Water can be regarded as a nuisance or a delight in electrolytes, depending upon the electrochemical application. The presence of water is seen as a key issue for high-voltage lithium or sodium batteries. First, aqueous electrolytes are incompatible with high-voltage electrochemistry, and second, in traditional electrolytes, water reacts with lithium or sodium, generating oxides, hydroxides, and liberating hydrogen gas. The addition of water in IL-based electrolytes, on the other hand, has been shown to have interesting impacts on both the physicochemical properties of the solvent and the surface reactions that occur.<sup>63</sup> It is suggested that there is no “free water” in ILs because water is highly coordinated to the IL (when water content is much lower than saturation point), preventing aggressive reactions with sodium or lithium metals.<sup>63,142</sup> The question as to whether the moisture content

in IL electrolytes plays a role in stable SEI formation and to what degree has improved understanding of the use of IL-based electrolytes for high energy metal battery technologies. Water miscibility in IL is mostly determined by anion as water molecules tend to form more hydrogen bonds with the anions as compared to the cations of the IL.<sup>143</sup> As a result, water is more soluble in ILs with hydrophilic anions (e.g.,  $[\text{BF}_4]^-$  and  $[\text{PF}_6]^-$ ) than ILs with hydrophobic anions [e.g.,  $[\text{TFSI}]^-$  and  $[\text{FAP}]^-$  (tris(perfluoroalkyl)trifluorophosphate anion)].<sup>143</sup> However, water also impacts the electrochemical stability window of the IL, which usually decreases with the addition of water.<sup>144</sup> Understanding of the electrode-IL interfacial phenomena in the presence of water is crucial for stable metal anode cycling. In this regard, the nature of the electrode, the IL chemical composition, the solute and water content should be carefully selected for a particular metal battery.<sup>143</sup>

Controlled moisture content ( $\sim 100$ – $200$  ppm) in non-fluorinated IL electrolytes has been shown to boost cycling performance in metal batteries,<sup>105,108</sup> while fluorinated anions (TFSI or FSI) based IL electrolytes were able to cycle sodium and lithium metals with water content up to 10 000 ppm.<sup>63,145,146</sup> Hence, presence of moisture during cell manufacturing allows for greater adaptability in

designing electrolyte and cell construction. The viscosity and conductivity concerns may be resolved by using a higher concentration of water, allowing cells to exhibit the low overpotentials required for the  $\text{Na}^{0/+}$  redox process.<sup>63,147</sup> Extraordinary stability for Na cycling in an FSI IL in the presence of water is feasible, given some important physicochemical parameters such as  $\text{Na}^+$  concentration and diffusion, and cation structure.<sup>63,147</sup> The chemistry of the IL cation cannot be neglected in this regard. Changing from a pyrrolidinium cation to an alkylphosphonium or alkoxyammonium cation revealed contrasting results because of the difference in interactions between cations and sodium ions. Even with 500 ppm water, the effect of water in a

phosphonium-based IL was equivalent to that of a pyrrolidinium-based IL, but deleterious to an ammonium-based IL. However, in the case of a Li metal electrode, the cation plays a crucial role in stabilizing water at the electrode surface. The phosphonium cation is better stabilized by the Li electrode compared to pyrrolidinium cations in the presence of water.<sup>145,148–150</sup>

Howlett *et al.* conducted the first in-depth study on the composition and structure of the SEI generated on Na metal anodes in water containing a superconcentrated pyrrolidinium-based IL electrolyte (50 mol. % solution of NaFSI, see Fig. 3).<sup>62</sup> High stability of the Na metal anode was observed (cycling efficiency >99%) by cycling the

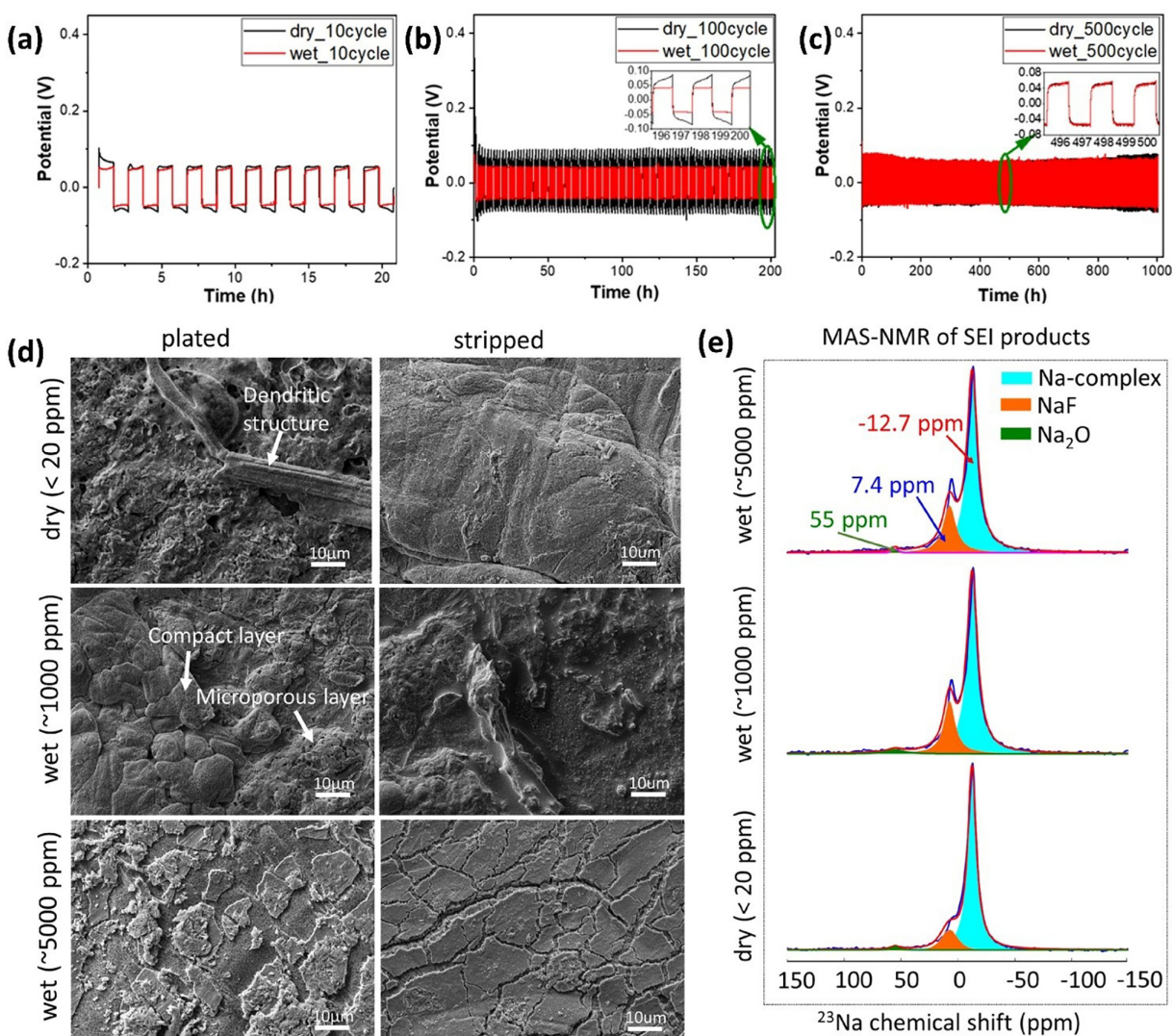


**FIG. 3.** Dry and wet electrolyte comparison (a)–(c) Potential vs Time cycling profile from Na|Na cells after 10, 100, and 500 cycles with fixed concentrations for dry and wet samples ( $1.0 \text{ mA}\cdot\text{cm}^{-2}$  current density, 1 h polarization at  $50^\circ\text{C}$ ) for superconcentrated 50 mol. % NaFSI in  $[\text{C}_3\text{mpyr}][\text{FSI}]$  ionic liquid electrolyte systems; (d) SEM micrographs obtained from Na|Na cells with different water content (0–5000 ppm) ( $1.0 \text{ mA}\cdot\text{cm}^{-2}$  current density, 1 h polarization at  $50^\circ\text{C}$ ) for superconcentrated 50 mol. % NaFSI in  $[\text{C}_3\text{mpyr}][\text{FSI}]$  ionic liquid electrolyte systems after 20 cycles (e)  $^{23}\text{Na}$  magic angle spinning nuclear magnetic resonance (MAS-NMR) spectra of electrodeposited Na from dry (< 20 ppm) and wet electrolyte (1000 and 5000 ppm water) after 20 cycles. Reproduced with permission from Ferdousi *et al.*, Appl. Mater. Interfaces **13**, 5706 (2021). Copyright 2021, American Chemical Society.<sup>62</sup>

anode in the electrolyte with various water content (1000 and 5000 ppm) for 1000 h at  $1 \text{ mAcm}^{-2}$  [see Figs. 3(a) and 3(c)]. After cycling Na anode in both dry and wet electrolytes, morphological analysis revealed two distinct deposit morphologies [Fig. 3(d)]. The cell with wet electrolyte (1000 ppm) showed more microporous deposits, while the dry electrolyte ( $< 20$  ppm) showed more compact deposits. The presence of water ( $\sim 1000$  ppm) enhances bond formation between IL anions and metal cations, resulting in the formation of large quantities of inorganic compounds (NaF and  $\text{Na}_2\text{O}$ ) by the decomposition of the anion at the anode surface,<sup>63</sup> as evidenced by spectroscopic investigations. Authors postulated the SEI composition as  $\text{Na}_2[\text{SO}_3\text{-NSO}_2\text{F}]$  complex for dry electrolyte while  $\text{Na}_2[\text{SO}_3\text{-N-SO}_2\text{F}]\cdot n\text{H}_2\text{O}$  complex for wet electrolyte [Fig. 3(e)].<sup>62</sup> Hence, the presence of a homogeneous surface with microporous structures on Na anode cycled in water containing electrolyte together with distinct SEI appeared to contribute to efficient cell charging and discharging over extended cycles. On the other hand, the presence of compact deposits lacking microporous structures when Na anode cycled in a dry electrolyte was related to unstable SEI and dendrite growth.<sup>62</sup>

As mentioned previously, the optimum water content in the IL-electrolyte influences the metal anode/IL interface. For Mg-based IL electrolytes, water can enhance the electrolyte's ionic conductivity, allowing a greater charge transport rate. In addition, water can change the chemical composition and characteristics of the surface layer evolved during Mg deposition on the magnesium surface, which then regulates the diffusion rates of ions to magnesium metal's surface.<sup>112,139</sup> Despite the obvious interest in water-IL mixtures, research on Mg anode behavior in these electrolytes, including the involvement of IL cations and anions in interfacial reactions, is limited. The interaction of Mg with water-IL mixtures is believed to be influenced by an IL with an etheric-substituted cation [such as poly-etheric ( $(-\text{O}-\text{CH}_2-\text{CH}_2-)_n$ ) substituted N-methylpyrrolidinium];<sup>125</sup> however, this hypothesis requires further in-depth analysis. In a nutshell, the investigation of optimal water concentration for specific IL systems is necessary to avoid undesirable reactions at Mg anode—corrosion and hydrogen evolution.

In many cases, the mass transport and electrochemical cycling of zinc in IL electrolytes can be further enhanced by introducing water as an additive or co-solvent.<sup>127,151-154</sup> For example, the introduction of 2.5 wt. % water to the electrolyte  $0.1 \text{ M Zn}(\text{TFSI})_2/[\text{N}_{2(20201)3}][\text{TFSI}]$  electrolyte can shift the zinc deposition potential to almost  $250 \text{ mV}$ <sup>127</sup> more positive. This suggests that water can decrease the energy activation barrier for Zn electrodeposition, assisting zinc's long-term cycling. Unlike in aqueous electrolytes, the formation of irreversible ZnO on the metal substrate is reduced in such water-IL mixtures since the solvation of  $\text{Zn}^{2+}$  ion in these systems is still largely dominated by the ionic liquid cation and anions.

Adding water minimizes the need for volatile organic additives and complex surface treatments and provides a new avenue to design water-tolerant electrolytes for high-stability cycling of metal anodes.<sup>62</sup> However, several reports point toward water's intricate behavior at the electrical double layer (EDL) in ILs, owing to strong intermolecular interactions with the ions.<sup>108,143,155</sup> As a result, more research is required to fully comprehend the impact of water on the metal anode/IL interface, particularly when using various IL cations and anions, for commercial practicality around scale-up and safety.<sup>143</sup>

## B. Interfacial electrochemistry of metal anodes in IL electrolytes

In Sec. III A, the issues related to specific metal anodes are described, where ionic liquid-based electrolytes were explored as an avenue to resolve issues related to traditional organic solvent-based electrolytes. The detailed interfacial chemistry of Na, Al, and Mg anodes in ILs will be discussed in Secs. III B 1–III B 3. The fundamental aspects underlying the advancements in ionic liquid electrolytes for specific metal batteries are presented. Additionally, the issues and controversies related to the usage of ILs are highlighted, and the proposed solutions are discussed with the help of some specific examples.

### 1. Na anode

The electrochemical, chemical, and thermal stability of ILs against Na metal is important when using Na metal as an anode. Various *in situ* surface-characterization techniques and MD simulations revealed that the interfacial structuring of pure ILs forms more and better-defined layers at the surface of the electrode under an applied potential.<sup>156</sup> The microscopic inhomogeneity and nanostructuring are demonstrated to be correlated with the Na anode's electrochemical performance in IL.<sup>156,157</sup> At higher temperatures, ion mobility in ILs increases as conductivity increases (independent of the type of Na solute), and viscosity decreases due to dissociation of ion clusters or ion pairs.<sup>116</sup> Combining the optimized  $\text{Na}^+$  concentration and raised temperature conditions increased the cycle efficiency of Na deposition/dissolution synergistically.<sup>158</sup> As  $\text{Na}^+$  diffuses fast across the surface of the electrode at  $90^\circ\text{C}$  ( $\sim$  the melting point of Na), increasing temperature can reduce dendrite growth and facilitate SEI-layer stabilization.<sup>159</sup> In the case of Li-based ILs, the electrolyte's thermal stability is related to SEI stability even at elevated temperatures.<sup>1</sup> However, there have been few investigations on the thermal characteristics of IL-based electrolytes for SMBs. To avoid thermal runaway, it is crucial to explore the thermal degradation of ILs at charged Na anode. Apart from the IL anion and cation chemistry, which is discussed in Sec. III A 1, the sodium salt concentration has a marked effect on the bulk properties of IL electrolytes and the interfacial layering at the electrode, and hence the enhanced cycling of the Na anode.

*a. Superconcentrated ILs for Na metal anodes.* Salt concentration significantly impacts the electrolyte properties and stability of the electrolyte/electrode interface. Highly concentrated/superconcentrated ILs (containing  $\sim 50$  mol. % of Na salt) electrolytes are a new dimension in IL research to solve the issue of instability of alkali metal anodes, enabling higher energy density technologies. Yoon *et al.* were the first to exhibit the cycling performance of a Li|LiCoO<sub>2</sub> cell using a pyrrolidinium-based IL electrolyte ( $[\text{C}_3\text{mpyr}][\text{FSI}]$ ) with a lithium salt concentration of up to  $3.2 \text{ mol kg}^{-1}$  at ambient temperature. Cells containing the largest electrolyte salt concentration exhibited enhanced rate capability, even at high C rates (3 and 5C), compared to cells with an organic electrolyte.<sup>149</sup> In such inorganic-organic IL electrolytes, metal cations become the dominant cation in the mixture, and unlike dilute solutions, device performance is not merely correlated with ionic conductivity.<sup>158,160,161</sup>

An increase in the alkali metal ions' concentration decreases the ionic conductivity of ILs due to the strong coordination and clustering of alkali metal ions ( $\text{Li}^+$  or  $\text{Na}^+$ ) to anions. At ambient temperatures,

the  $\text{Na}^+$  ion has a greater impact on increasing viscosity (lowering conductivity) than the  $\text{Li}^+$  ion because of a larger cation size and higher coordination number. However, at higher temperatures, the discrepancies tend to be less pronounced.<sup>160</sup> For FSI-based ILs, the transference number of alkali metal cations increases with the alkali metal salt's concentration (LiFSI or NaFSI), even though conductivity decreases and viscosity increases. The number of accessible FSI anions to meet the coordination number of the alkali metal cation—typically between three and five—decreases and becomes insufficient at a 1:1 molar salt concentration unless each anion starts to coordinate multidentately or to multiple metal cations. This aggregation and structuring impacts the alkali metal cation transport mechanism in superconcentrated electrolytes, which is different from traditional dilute electrolytes.<sup>160,161</sup>

MD simulations point toward a change in the basic diffusion mechanism, i.e., a shift from vehicular transport to hopping of alkali metal cations at such higher concentrations. The decoupling of alkali ions from vehicular transport not only leads to unique metal anode/IL interfaces but also improves the electrochemical stability and device rate performance. This suggests that the  $\text{Na}^+$  transference number, rather than the ionic conductivity, is crucial in the development of SEI layers.<sup>17</sup> At high  $\text{Na}^+$  concentrations, the high nucleation rate observed during metal deposition is due to a transport mechanism that is less susceptible to mass transport limits. Hence, Na anodes cycled in superconcentrated IL electrolytes demonstrated stable cycling due to having a compact layer with nanostructures. The absence of dendrites also reflects the nucleation and growth mechanism of the electrodeposit.<sup>160,162</sup>

By using computational and experimental investigations, Forsyth *et al.* recently elucidated the role of the concentration of NaFSI and applied potential on the electrolyte structure and composition of pyrrolidinium-based IL at metal anodes for increasing Na electrodeposition and the stability of the SEI film.<sup>156</sup> AFM force measurements and atomistic MD simulations showed distinct effects on the interfacial structure by increasing the NaFSI concentration from 0 to 50 mol. % in  $[\text{C}_3\text{mpyr}][\text{FSI}]$ . The interfacial structure is markedly different for 50 mol. % NaFSI, pointing toward a change in the strength of the ion-ion association and physical dimensions of interfacial ion packing. Furthermore, MD simulations suggest the enrichment of the innermost layer with both FSI and Na ions as the concentration of salt increases.<sup>156</sup> The higher coordination number of Na-FSI in superconcentrated ILs compared to ILs containing low salt concentrations is attributed to the formation of extended  $\text{Na}_x(\text{FSI})_y$  ion aggregates (as discussed before) due to reduced binding strength between  $\text{Na}^+$  and FSI anions. Thus, an enhanced Na hopping mechanism enriched the innermost layer at the electrode surface with more  $\text{Na}^+$  ions. The highly aggregated molten-salt-like structure  $[\text{Na}_x(\text{FSI})_y]$  in the innermost layer, particularly at a negatively charged surface, reduced the nanostructuring of the layers at the interface, which is evident by both AFM and MD simulations. As a result, a more uniform and homogeneous SEI layer is formed due to the dominance of Na and FSI ions and the expulsion of  $[\text{C}_3\text{mpyr}]^+$  near the anode surface. Uniform FSI anion distribution and decomposition to NaF results in dendrite-free Na deposition, which is favorable for stable Na cycling as evident by the Li metal system.<sup>157,163</sup> Notably, these results are for cations with shorter chained alkyl substituents in terms of packing and nanostructuring at charged electrode. This highlights that the effect of the nature

of cation substituent and cation structure on the surface organization of IL must be considered.<sup>111</sup>

Overall, the benefits of using superconcentrated ILs as electrolytes include (1) avoiding parasitic reduction of organic cations, which causes a poorer SEI layer; (2) anion-driven fluorinated SEI build-up; and (3) a substantial enrichment of interfacial layers with  $\text{Na}^+$  ions, which supports uniform metal deposition. Coupling superconcentrated ILs with anode preconditioning (at high current densities) improves the efficiency and life of metal anode batteries. However, such high salt-concentrated solutions are only attainable in a few systems, and there is scarce literature on the selection of organic cations for sodium electrochemistry. There is a need to develop molten-salt electrolytes and/or ILs solvents with high salt solubility.

*b. Localized high-concentration electrolytes.* The cosolvent method has the capability to address the disadvantages of IL-based electrolytes in Li metal batteries.<sup>164</sup> Due to insignificant interactions with cations, 1,1,2,2-tetrafluoroethyl 2,2,3,3-tetrafluoropropyl ether (TTE) as a cosolvent can dilute highly concentrated IL-electrolytes (decrease viscosity) and generate localized high-concentration electrolytes. Similarly, NaTFSI with  $[\text{C}_3\text{mpyr}][\text{FSI}]$  and TTE as cosolvent validated the efficacy of localized  $\text{Na}^+$  ion concentrated ionic liquid (LNCIL) electrolyte in improving safety and cycling stability of SMBs vs a Na ion containing IL (NIL),  $\text{Na}^+$  ion concentrated IL (NCIL), traditional carbonate-based electrolyte (EC/PC), and ether-based electrolyte [bis(2-methoxyethyl) ether (2G)].<sup>165</sup> Overall, LNCIL may maintain the NCIL's  $\text{Na}^+$  solvation structure with greater concentrations of Na-bound anionic species, generating an outside non-solvation sphere to promote fast Na ion transfer [Fig. 4(a)]. TTE dilution, in conjunction with FSI/TFSI anion pairs, fostered the establishment of a NaF-based SEI at the Na metal anode, suppressed dendrite growth, and improved coulombic efficiency ( $\sim 99\%$ ) [Figs. 4(b) and 4(e)]. SMB with Na as anode, NVP as cathode, and LNCIL as electrolyte demonstrated improved electrochemical performance with high-rate cycling of  $\sim 2.4 \text{ mA cm}^{-2}$  at 6C and capacity retention of 96.6% during 500 cycles as compared to the 2G electrolyte [Fig. 4(f)]. Moreover, even after TTE introduction, LNCIL maintained a remarkable oxidative stability ( $\sim 4.9 \text{ V}$  vs  $\text{Na}/\text{Na}^+$ ), rendering it appropriate for high-voltage SMBs.<sup>165</sup>

In most situations, surveying the literature reporting the utilization of Na-metal anode in ILs as an electrolyte yields no concrete insight related to SEI formation, composition, and cycling stability. SEI formation and surface composition are often documented using various approaches and operation conditions. A variety of IL electrolytes, additives (organic or water), metal salts, and surface treatments have been studied, with an emphasis on performance measurements and minimal data on the relationship of SEI evolution and stability with deposit morphology. More fundamental research is needed to completely understand the impacts of using mixed anions IL systems or superconcentrated ILs to regulate the interfacial behavior and ion nanostructuring at the charged electrode in order to achieve desirable SEI-forming features and improved recyclability, as well as to prevent battery failure and safety incidents on a practical level.

## 2. Al anode

In Al-batteries, IL-based electrolytes generally consist of  $\text{AlCl}_3$  and an organic salt. Among the different organic cations, alkyl

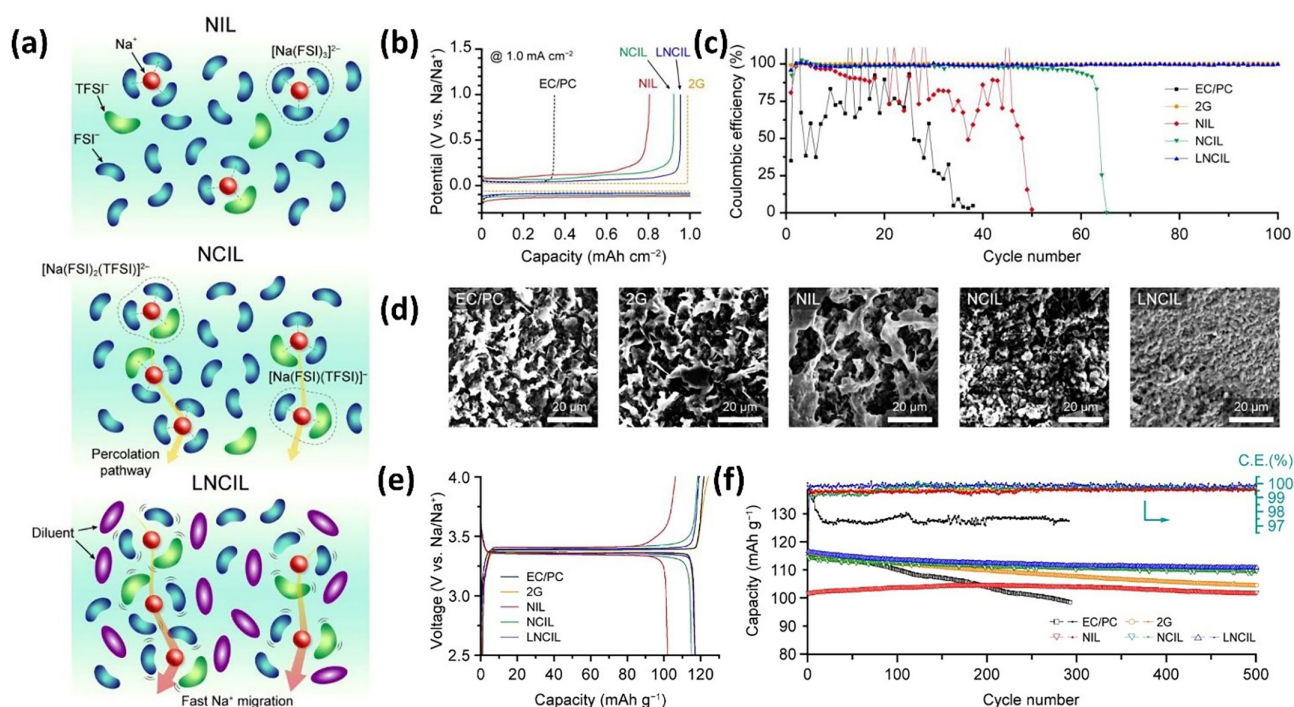


**FIG. 4.** (a) Schematic representation of the solution structures of NIL, NCIL, and LNCIL electrolytes: NIL, NCIL, and LNCIL; description of (b) voltage profiles (for first cycle) and (c) coulombic efficiency and cyclic stability of Na||Cu cells with electrolytes containing Na<sup>+</sup> ion (NIL, NCIL, LNCIL, 2G, and EC/PC) upon cycling (1 mA cm<sup>-2</sup>/1 mAh cm<sup>-2</sup>); (d) Na electrodes's surface SEM images cycled in various electrolyte (1 mA cm<sup>-2</sup>/1 mAh cm<sup>-2</sup>); Na||NVP cells with Na<sup>+</sup> ion containing different electrolytes demonstrating (e) voltage profiles in the voltage range of 2.5–4.0 V (vs Na/Na<sup>+</sup>) at 0.1C-rate; (f) Coulombic efficiencies and capacity retention at 1C-rate. Reproduced with permission from Lee *et al.*, *J. Chem. Eng.* **425**, 130612 (2021). Copyright 2021, Elsevier.<sup>165</sup>

imidazolium cations such as [EMIM]<sup>+</sup> and [BMIM]<sup>+</sup> are widely used in IL-based Al-battery systems due to ease of Al's electrodeposition at current densities  $\leq$  ca. 40 mA cm<sup>-2</sup>.<sup>166–170</sup> The ion speciation, physicochemical, and electrochemical properties of chloroaluminate ILs are dictated by the electrolyte's Lewis acidity, which is estimated by the molar ratio ( $r$ ) of aluminum chloride to the IL. In Lewis acidic ILs, the molar ratio ( $r$ ) is in the range  $1 < r < 2$  (AlCl<sub>3</sub> becomes insoluble for  $r > 2$ ), while  $r$  is less than 1 indicates Lewis basic IL and equimolar AlCl<sub>3</sub>/IL mixtures indicates neutral IL. The impact of  $r$  on the ion speciation of AlCl<sub>3</sub>/[EMIM][Cl] electrolyte is displayed in Fig. 5(a). In a Lewis acidic chloroaluminate, both AlCl<sub>4</sub><sup>-</sup> and Al<sub>2</sub>Cl<sub>7</sub><sup>-</sup> anions are present, while Al<sub>2</sub>Cl<sub>7</sub><sup>-</sup> has the ability to accept electron pairs and, therefore being termed as Lewis acidic.<sup>36</sup> Theoretically, increasing the IL's Lewis acidity increases the concentration of Al<sub>2</sub>Cl<sub>7</sub><sup>-</sup> anions resulting more Al electrodeposition during the charging cycle, hence, enhanced the anodic specific capacity of the battery.<sup>171</sup> Empirical evidence suggests that this is only feasible when specific currents are low (ca. 20 mA g<sup>-1</sup>) because above this limit, the rate of diffusion of Al<sub>2</sub>Cl<sub>7</sub><sup>-</sup> anions is restricted, resulting in a localized depletion of Al-containing anions at the electrode surface.<sup>171</sup> Hence chloroaluminate IL with low to moderate Lewis acidity ( $r = 1.1–1.3$ ) exhibits stable battery charging and discharging due to higher ionic conductivities and lesser corrosivity to Al anode.<sup>172</sup> The “self-cleaning” ability of slightly acidic melts due to their mild corrosive nature is beneficial in removing the aluminum oxide layer from the Al electrode,<sup>129</sup> as detailed in Sec. III B 2. d. Theoretical

calculations showed that the surface tension of the oxide layer is a key controlling parameter for efficiently breaking down the inert oxide coating.<sup>173</sup> In this regard, the anion (Cl<sup>-</sup>) content of the chloroaluminate-based IL has a favorable effect by decreasing the surface tension of the layer. An Al anode immersed in the most reported Lewis acidic IL electrolyte ( $r = 1.5$ ) can form cracks in the oxide film by 21%.<sup>173</sup>

Lewis basic ILs contain both AlCl<sub>4</sub><sup>-</sup> and Cl<sup>-</sup> ions, whereas neutral ILs contain predominantly neutral AlCl<sub>4</sub><sup>-</sup> anions [Fig. 5(a)]. AlCl<sub>4</sub><sup>-</sup> reduces at an electrode potential lower than that of the IL cation, so electrodeposition of Al is often not possible from neutral and basic ILs due to electrolyte decomposition before Al electrodeposition. Hence, the use of chloroaluminate ILs in Al-batteries is almost entirely limited to Lewis acidic ILs. The electrodeposition of Al from AlCl<sub>4</sub><sup>-</sup> anions in Lewis neutral ILs has been recently demonstrated by selecting IL cations with high electrochemical stability.<sup>174,175</sup> For example, forming ionogels of Lewis neutral ILs increases the electrochemical stability window up to 5 V and allows the deposition of dendrite-free Al. However, because of the high viscosity and low ionic conductivity of ionogel, electrodeposition occurs at coulombic efficiencies below 60%.<sup>175</sup>

The reactions occurring at the rechargeable Al-based batteries' anode (RABs) are almost consistent in chloroaluminate-IL electrolytes. The reversible deposition/dissolution of Al is achieved by a redox reaction between AlCl<sub>4</sub><sup>-</sup> and Al<sub>2</sub>Cl<sub>7</sub><sup>-</sup>, which corresponds to charging and discharging and is described as follows:

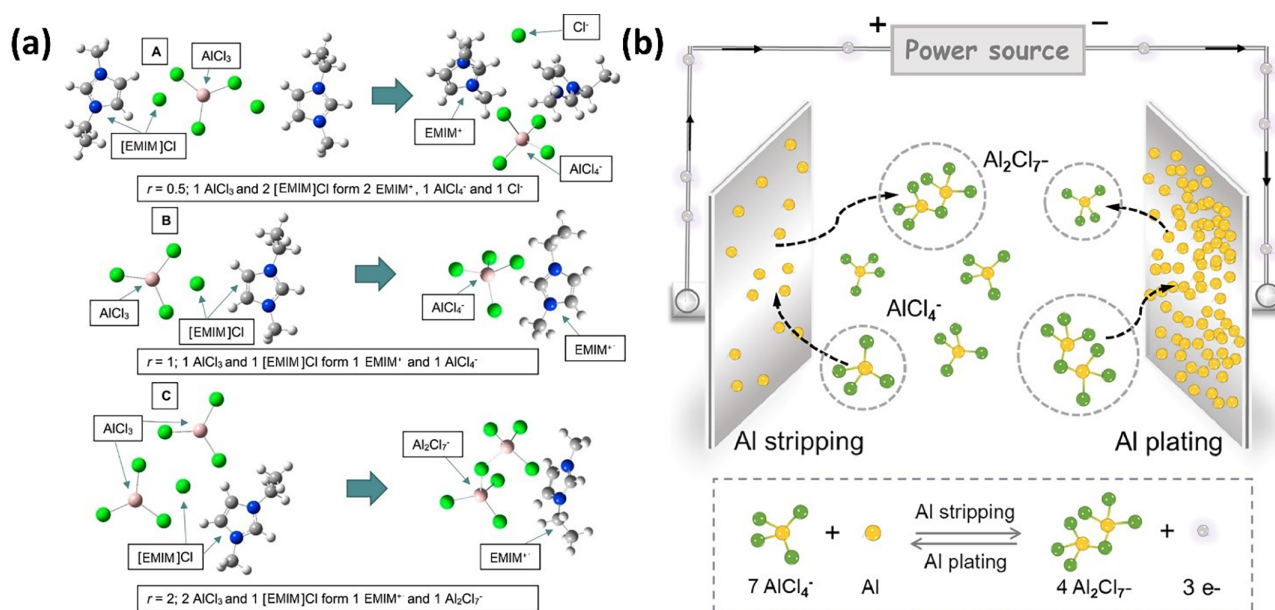
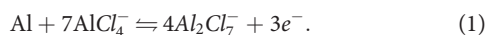


**FIG. 5.** Schematics demonstrating: (a) Chloroaluminate species formation at differing  $r$  values of  $\text{AlCl}_3$ -[EMIM][Cl]. Reproduced with permission from Renewable Sustainable Energy Rev. **133**, 110100 (2020). Copyright 2020, Elsevier.<sup>36</sup> (b) Schematic illustration of Al stripping/plating in chloroaluminate ionic liquid electrolyte on an Al anode. Reproduced with permission from Long *et al.*, Energy Storage Mater. **34**, 194 (2021). Copyright 2021, Elsevier.<sup>50</sup>



The reversible deposition/dissolution mechanism of Al can easily be understood in electrolytic cells with Al metal both as the cathode and anode and an ionic liquid electrolyte ( $\text{AlCl}_3$ /[EMIM][Cl]), as illustrated in Fig. 5(b).<sup>50</sup> The cathodic reaction involves the Al plating in which  $\text{Al}_2\text{Cl}_7^-$  ions gain electrons and are converted to  $\text{AlCl}_4^-$  ions and deposit Al. On the other hand, the reverse process (Al stripping) is observed at the anode.<sup>50</sup> The Al metal is dissolved in the IL electrolyte during the stripping or discharge process, as outlined by Eq. (1), which is the primary electrochemical reaction at the anode. As the Al anode is covered with an oxide layer ( $\text{Al}_2\text{O}_3$ ), the fissures in the pristine oxide layer allow only limited  $\text{Al}^{3+}$  diffusion and electrolyte conductivity, significantly reducing the surface area accessible for Al dissolution. This contributes to a potential drop at the film surface between the solid anode and the electrolyte.<sup>173</sup>

Aside from chloroaluminate ILs, successful reversible plating/stripping of Al in water and air-stable ILs such as [EMIM][TFSI] and [C<sub>4</sub>mpyr][TFSI] has also been reported.<sup>176–178</sup> When  $\text{AlCl}_3$  is mixed with [C<sub>4</sub>mpyr][TFSI] or [EMIM][TFSI], biphasic fluids are obtained at molar concentrations greater than 0.33 and 0.39, respectively, and Al reversible deposition/dissolution is obtained from the upper (lower density) phase in both cases. Detailed NMR, Raman spectroscopy, and computational analysis revealed that the lower density phase is rich in reducible  $\text{AlCl}_4^-$  species, whereas the more dense phase contains the non-reducible TFSI anion and  $\text{Al}[\text{TFSI}]_3$  species.<sup>176–178</sup>

Despite the fact that chloroaluminate ILs have extensive electrochemical stability windows ( $\sim 4.0$  V),<sup>3,170</sup> their hygroscopic character and sensitivity to moisture lead to undesirable reactions such as the generation of hydrogen chloride (HCl) and other oxide- and proton-containing species, which can further react irreversibly with other

solutes.<sup>179,180</sup> These concerns can be addressed to some extent by fine-tuning the composition and nature of the Al salt, prompting researchers to look into alternative IL-based electrolytes.<sup>172,181,182</sup> In this regard, researchers have investigated various strategies—such as investigating ILs based on organic amines such as trimethylamine (TMAHCl- $\text{AlCl}_3$ )<sup>167</sup> and triethylamine ( $\text{Et}_3\text{NHCl}$ ),<sup>183,184</sup> or replacing  $\text{Al}_2\text{Cl}_7^-$  anions with neutral pyridine-based ligands<sup>180</sup>—to mitigate issues associated with commonly used imidazolium-based ILs. TMAHCl- $\text{AlCl}_3$  and  $\text{Et}_3\text{NHCl-}\text{AlCl}_3$  ILs are cheaper alternatives to [EMIM][Cl] and display outstanding cycling stability in aluminum-metal batteries.<sup>167,183,184</sup> When compared to the standard [EMIM][Cl]- $\text{AlCl}_3$  IL, neutral (4-ethylpyridine or 4-propylpyridine) ligand substituted pyridine based IL- $\text{AlCl}_3$  electrolytes are not only moisture-insensitive, but are also significantly less corrosive toward Al, Cu, and Ni electrodes.<sup>180,185</sup> The difference is in the nature of the Al-containing ion. Instead of Al-containing anions (for example,  $\text{Al}_2\text{Cl}_7^-$  in [EMIM][Cl]- $\text{AlCl}_3$  IL), the electroactive species in neutral ligand-pyridine- $\text{AlCl}_3$  IL is an Al-containing cation, which is advantageous to aluminum electrodeposition. Furthermore, because Al-containing cations are less prone to attack metals than  $\text{Al}_2\text{Cl}_7^-$ , the neutral ligand-pyridine- $\text{AlCl}_3$  IL is chemically benign. Exploration of such  $\text{Al}_2\text{Cl}_7^-$  free IL electrolytes may result in rechargeable aluminum batteries (RABs) with higher reliability, less corrosion damage, and fewer safety issues.

The challenges associated with implementing Al-batteries in practice include poor reversibility of the metal anode, insignificant amount of charge stored, and areal specific capacities, which are unfeasibly low and range from 0.01–0.18  $\text{mAh cm}^{-2}$ , which is roughly two orders of magnitude lower compared to state-of-the-art Li-ion batteries (1–3  $\text{mAh cm}^{-2}$ ).<sup>48</sup> The slow progress in addressing these challenges raises concerns regarding the true viability of RABs as energy



storage devices of next-generation. In comparison to the substantial progress made in RAB cathodes, there are a few papers on the electrochemical characteristics of Al anodes in ILs.<sup>73,186</sup> The interface between the IL and the Al anode is critical to the performance of Al-based batteries because the instability of Al/electrolyte during stripping and plating process can result in degradation of battery capacity, fluctuations in the voltage, and unstable cycling.<sup>50</sup> In Secs. III B 2 a–III B 2 e, a basic understanding of Al anode–IL interfacial challenges is presented, and the development of various strategies to overcome these challenges is discussed.

*a. Double-edged role of Al<sub>2</sub>O<sub>3</sub> film on Al anode.* Unlike other metals, the Al surface has a natural aluminum oxide (Al<sub>2</sub>O<sub>3</sub>) layer, which forms upon exposure to air. It is well understood that bulk aluminum oxide exhibits insulating properties for both electrons and ions. However, Al<sub>2</sub>O<sub>3</sub> generated on Al metal surface is amorphous, compact, and defect-rich. Notably, electron tunneling is feasible through an oxide film at thicknesses of several nanometers; thus, the surface alumina can allow charge transfer and possibly ion conduction.<sup>186</sup> Moreover, the oxide film protects the Al anode by preventing galvanic reactions when exposed to acidic electrolytes.<sup>187</sup> Conversely, a passive oxide layer can influence the reversible reactions occurring at the anode during charge/discharge cycles due to its insulating properties. So, the ideal properties and thickness of the Al<sub>2</sub>O<sub>3</sub> oxide film for RABs are yet to be established. A thin oxide coating can inhibit dendritic formation in Aluminum-ion batteries (AIBs). Gao *et al.* emphasized the critical role of a native surface aluminum oxide film with a high Young's modulus in decreasing dendrite growth and stabilizing the anode. It does this by reducing nucleation sites and limiting metallic dendrite growth in AlCl<sub>3</sub>/[EMIM][Cl].<sup>52</sup> Defects sites in the protective Al<sub>2</sub>O<sub>3</sub> film provide a confined reaction space for subsequent stripping/depositing at the oxide/metal interface.<sup>52</sup>

Some researchers have suggested that the oxide film negatively impacts the charge/discharge performance. As a result, the alumina should be removed from the anode surface to expose a more active Al surface.<sup>187</sup> For example, in one study, an aluminum battery utilizing an electropolished Al metal in AlCl<sub>3</sub>/[EMIM][Cl] demonstrated a high capacity compared to Al metal with a native oxide film due to the balanced Al<sup>3+</sup> insertion/extraction.<sup>187</sup> The presence of the oxide film reduced the area available for the electrochemical process by blocking the IL from reaching the active Al surface. The thickness and microstructure of the oxide coating determine its effectiveness. A thin, porous alumina layer has the potential to increase battery performance. To summarize, the surface Al<sub>2</sub>O<sub>3</sub> can stabilize and passivate the Al anode, but the major challenge is to find the balance between these two effects.

*b. Dendritic puzzle and Al anode.* Dendrite formation is common in RABs because the anode reaction involves Al plating. The Al anode's surface morphology after electrochemical cycling in IL-based electrolytes can be categorized into three cases: (1) no dendrite growth and a smooth surface;<sup>52,183,188</sup> (2) an etched Al anode surface;<sup>189</sup> and (3) a pulverized Al negative electrode.<sup>190</sup> Al dendrite issues have often been overlooked, and there is considerable disagreement over the formation of “dendrites” of Al in IL electrolytes due to a lack of direct evidence.<sup>50</sup> For example, Lin *et al.* reported dendrite-free Al plating from AlCl<sub>3</sub>/[EMIM][Cl] in an ultrafast rechargeable AIB consisting of Al anode and graphite cathode.<sup>188</sup> On the other hand, several independent investigations revealed the growth of dendrites on Al anodes following extensive charge/discharge cycles by using ILs.<sup>52,191</sup> Figures 6(a) and 6(b) depicts surface and optical microscopy observations of Al dendrite growth, which begins with fluffy Al formation on the surface followed by an increase in Al foil thickness due to protrusions of dendritic Al.<sup>50</sup> With increased electroplating time, massive dendrites in a tip-

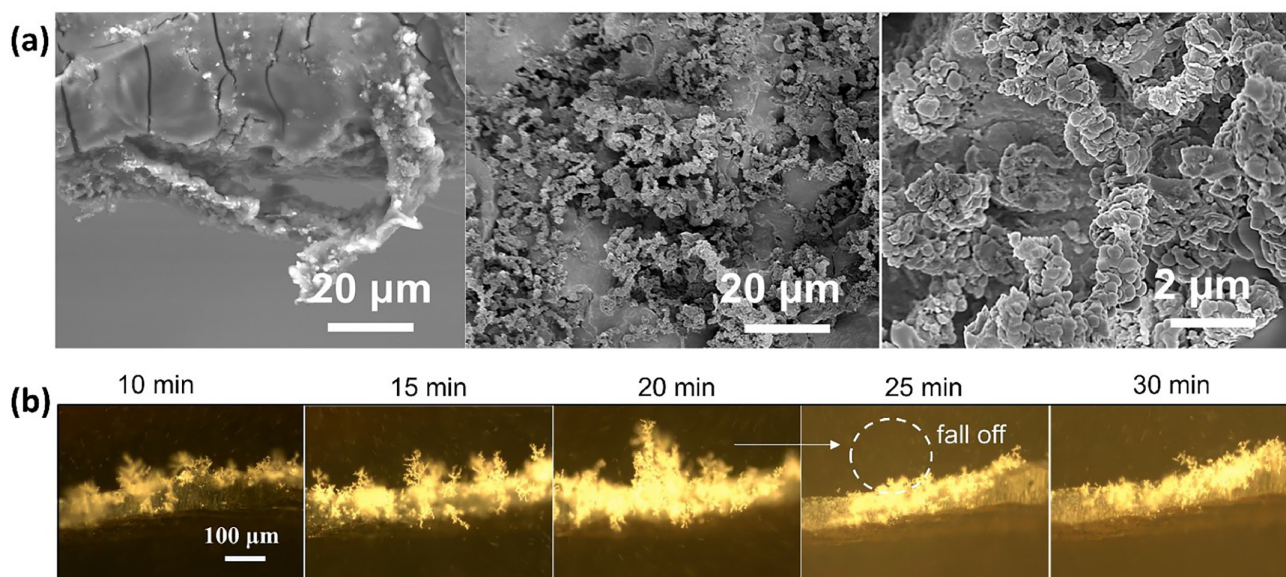


**FIG. 6.** Analysis of the formation of Al dendrite (a) morphology of the Al electrodes using SEM images (side-view and top-view); (b) Al dendrite growth on Al electrode shown by the *in situ* optical microscope images taken at different time intervals. Reproduced with permission from Long *et al.*, Energy Storage Mater. **34**, 194 (2021). Copyright 2021, Elsevier.<sup>50</sup>

growth pattern form on the Al surface. Furthermore, “dead” Al dendrites were observed to slide off the anode into the electrolyte, resulting in Al loss.<sup>50</sup>

Although the literature on dendritic formation on Al foil is inconsistent, the metallic character of Al foil is prone to dendrite formation, leading to disintegration of the electrode and, eventually, cell failure.<sup>52</sup> Gao *et al.* experimentally proved the existence of aluminum dendrites during reversible Al plating/stripping in  $\text{AlCl}_3/[\text{EMIM}][\text{Cl}]$  (see Fig. 7).<sup>52</sup> However, dendrites are restricted beneath the protective oxide layer, resulting in nearly undamaged Al foil with a smooth surface after cycling, giving the impression of dendrite-free Al deposition. Figures 7(d)–7(f) schematically demonstrates that despite the nearly full interfacial protection by surficial oxide coating, Al metal serves as a reactive anode only at the fissures. The defect sites in the  $\text{Al}_2\text{O}_3$  film offer pathways for electrolyte penetration and confined reaction space for subsequent stripping/plating at the oxide/metal interface. On the other hand, unrestricted dendritic growth is observed on the Al surface, lacking oxide coating, which leads to a rugged Al surface with dead Al dendrites [Figs. 7(a)–7(c)]. Due to the unconstrained volume variation and inhomogeneous dendritic dissolution, aluminum dendrites can easily detach from the original aluminum foil after continuous cycling, resulting in active material loss and subsequent electrode degradation, as shown in Fig. 7(g).<sup>52</sup>

Dendrite growth in ILs is influenced by current density and involves a series of intricate processes such as nucleation, growth, and stripping. *In situ* optical observations showed that with an increase in the current density, the density of the dendrites increased, and the morphology altered accordingly.<sup>53</sup> Theoretical simulations revealed that Al electrodeposition on the anode surface was localized either at the defect or active sites. Al dendrites’ electrochemical activity was

found to be lower than the pure Al anode, as dendrites obstructed the Al electrode surface’s uniform evolution due to an inhomogeneous ion concentration interface and an irregular current distribution on the electrode.<sup>53</sup> Aside from surface stability, progress on dendrite growth on an Al metal electrode suggests that electrodeposition of Al is similar to plating, with the deposition morphology determined by surface modification, concentration gradient, ion concentration, self-diffusion of the metal atom, temperature, and distribution of the electric field.<sup>19,53,186</sup> In particular, slow ion diffusion and high viscosity are important considerations for ILs as electrolytes. Therefore, while addressing dendrite issues in IL, the intrinsic factors (Al plating process) and kinetic factors (concentration gradient) on nucleation and growth mechanism must be taken into account.

The use of untreated Al metal as anodes continues to pose a significant challenge to the cycling performance of aluminum batteries due to the existence of an oxide film and Al corrosion, particularly in air and moisture-sensitive ILs.<sup>192</sup> Several strategies for optimizing metallic Al anodes and addressing these issues have been proposed. Al’s alloying with other elements (Ga, Zn, and Cu) or producing low melting eutectic alloys such as galinstan—tin (10.0%), gallium (68.5%), and indium (21.5%) (by weight)—and Al-In-Zn has been shown to alleviate the problem of the passivating oxide layer and pulverization and improve the corrosion resistance.<sup>190,193–196</sup> The soaking or electro-etching of the Al anode as a pretreatment resulted in unique interfacial chemistry and increased performance (detailed discussion is given in Sec. III B 2 d).<sup>50,52,187</sup> Although these strategies have improved Al metal anodes, it is difficult to change the Al anodes’ planar nature, which are susceptible to non-uniform and dendritic deposition in an IL.<sup>192</sup> Unresolved dendrite issues in the Al metal anode—such as protrusions of dendritic Al and electrical disconnection from electrode

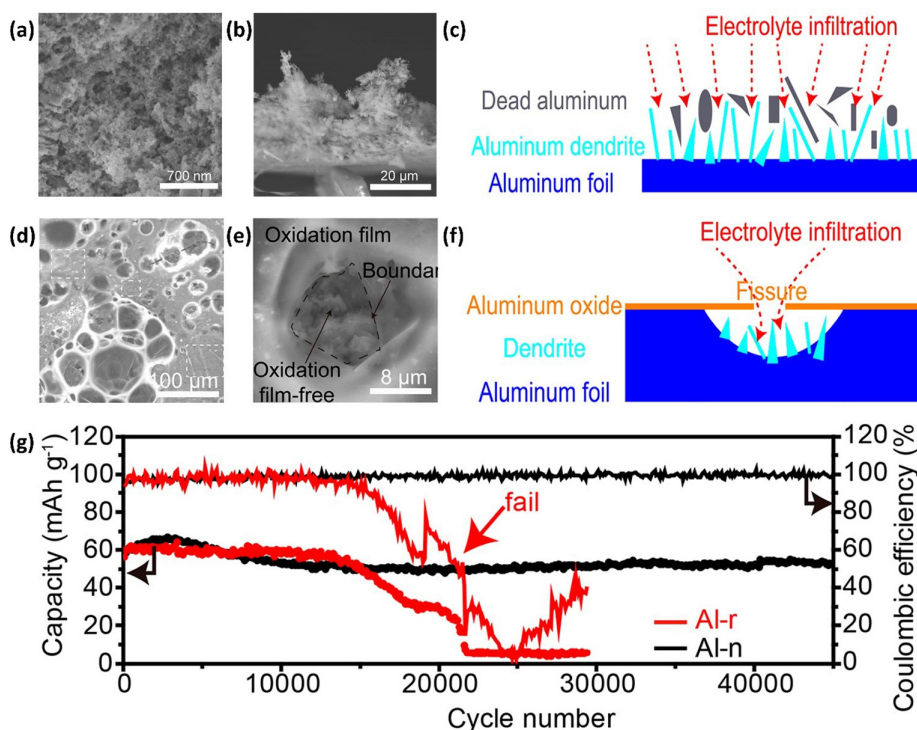


**FIG. 7.** Investigation of the existence of Al oxide on the electrochemical behavior of Al-n (Al foil with oxide film) and Al-r (Al foil without oxide film) anodes. (a) SEM image and (b) SEM image of the cross section of Al-r anode taken out from Al-graphene cell after 1000 cycles; (c) Schematic illustration of dendrite growth on Al-r foil. (d) SEM image and (e) high magnification SEM images of Al-n anode taken out from Al-graphene cell after 10000 cycles. The presence of dendrites beneath the hole in Al oxide film is shown by the magnified SEM image. (f) Dendrite growth on Al-n foil’s schematic illustration. (g) Comparison of cycling performance between aluminum—graphene full cells adopting Al-r or Al-n as anodes. Reproduced with permission from Chen *et al.*, *Appl. Mater. Interfaces* **9**, 22628 (2017). Copyright 2017, American Chemical Society.<sup>52</sup>

due to the 2D metal foil's inherent characteristics—necessitate additional investigation. In this regard, employing porous Al rather than planar Al as an anode offers a stable framework for reversible Al deposition/dissolution in ILs.<sup>50</sup> It not only enhances the available electroactive surface area for Al nucleation, but it also reduces the local current density, resulting in homogenous Al deposition inside the inner pores depicted in Figs. 8(a)–8(d). Porous Al has consistent and negligible voltage hysteresis with an average coulombic efficiency of  $\sim 100\%$  for stripping/plating, as shown in Fig. 8(b).

The low active surface area and low conductivity of the 2D Al anode can be addressed by using Al electrodeposited on a 3D carbon cloth (Al/CC) as anode.<sup>192</sup> Furthermore, to ensure anode cycle stability and corrosion resistance, IL-based electrolytes with appropriate Lewis acidity are required. Recently Li *et al.* ameliorated the corrosivity of [EMIM][Cl]/AlCl<sub>3</sub> (IL-O) by treating it with an Al pellet of high-purity at an elevated temperature (60 °C) for a day till the electrolyte became colorless.<sup>192</sup> In a treated IL (IL-T), the Al palette's surface was etched as a result of Al reacting with small amounts of H<sub>2</sub>O and HCl present in the chloroaluminate IL, producing AlCl<sub>4</sub><sup>-</sup> and Al<sub>2</sub>Cl<sub>7</sub><sup>-</sup> (see Fig. 9). Figures 9(a) and 9(b) compare the morphological changes that occurred on planar Al foil and Al/CC after 10 cycles in IL-T, with the Al foil anode being consumed and pulverized, indicated by red dotted lines in Fig. 9(a), while Al/CC retained its original structure as seen in the optical image [Fig. 9(b)]. Uncontrolled plating/stripping in the case of the Al foil led to an enormous pit and cracks, thus gradually destroying the metallic Al anode. In contrast, 3D Al anodes have

effective surface areas and conductive frameworks that boost ionic and electronic conductivities, resulting in homogeneous Al deposition [Fig. 9(b)] and accommodating the volume variation during reversible deposition/dissolution [Fig. 9(c)]. Figure 9(d) shows a comparison of the graphite||aluminum battery cycling stability using 2D and 3D Al anodes, with the 3D Al anode performing much better with a high initial discharge capacity of 89 mAh g<sup>-1</sup> which was stable after 800 cycles (54 mAh g<sup>-1</sup>) and high CE ( $\sim 97\%$ ). Thus, using a 3D Al anode in conjunction with the treated IL effectively prevented dendrite formation, accommodated volume variation, and enhanced reversible Al plating/stripping processes.<sup>192</sup>

To summarize, disagreement persists over the “dendritic” Al deposition from the IL, and the current research focus is primarily on the morphology of the Al deposit, with limited studies investigating the Al anode's evolution. Al anode's surface evolution includes a number of complex processes, including corrosion, removal of surface oxide film, and Al deposition and dissolution. Thus, dendritic concerns in rechargeable Al-based batteries cannot be addressed without understanding the processes that dominate the deposition morphology.

*c. SEI on Al anode.* In chloroaluminate electrolytes, Al anodes do not form an SEI layer; therefore, plating and stripping occurs at the electrolyte/Al interface,<sup>36</sup> meaning that the Al anode experiences chemical instability in the Lewis acidic IL electrolyte. One of the primary challenges in using RTILs in Al-based batteries is the stability of the alumina coating on Al surface, which is challenging to dissolve or remove. There is evidence of dissolution of the pristine oxide layer

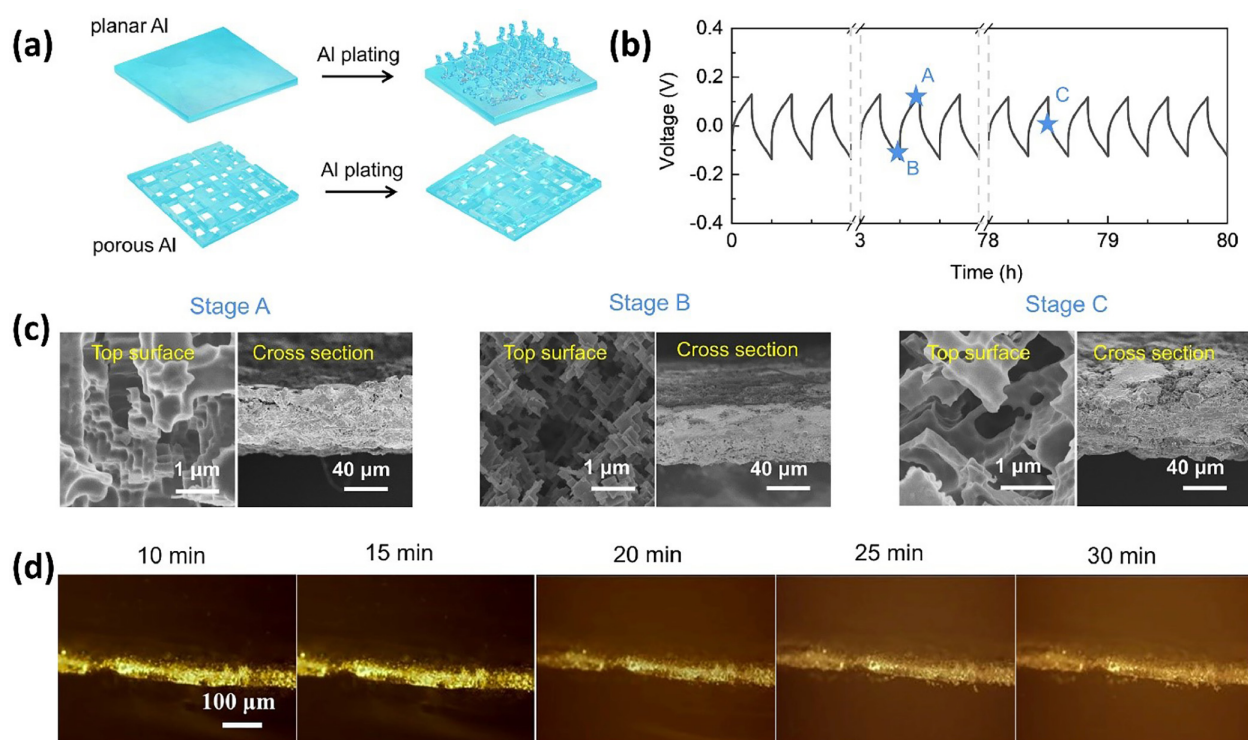


**FIG. 8.** (a) Schematic illustration of the dendrite growth and Al electrodeposition on planar Al and porous Al; (b) Voltage vs time profiles of Al stripping/plating on porous Al anode; (c) SEM images (top-view and side-view) demonstrating morphology of porous Al at different stages of stripping/plating; (d) Morphology of Al deposition on porous Al shown by *in situ* optical microscope images. Reproduced with permission from Long *et al.*, Energy Storage Mater. **34**, 194 (2021). Copyright 2021, Elsevier.<sup>50</sup>

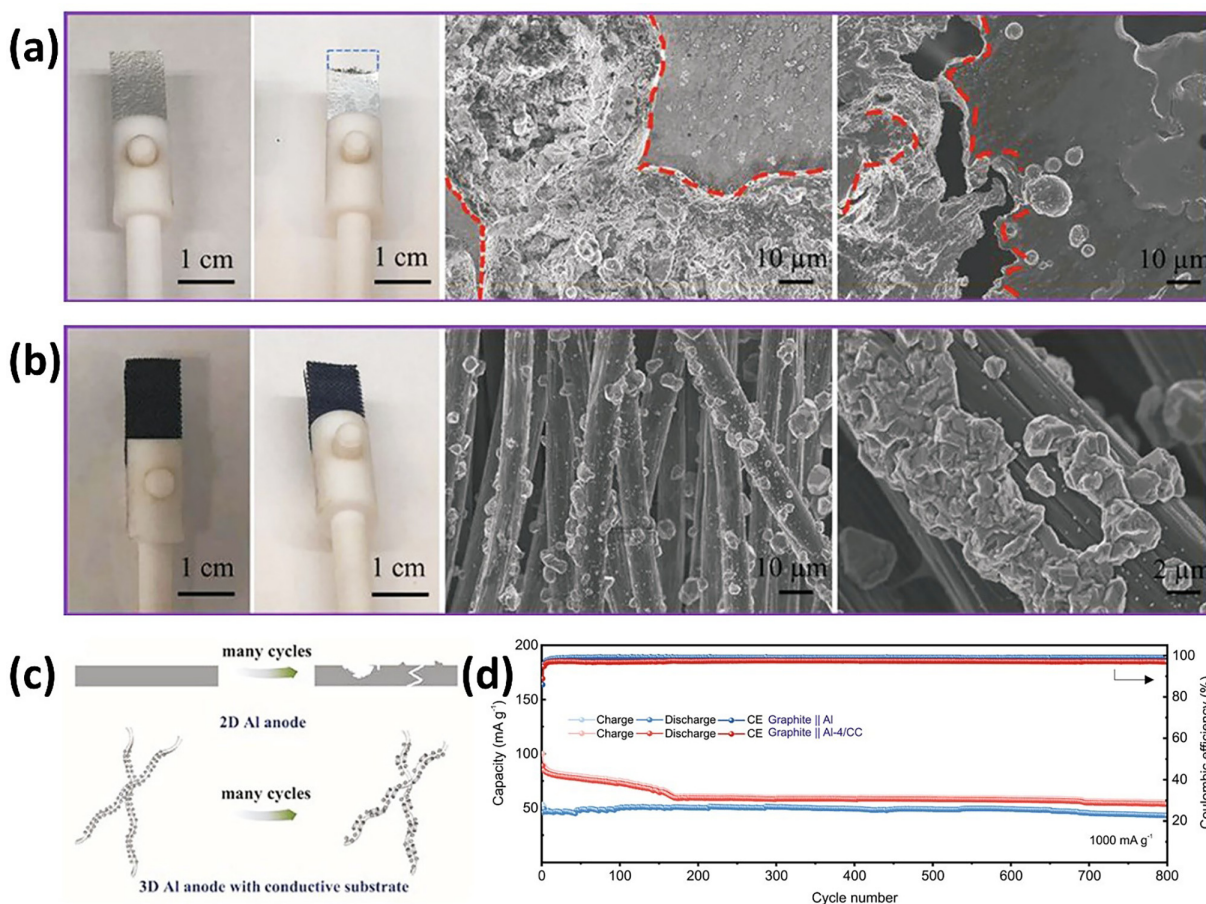


**FIG. 9.** Optical and SEM images of (a) the Al foil anode and (b) the Al-4/CC anode cycled in the IL-T electrolyte for 10 cycles (current density =  $0.5 \text{ mA cm}^{-2}$ ). (c) Schematic illustration demonstrating the cycling comparison between 2D Al foil and the 3D Al/CC anode. (d) Comparison of stability and Coulombic efficiency between graphite||Aluminum and graphite|| Al-4/CC cell operated at  $1000 \text{ mA g}^{-1}$  in IL-T electrolyte. Reproduced with permission from Li *et al.*, Carbon Energy 4, 155 (2022). Copyright 2022, Wiley.<sup>192</sup>

( $\text{Al}_2\text{O}_3$ ) in the IL electrolyte, accompanied by the creation of a new interphase instead of  $\text{Al}^{3+}$  diffusing into the electrolyte.<sup>197</sup> The limited solubility of  $\text{Al}_2\text{O}_3$  in commonly used ILs is usually due to the presence of weakly coordinating anions like  $\text{BF}_4^-$ ,  $\text{PF}_6^-$ , or  $\text{TFSI}^-$ .<sup>198</sup> The use of appending coordinating groups, such as oligo-fluorinated species, especially  $\text{H}_2\text{F}_3^-$ , increases the solubility of the Al metal oxide and transforms the Al surface from a passive to an active state. Several surface and electrochemical characterization methods supported oligo-fluorohydrogenate-based ILs to dissolve pristine oxide surface films, allowing the development of a protective amorphous Al-O-F layer instead.<sup>198,199</sup> Al activation in  $[\text{EMIM}][(\text{HF})_{2.3}\text{F}]$  (1-ethyl-3-methylimidazolium oligofluorohydrogenate) begins with the thinning of the  $\text{Al}_2\text{O}_3$  film, then exposing Al surfaces to form  $\text{Al}_x\text{O}_y\text{F}_z$ . The dissolution of pristine Al oxide continues with the growth of  $\text{Al}_x\text{O}_y\text{F}_z$  until the new amorphous film covers the bulk of the Al surface. Figure 10(a) depicts this process, which is corroborated by cross-sectional STEM images taken before [Figs. 10(b) and 10(c)] and after 0.5 h [Fig. 10(d)] of Al immersion. This newly built-up layer allows both processes to occur simultaneously, i.e., a dramatic restriction of Al corrosion while still allowing for high amounts of Al anodic dissolution.<sup>198</sup> During

Al-air battery discharge with different RTILs, only the Al-air batteries with  $[\text{EMIM}][(\text{HF})_{2.3}\text{F}]$  were discharged, as depicted in Fig. 10(e). The cells containing  $[\text{EMIM}][\text{TFSI}]$  and  $[\text{EMIM}][\text{OTF}]$ , on the other hand, were unable to operate with cell voltages rapidly dropped to 0 V, demonstrating their incapability to meet and maintain the current demand as they could not penetrate the native  $\text{Al}_2\text{O}_3$  surface film.

In this regard, air and water stable  $[\text{EMIM}][(\text{HF})_{2.3}\text{F}]$  and tetrabutylammonium dihydrogen trifluoride ( $\text{TBAH}_2\text{F}_3$ ) ILs are a good alternative to chloroaluminate ILs.<sup>133,200</sup> The oligo-fluorohydrogenate based IL sustains two different conditions upon contact with the Al anode: (1) electrochemical Al discharge at high rates ( $\sim 1.5 \text{ mA cm}^{-2}$ ), (2) preventing rapid Al corrosion and exhibiting a low corrosion rate ( $\sim 25 \mu\text{A cm}^{-2}$ ). These distinctive characteristics allow above 70%–75% utilization of the Al anode and thus a more efficient battery operation.<sup>199</sup> Despite the fact that both  $[\text{EMIM}][(\text{HF})_{2.3}\text{F}]$  and  $\text{TBAH}_2\text{F}_3$  electrolytes include active oligo-fluorinated species and exhibit promising results, there are considerable differences in Al anode activation and corrosion rates. At low discharge current rates of  $0.1 \text{ mA cm}^{-2}$ , the cell using  $[\text{EMIM}][(\text{HF})_{2.3}\text{F}]$  as electrolyte's has a lower capacity (14.5% of the theoretical capacity) compared to the cell using

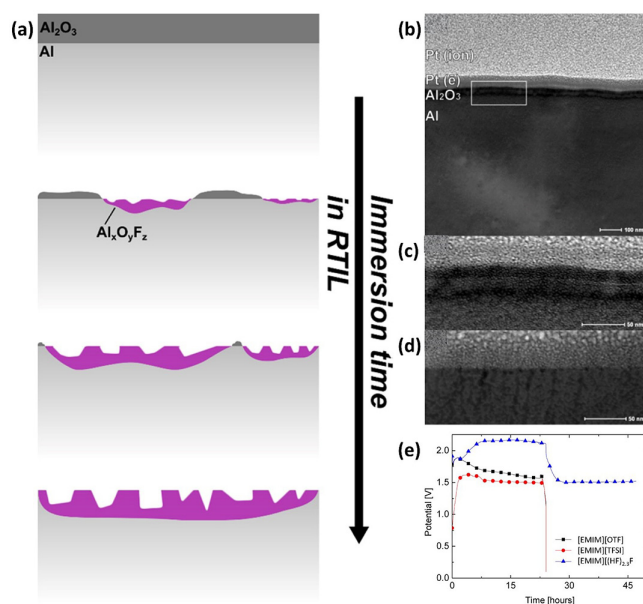


**FIG. 10.** (a) Schematic illustration of the Al activation mechanism in oligo-fluorohydrogenate ([EMIM][(HF)<sub>2.3</sub>F]) IL; High-angle annular dark-field scanning transmission electron microscopy (HAADF STEM) images demonstrating cross section view of (b) and (c) oxidized Al before interaction and (d) after 30 min of interaction of oxidized Al with 10  $\mu$ L of [EMIM][(HF)<sub>2.3</sub>F]. The rectangular area in (b) is focused in (c) and (d) for a clear description of the evolution of interfacial morphology. The layer in the dark contrast shows Al<sub>2</sub>O<sub>3</sub> which is present in (b) and (c) but absent in (d). The Pt deposited on the sample as shown in (b) is part of the preparation of the sample for microscopic imaging; (e) Potential vs time profile for aluminum–air battery (current density = 0.5 mA·cm<sup>-2</sup>) using Al anode with different electrolytes—[EMIM][OTF] (black squares) [EMIM][TFSI] (red circles), and [EMIM][(HF)<sub>2.3</sub>F] (blue triangles). Reproduced with permission from Shvartsev *et al.*, *Langmuir* **31**, 13860 (2015). Copyright 2015, American Chemical Society.<sup>198</sup>

TBAH<sub>2</sub>F<sub>3</sub> (65%). Notably, the theoretical capacity of the Al anode varies dramatically, with 20 vs 200 mAh·cm<sup>-2</sup> for TBAH<sub>2</sub>F<sub>3</sub> and [EMIM][(HF)<sub>2.3</sub>F], respectively.<sup>133</sup> Consequently, Al anode in TBAH<sub>2</sub>F<sub>3</sub> experienced lower corrosion. However, a higher discharge voltage is attained for [EMIM][(HF)<sub>2.3</sub>F] (1.7 V) vs 1.55 V for TBAH<sub>2</sub>F<sub>3</sub>. This is because of the weak interactions between the anion and cation of [EMIM][(HF)<sub>2.3</sub>F] compared to the ionic constituents of TBAH<sub>2</sub>F, which results in higher ionic conductivity.

*d. Interface reconstruction effect.* Passivation and corrosion limit the performance of the Al negative electrode. The paradigm for Al anode interfacial engineering involves both Al activation and stabilization, with the goal to prevent corrosion and dendrite formation.<sup>186</sup> According to a recent study in the acidic AlCl<sub>3</sub>/[EMIM][Cl] electrolyte, galvanic corrosion occurs when the Al anode interacts with the electrolyte.<sup>197</sup> Comprehensive investigation into interfacial chemistry revealed the dissolution of the native Al<sub>2</sub>O<sub>3</sub> surface film and reconstruction of the SEI prior to dendrite growth in the IL electrolyte during Al plating (Fig. 11). Spectroscopic and composition analysis showed that the newly formed SEI was comprised of Al–Cl and Al–O like species.<sup>50</sup> For an efficient electrochemical reaction at the anode, pretreatment of the native Al<sub>2</sub>O<sub>3</sub> is required to expose active Al metal.

It was demonstrated that complete removal of the surface oxide film by employing intense treatments such as electropolishing or strong protic acid etching is detrimental.<sup>52,186</sup> Because of the unrestricted growth of aluminum dendrites all over the pretreated surface, the Al metal anode develops a rugged surface, resulting in a cell short circuit. As opposed to complete oxide film removal, partial removal of the passive surface film is shown to promote stable cycling performance.<sup>181,201</sup> In this regard, the chloroaluminate IL (AlCl<sub>3</sub>/[BMIM][Cl]) efficiently removes the oxide film compared to Al(OTF)<sub>3</sub>/[BMIM][OTF] because of its acidic nature. Figure 11(a) shows a schematic comparison of the Al<sup>3+</sup> plating/stripping on an untreated (blocked by Al<sub>2</sub>O<sub>3</sub> film) and treated Al anode. Surface morphologies of the Al anode immersed in Al(OTF)<sub>3</sub>/[BMIM][OTF] and AlCl<sub>3</sub>/[BMIM][Cl] are shown in Fig. 11(b). When Al foil is submerged in Al(OTF)<sub>3</sub>/[BMIM][OTF] IL, no change is observed; however, pitting corrosion is clearly visible when Al foil is treated with AlCl<sub>3</sub>/[BMIM][Cl]. A cycling comparison of a treated and untreated Al anode in Al(OTF)<sub>3</sub>/[BMIM][OTF] shows that after the removal of oxide film, Al<sup>3+</sup> deposition/dissolution proceeds unimpeded, revealing that the interface between the freshly exposed Al negative electrode and the electrolyte is a crucial aspect influencing battery performance.

Reconstruction of the interface through facile pretreatment is advantageous for producing fresh Al that reacts with oxygen and moisture after being exposed to the electrolyte in the battery, eventually forming a thin, flat, and uniform SEI layer that can shield the anode underneath and improve cycling stability.<sup>201</sup> Morphological analysis revealed that Al<sub>2</sub>O<sub>3</sub> and Al(OH)<sub>3</sub> makeup the restored SEI. The interaction of exposed Al and traces of oxygen and moisture dissolved in AlCl<sub>3</sub>/[BMIM][Cl] produces Al<sub>2</sub>O<sub>3</sub>, while the hydrolysis reaction of Al<sup>3+</sup>—when Al comes in contact with acidic electrolyte—produces Al(OH)<sub>3</sub>. Water in the IL electrolyte has been shown to be critical in the development of the SEI layer. During the interface-reconstruction process, many hydrogen ions are consumed, thereby reducing the IL electrolyte's acidity to basic or neutral. The duration of Al immersion in the corrosive IL is important because immersion of Al foil for greater than 6 h causes cracks.<sup>201</sup> Nonetheless, prolonged immersion induces pulverization of the Al anode during electrochemical cycling.

*e. IL-artificial SEI film: Reality or illusion.* Corrosive IL electrolytes such as AlCl<sub>3</sub>-[EMIM][Cl] are thought to be beneficial in Al batteries as they dissolve the passivating oxide layer and allow the construction of a new SEI layer. The reconstructed interphase on Al electrodes enables reversible operation not only in IL-based electrolytes (as previously discussed) but also in aqueous electrolytes.<sup>74,202</sup> Archer *et al.* demonstrated the use of IL-rich artificial SEI (ASEI) for reversible plating/stripping at Al anode, enabling high-capacity aqueous Al-batteries.<sup>74</sup> More comparable works using an ASEI formed by an IL or a DES have since been reported for aqueous Al-batteries.<sup>202–204</sup> However, there are reservations about the efficacy and validity of the ASEI engineering approach. First, due to a lack of experimental and computational results showing the only reaction occurring is metal stripping/plating, the ability of an IL residual layer on Al to operate as an ASEI is questionable. On the other hand, though some electrochemical performance data supports its superior performance, fundamental characteristics such as electronic insulation, ionic mobility, and stability are essentially unknown. Azimi *et al.* investigated the origin of the passivation and the “IL-ASEI” functioning mechanisms. They

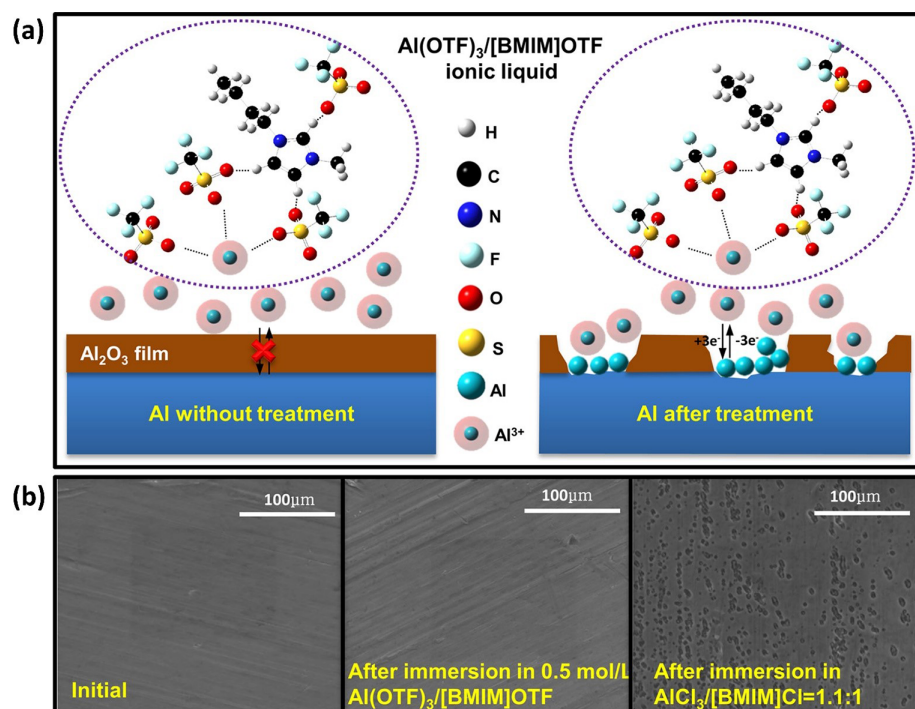


**FIG. 11.** (a) Schematic illustration demonstrating dissimilarities in Al deposition/dissolution process on the untreated Al anode and AlCl<sub>3</sub>/[BMIM][Cl] treated Al surface; (b) Al foil SEM images taken before immersion and after 24 h of interaction with 0.5 mol/L Al(OTF)<sub>3</sub>/[BMIM][OTF] and AlCl<sub>3</sub>/[BMIM][Cl] (1:1:1). Reproduced with permission from Wang *et al.*, ACS Appl. Mater. Interfaces **8**, 27444 (2016). Copyright 2016, American Chemical Society.<sup>181</sup>

discovered conflicting results despite the significantly better performance of IL-pretreated Al, as widely reported in the literature.<sup>10</sup> According to the authors, the IL-ASEI is unstable, and its function as an artificial solid electrolyte interphase is disappointingly an illusion stemming from insufficient experimental validations and misinterpretations of data. A fortuitous combination of factors such as a short interface life, inconsistency of the IL film thickness, and the pitting of Al caused by it, evaluation of the electrochemical results without considering the possible interfacial reactions often leads to enticing but misleading results.

It is crucial to broaden the understanding and material selection for the Al surface activation in ILs, while also enabling the introduction of new IL-based electrolytes (either as a “stand-alone” electrolyte or IL hybrid mixtures) for Al-based batteries. One-dimensional micro-macro homogenous mathematical model and experimental analysis revealed that eliminating the oxide film on Al is critical for lowering the anodic potential loss and improving cell performance. A fundamental understanding of the mechanism of oxide film growth/breakdown in the IL solution will be beneficial in determining appropriate strategies to partially/completely remove the oxide film. In addition, fundamental characteristics such as ionic mobility, electronic insulation, and the stability of the IL-ASEI in IL and aqueous electrolytes need to be critically evaluated by incorporating both electrochemical and chemical characterization (*in situ* and *ex situ*) and high-throughput computational screening and machine learning.

The manufacturing of high-performance aluminum batteries is hampered by insufficient knowledge of the SEI evolution and operation mechanism. To address this issue, more systematic studies should be conducted to fully comprehend the underlying reasons for the surface evolution of the Al electrode and to design corresponding strategies for the Al anode in Al batteries. Chloroaluminate ILs are widely

employed in Al-battery research; nevertheless, as previously stated, controversial aspects of interfacial electrochemistry of the Al anode in electrolytes necessitate in-depth investigations of novel IL electrolytes with good interfacial stability, or alternatively, the use of an alloy anode or surface modification. Computational and theoretical studies can serve as useful tools for forecasting structure/properties correlation, ions speciation at different compositions, electrochemical properties, and gaining a better understanding of the underlying electrochemical mechanisms at the interface.

### 3. Mg anode

Given the prominence of the advancements of the suitable electrolyte and cathode, interfacial processes at the Mg anode have garnered considerably less focus. Nonetheless, these processes have an impact on the overall cell performance and are frequently mistaken for poor cathode performance.<sup>205</sup> For the progress of Mg metal battery technologies, direct visualization of the mechanism of interfacial formation is crucial. A direct correlation has been found between the interfacial structure evolution and the long-term cycling of the Mg metal anode in diglyme (DEG)/N-methyl-N-butylpiperidinium bis(trifluoromethylsulfonyl)imide ([PP<sub>14</sub>][TFSI]) IL electrolyte.<sup>65</sup> Figure 12 depicts the morphological changes corresponding to dynamic interfacial evolution at Mg anode during plating/stripping observed via *in situ* optical microscopy.<sup>65</sup> The plating process begins with the development of Mg particles, which are sphere-shaped, followed by the establishment of irregular grains and the growth of crystallized Mg. The interface can lead to the dissolution of crystallized Mg during stripping, leaving uneven-grained fractures in the Mg.<sup>65</sup> Hence, severe capacity fading stems from the limited morphological reversibility displayed by this system.

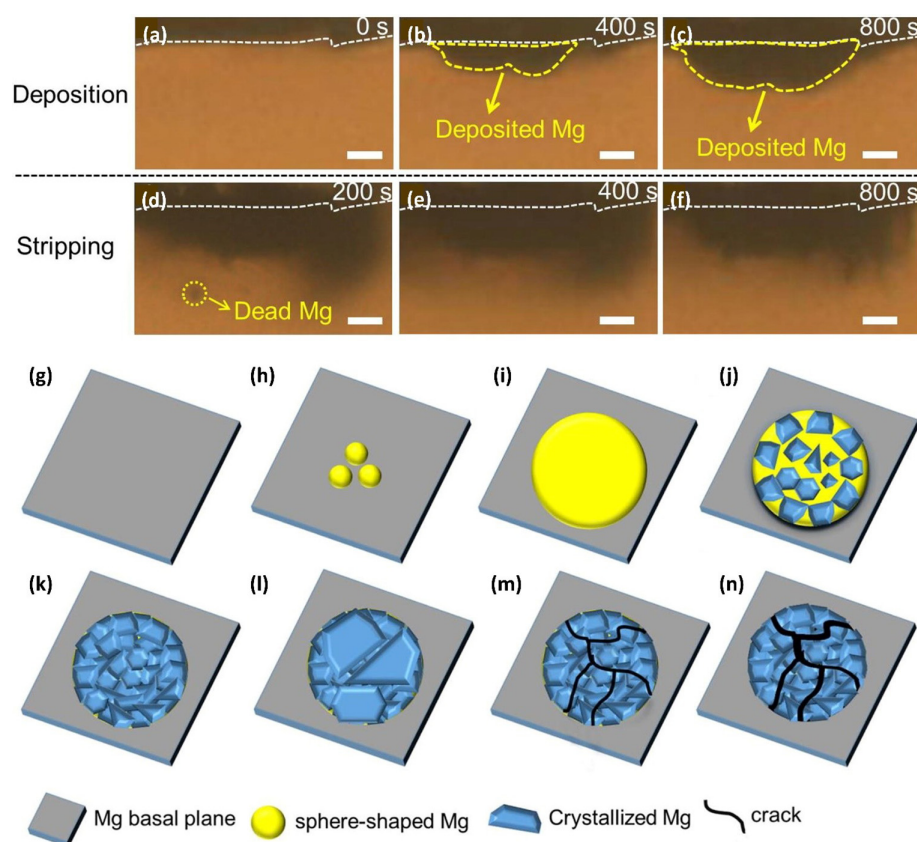


**FIG. 12.** Mg deposition/stripping mechanism in diglyme/IL system: *In situ* optical images of the plating and stripping processes on Mg electrode (a) at the OCP (open circuit potential) (b) and (c) after deposition for 400 and 800 s respectively (current = 10  $\mu$ A); after dissolution for (d) 200, (e) 400, and (f) 800 s (current = 10  $\mu$ A). The scale bars are 10  $\mu$ m; Schematic illustration of the corresponding Mg deposition/stripping processes on Mg anode: (g) at OCP, (h) sphere-shaped Mg formation, (i) sphere-shaped Mg growth, (j) and (k) irregular graininess evolution, (l) formation of crystallized Mg upon deposition, (m) stripping of crystallized Mg, (n) irregular graininess fracture. Reproduced with permission from Hu *et al.*, *J. Electroanal. Chem.* **896**, 115301 (2021). Copyright 2021, Elsevier.<sup>65</sup>

Few investigations have demonstrated the formation of a stable interfacial anodic film in ILs, which can stabilize the magnesium surface.<sup>112,139</sup> The surface film has a gel-like structure which is composed of a magnesium, phosphonium cation, and chloride-based hydrated complex. The presence of IL cationic elements in the interfacial film suggests the vital role of IL species in the development of the interfacial film. Unlike lithium, which generates an ion-conducting SEI when exposed to aprotic nonaqueous electrolytes,<sup>206</sup> Mg forms an ionically insulating surface layer (rich in organic compounds) when exposed to most organic solvent-based electrolytes,<sup>207</sup> necessitating a surface-layer-free or pretreated Mg.<sup>208</sup>

Research on ILs for magnesium electrochemistry is still in its infancy. Despite significant efforts to produce efficient Mg primary batteries, Mg rechargeable batteries remain a long way off.<sup>72</sup> To be used as an electrolyte, ILs must have a high salt solubility, high ionic conductivity, wide electrochemical window, interface compatibility, and sufficient reducing stability to Mg. In this regard, constituents of ILs, especially anions, play a major role in determining the physicochemical and electrochemical stability of the Mg battery electrolyte.<sup>70,138,209</sup> Earlier reports on magnesium IL electrolytes comprised a mixture of Mg salt magnesium triflate [Mg(OTF)<sub>2</sub>] with ILs such as [BMIM][BF<sub>4</sub>]<sup>209</sup> or [PP<sub>13</sub>][TFSI]<sup>210</sup> or a mixture of both.<sup>211</sup> On a platinum electrode, the IL containing BF<sub>4</sub><sup>-</sup> not only features low melting point and high ionic conductivity but also exhibits good stability within the range of -1 to +3 V with respect to Mg. Experimental results show that the Mg stripping/plating with Mg(OTF)<sub>2</sub> occurs at a low current within this

electrochemical window. Despite this system delivering CE ~100%, significant voltage fluctuations prevented Mg plating/stripping from being repeated for more than 165 cycles.<sup>209</sup> It is worth noting that despite the reduction of OTF<sup>-</sup> that formed a film on the electrode, magnesium was nevertheless plated from this electrolyte system.

The same group reported reversible magnesium deposition on a silver working electrode from a 1 M Mg(OTF)<sub>2</sub> in [PP<sub>13</sub>][TFSI] electrolyte.<sup>210</sup> The plating/stripping current potential response, on the other hand, was slow, and there was no evidence of complete dissolution (anodic current decrease to zero). Although the TFSI anion demonstrates significant oxidation stability than [BMIM][BF<sub>4</sub>], but due to insufficient reductive stability it is unable to sustain reversible Mg stripping/plating over a prolonged duration. Furthermore, the decomposition of TFSI anions in ILs forms a protective layer on Mg metal.<sup>70,138,212</sup> It is worth noting that using a mixed IL composed of [BMIM][BF<sub>4</sub>] and [PP<sub>13</sub>][TFSI] and the same Mg salt [Mg(OTF)<sub>2</sub>] provides a lower initial plating/stripping overpotential compared to individual IL system.<sup>211</sup> According to these early investigations, Mg can be reversibly deposited/stripped from Mg-based IL electrolytes; however, the results could not be easily duplicated and resulted in high overpotentials.<sup>35,72,208</sup> Hence, the composition of the IL electrolyte must be tuned for the magnesium/electrolyte interface for successful reversible deposition/dissolution of magnesium at room temperature.

*a. Strategies to construct stable and active Mg/IL based-electrolyte interface.* As discussed previously, regulating the interface by careful

selection of the IL constituents, co-solvents, water content, and Mg salts may result in favorable interfacial properties like low leakage currents, high stability, wide electrochemical window,<sup>208</sup> and reversible plating/stripping with good cell performance under load.<sup>112</sup> Low oxidative (anodic) stability of Mg electrolytes limits the selection of positive electrodes because high-voltage cathodes, such as vanadium phosphate,  $\text{Na}_3\text{V}_2(\text{PO}_4)_3/\text{C}$ , amorphous  $\text{V}_2\text{O}_5\text{-P}_2\text{O}_5$ , cannot be used, posing a challenge to compete with Li-based systems.<sup>208</sup> The choice of conductive salt, solvent, and additive can make a substantial difference on the oxidative stability of Mg electrolytes.

Certain ILs [such as trihexyl(tetradecyl)phosphonium diphenylphosphate ( $[\text{P}_{66614}][\text{DPP}]$ ) or trihexyl(tetradecyl)phosphonium bis 2,4,4-trimethylpentylphosphinate ( $[\text{P}_{66614}][\text{TMPP}]$ )] can form passive films when exposed to Mg metal and alloys, resulting in high cell resistivity, and in extreme cases, impractical devices.<sup>112,213,214</sup> Although imidazolium-based ILs are readily available from renewable resources and are frequently utilized as electrolytes, the instability of the imidazolium ring raises concerns.<sup>70</sup> Furthermore, the introduction of magnesium borohydride impairs the reductive stability of  $[\text{BMIM}][\text{TFSI}]$ .<sup>70</sup> Replacing conventional imidazolium-based ILs with a 1-butyl-3-methylimidazol-2-ylidene borane zwitterionic liquid proved to be a better host for  $\text{Mg}(\text{BH}_4)_2$  due to strong intermolecular interactions. The zwitterionic liquid not only allowed electrodeposition but also reversible deposition/dissolution of Mg on a stainless steel electrode, thus circumventing the stability issues of both imidazolium cations and TFSI anions.<sup>70</sup> However, the efficiency of this electrolyte system needs to be evaluated against the Mg anode along with a suitable cathode in a full-cell configuration.

Chelating ILs or IL/tetraglyme systems are viable strategies for changing  $\text{Mg}^{2+}$  speciation in TFSI-containing electrolytes.<sup>124,215–217</sup> The polyether group in these systems can substitute both  $\text{BH}_4$  and TFSI anions from the coordination sphere of  $\text{Mg}^{2+}$ , suppressing reductive decomposition of TFSI anion as well as the generation of cationic speciation for  $\text{Mg}^{2+}$ , which improves electromigration transport.<sup>124</sup> However, mixing chelating solvents (glymes) with an IL-based Mg source  $[\text{Mg}(\text{TFSI})_2]$  may negate the benefits of an IL-based electrolyte. When using  $\text{Mg}(\text{BH}_4)_2$  as conducting salt, these well-designed ILs enable Mg stripping/plating at adequately low overpotentials ( $<0.5$  V vs  $\text{Mg}|\text{Mg}^{2+}$ ). However, difficulty in the synthesis of these chelating ILs and cost could pose a further challenge.

Recently, a hybrid Al/Mg electrolyte based on ILs was described for reversible alloy (simultaneous Mg and Al) plating/stripping with a CE of 99.66%, an overpotential less than 50 mV, and anodic stability of 2.35 V vs  $\text{Mg}|\text{Mg}^{2+}$  ( $+3.02$  V vs  $\text{Li}|\text{Li}^+$ ).<sup>64</sup> When compared to Mg-based electrolytes, this twin metal hybrid system demonstrated better specific capacity and reduced overpotential for Mg/Al alloy deposition/dissolution. The twin metal electrolyte is composed of  $[\text{C}_4\text{mpyr}]$  Cl and  $\text{AlCl}_3$  in a molar ratio of 1:1.5 and is doped with  $\delta\text{-MgCl}_2$  salt. Complex anions containing Mg–Al species connected via  $\text{Cl}^-$  bridges are present in bulk electrolytes as monomers and dimers of chloroaluminate repeating units, as shown in Fig. 13(a). The coexistence of Mg in chloroaluminate anion domains enhances  $\text{Mg}^{2+}$  solubility in the electrolyte, while a higher concentration of chloroaluminate ( $\text{Al}_2\text{Cl}_7^-$ ) dimers in complex anion improves Al codeposition. Figure 13(b) shows alloy deposit at a significantly low overvoltage (ca.  $-50$  mV vs  $\text{Mg}|\text{Mg}^{2+}$ ) that is independent of the scan rate.<sup>64</sup> Figure 13(c) shows

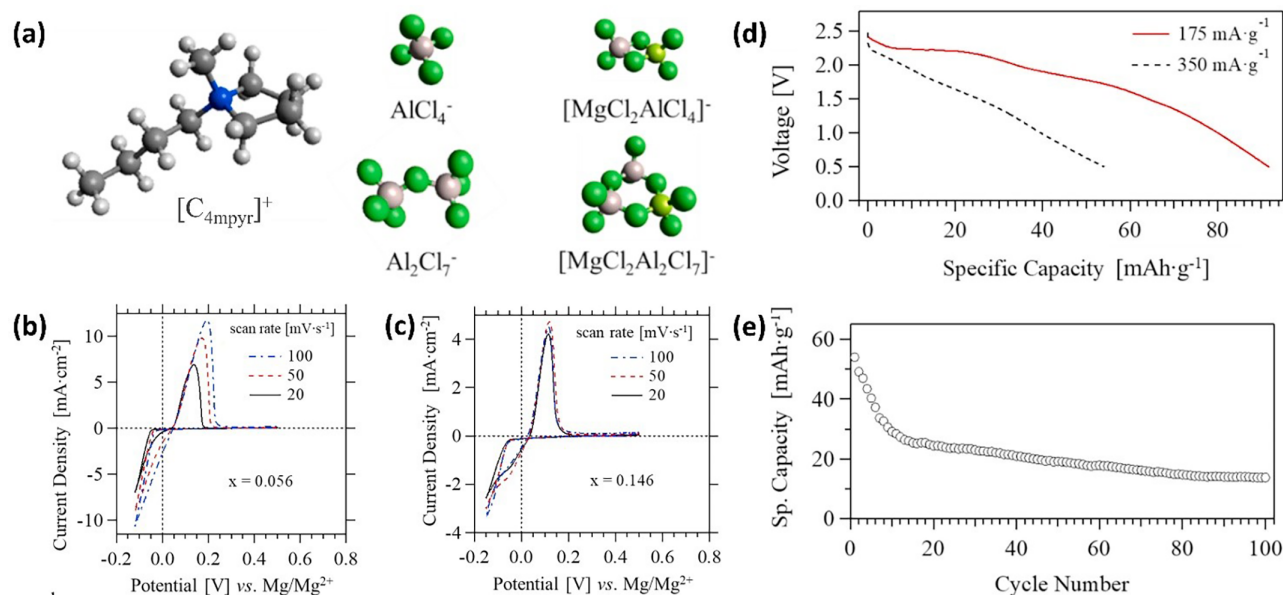


**FIG. 13.** (a) Proposed ionic species' molecular structures present in  $[\text{C}_4\text{mpyr}]\text{Cl}/(\text{AlCl}_3)_{1.5}/(\delta\text{-MgCl}_2)_x$  electrolytes. (Color legend: C black; H light gray; Cl dark green; Al gray; N blue; and Mg light green); Effect of changing scan rate ( $20\text{ mV}\cdot\text{s}^{-1}$  (black line),  $50\text{ mV}\cdot\text{s}^{-1}$  (red dashed line), and  $100\text{ mV}\cdot\text{s}^{-1}$  (blue dash-dot line)) on deposition of Al/Mg alloy using (b)  $[\text{C}_4\text{mpyr}]\text{Cl}/(\text{AlCl}_3)_{1.5}/(\delta\text{-MgCl}_2)_{0.056}$  and (c)  $[\text{C}_4\text{mpyr}]\text{Cl}/(\text{AlCl}_3)_{1.5}/(\delta\text{-MgCl}_2)_{0.146}$  electrolytes; (d) First-cycle of a  $\text{Mg}|\text{C}_4\text{mpyr}]\text{Cl}/(\text{AlCl}_3)_{1.5}/(\delta\text{-MgCl}_2)_{0.056}|\text{V}_2\text{O}_5$  battery between 0.5 and 2.5 V at different specific current values.  $175\text{ mA}\cdot\text{g}^{-1}$ , ca. 0.9C, red line; and  $350\text{ mA}\cdot\text{g}^{-1}$ , ca. 1.8C, black line.  $[\text{C}_4\text{mpyr}]\text{Cl}/(\text{AlCl}_3)_{1.5}/(\delta\text{-MgCl}_2)_{0.056}$  is used; (e) Full-cell specific capacity based on the cathode active mass over the first 100 cycles at  $350\text{ mA}\cdot\text{g}^{-1}$ , ca. 1.8C. Reproduced with permission from Pagot *et al.*, J. Power Sources **493**, 229681 (2021). Copyright 2021, Elsevier.<sup>64</sup>



that even when the concentration of Mg salt is increased, this system allows efficient alloy deposition/dissolution. A prototype device using  $[C_4\text{mpyr}][Cl]/(AlCl_3)_{1.5}/(\delta\text{-MgCl}_2)_{0.056}$  as electrolyte, a  $V_2O_5$ -based cathode and magnesium anode is capable of achieving impressive current rates with a gradual drop in specific capacity on cycling [Figs. 13(d) and 13(e)]. The initial discharge-specific capacity of this prototype device, when operated at  $175\text{ mA}\cdot\text{g}^{-1}$  is  $92\text{ mAh}\cdot\text{g}^{-1}$ , which is significantly greater than that of the imidazolium-based ILs and other types of electrolytes.<sup>218,219</sup> Cathode stability in chloroaluminate ILs should be considered when choosing the cathode material with this Al/Mg IL-based electrolyte; for example, Mg| $V_2O_5$  cell performed better with this electrolyte than Mg| $Mo_6S_8$ .

Adding a complexing additive is a simpler and more viable strategy than preparing chelating ILs<sup>124</sup> or combining a chelating solvent with ILs<sup>215–217</sup> to enhance the extent and reversibility of magnesium deposition/dissolution. Crown ethers are common complexing agents that have previously been used to improve Mg plating/stripping in an IL.<sup>138</sup> Use of  $Mg(BH_4)_2$ —or borohydrides in general,—is particularly desirable due to their high reductive stability and capacity to inhibit the development of a passive layer on Mg anodes due to the reductive nature.<sup>138</sup> It has been postulated that the  $BH_4^-$  anion acts as a  $Mg^{2+}$ -complexing agent capable of interacting with the anode surface via adsorption in a manner similar to chloride-containing electrolytes.<sup>122,123,138</sup> During electrolyte formulation, magnesium borohydride acts as a water scavenger, reacting with residual traces of water in the IL, resulting in a truly water-free electrolyte.<sup>70,138,215</sup>  $Mg^{2+}$  deposition, for example, is hindered in pure  $Mg(TFSI)_2$ -containing  $[C_4\text{mpyr}][TFSI]$  electrolytes due to strong interactions between  $Mg^{2+}$  and the surrounding TFSI anions. The addition of cyclic ether (18-crown-6) and  $Mg(BH_4)_2$  synergistically improved the deposition characteristics of  $Mg(TFSI)_2$ -containing  $[C_4\text{mpyr}][TFSI]$  electrolyte.<sup>138</sup> Coordination of the 18-crown-6 molecule with  $Mg(TFSI)_2$  or  $Mg(TFSI)_2 + [C_4\text{mpyr}][TFSI]$  significantly weakens the interaction between  $Mg^{2+}$  and the neighboring TFSI<sup>-</sup> anions, resulting in a considerable reduction in  $Mg^{2+}$ -induced TFSI decomposition during  $Mg^{2+}$  reduction. Hence, both additives, as well as their relative concentration compared to  $Mg^{2+}$ , are crucial for reversible Mg deposition/dissolution.

ILs, as an additive in organic solvent-based electrolytes, improve their ionic conductivity, thermal stability, electrochemical operating window, and electrochemical performance for Mg batteries.<sup>215,220–222</sup> Theoretically, the addition of ILs to ether-based electrolyte systems combines the advantages of both. However, experimentally, it is shown that although cycling is feasible with these hybrid electrolytes, the overpotentials for Mg plating/stripping at ambient temperature are frequently above 1 V vs  $Mg|Mg^{2+}$ .<sup>223,224</sup> The overpotential can be reduced further by reducing the amount of “free” ether solvents in such hybrid electrolytes.<sup>208</sup> Varying the solvent (ethers and ILs) and salt ratios of  $MgCl_2$ -based electrolytes can affect the *in situ* generated  $Mg_2Cl_z^{z+}$ -ether-complex concentration, which in turn affects the oxidation potential. The impact of the IL on the solution structure and the overpotential for Mg stripping/plating is dependent on the properties of the ether solvent. So, the oxidative stability of IL hybrid electrolytes can be enhanced to above 4.5 V vs  $Mg|Mg^{2+}$  by careful adjustment of the electrolyte composition.<sup>208</sup> However, these findings need to be verified in a full-cell system using suitable cathode materials.

An ideal electrolyte for high-voltage Mg-based batteries has low overpotentials for Mg plating/stripping and strong oxidative stabilities ( $>4\text{ V}$  vs  $Mg|Mg^{2+}$ ) at the cathode. Although investigations into IL-based electrolytes are in their early stages, this work indicates that they have the ability to meet both requirements as promising electrolytes for Mg anodes.

#### IV. SUMMARY AND FUTURE PROSPECTS

A fundamental understanding of the metal anode/IL interface evolution is crucial for designing practical post-Li metal anode batteries. Insights into electrode/electrolyte coupling will not only improve understanding of the superior performance of these systems but also provide directions to extend the electrochemical and chemical stability. This review discusses theoretical and experimental studies to understand the interfacial perspective of ILs as electrolytes for metal anodes, focusing on the current development and design strategies to combat the challenges of metal anodes. Fundamental issues with monovalent metal anodes include unstable SEI formation, dendritic growth, and abrupt volume changes during plating/stripping. Whereas in multivalent metal anodes, the incapacity of the electrolyte to form a beneficial SEI layer at the electrode interface to provide a passage for metal ions and facilitate reversible deposition/stripping of these metals with low overpotential and high efficiency is a key challenge. ILs are intrinsically conductive electrolytes with high electrochemical, chemical, and thermal stability and are highly tunable electrolytes for both monovalent and multivalent metal batteries.

Various strategies—including superconcentrated ILs, the use of additives including water, the use of mixed anions system, and high voltage pretreatment—have been proposed to improve metal-ion solvation and optimize the interfacial chemistry of monovalent anodes in ILs. However, more efforts are required to investigate the SEI evolution in ILs, its composition, and its relationship with the deposit morphology to realize commercialization. The key to enhancing the performance of multivalent metal anode batteries—especially rechargeable metal batteries—is an appropriate interfacial design between multivalent metal anodes and the electrochemically stable IL electrolyte. Various structural regulations of the anode along with electrolyte modification strategies—including alloying, dimensional engineering of metal anodes, anode surface pretreatment, use of complexing additives, IL-organic hybrid electrolytes—are also proposed to improve the anode performance by regulating interface. Furthermore, Al metal batteries have demonstrated significant cycle stability and cost savings when replacing corrosive and air-sensitive chloroaluminate ILs with ILs made from organic salts or  $Al_2Cl_7^-$  free IL electrolytes.

A new area of research in the realm of rechargeable multivalent metal batteries is the use of dual-salt-containing IL electrolytes. The twin-metal hybrid electrolyte system alleviates the metal salt solubility issues, and synergy between different multivalent metal ions improves the energy density of the battery. The challenges and strategies adopted for monovalent and multivalent anodes are illustrated in Fig. 14. Further research on the structure-effect relationship between these electrolytes, stability against cathodes, and battery performance may result in rechargeable metal batteries with better reliability, less corrosive damage, and fewer safety issues.

The following are suggestions for future work:

- The dynamic properties of ILs, as well as the electrode/electrolyte interfacial properties of ILs, require further insight. A

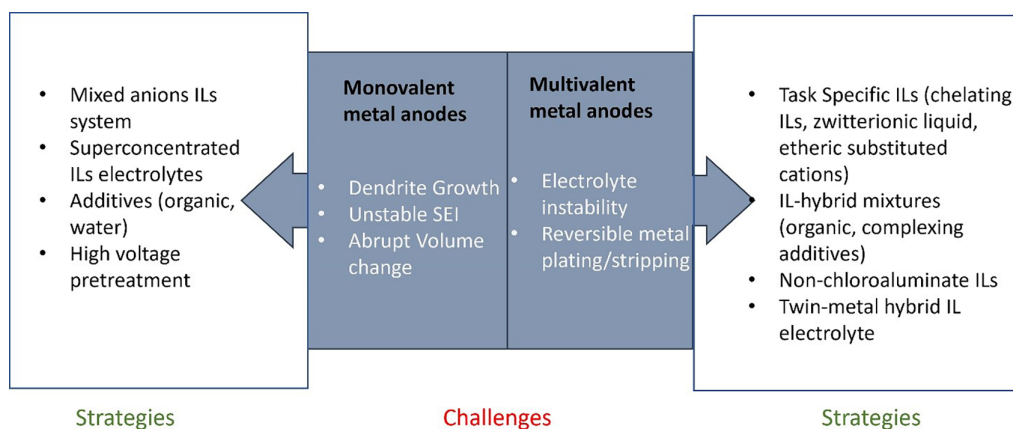


FIG. 14. Summary of the challenges of monovalent and multivalent metal anodes along with some respective strategies adopted for IL-based electrolytes.

comprehensive understanding of the difference in cation/anion size, structure, coordination of ion-counter ions, and metal ion solvation in the IL is helpful in tailoring them with beneficial properties required for superior battery performance.

- A better understanding of the role of additives in metal ion speciation and supporting stable and reversible metal plating/stripping is required for future breakthroughs. Future research on appropriate additives for specific metal anodes will combat the instability of IL-based electrolytes against metal anodes, especially multivalent metal anodes, realizing high-performance IL-based hybrid electrolytes for metal batteries.
- A systematic investigation of the initial stages of metal electrodeposition in IL-based electrolytes is indispensable to understanding dendritic growth under various circumstances. Operando techniques should be utilized to understand interaction at the metal anode/ILs interface, formation of SEI, and its stability along with the emergence of dendrites. These observations can be further elaborated using computational and theoretical studies, which are also useful tools for predicting both bulk and interfacial properties of IL electrolytes. Incorporating theoretical investigations to comprehend the coordination environment, changing ion dynamics, and local structure at charged electrodes is important in designing task-specific ILs.

Ongoing research on IL-based electrolytes for metal batteries has yet to establish concrete facts; however, it does indicate prospects of ILs meeting the requirements of perfect electrolytes. Despite some proof-of-concept results, considerable work remains to persuade the scientific community about the likelihood of IL-based electrolytes outperforming conventional electrolytes in terms of safety and performance.

#### ACKNOWLEDGMENTS

R.J. thanks Curtin University for a Ph.D. scholarship. DSS thanks the Australian Research Council (ARC) for a Future Fellowship (FT170100315). M.K. acknowledges the Australian Research Council funded StorEnergy Industrial Transformation

Training Centre (IC180100049) for financial support. N.M. acknowledges the Vice-Chancellor Fellowship Scheme at RMIT University and S.L. acknowledges RMIT University for the award of their RMIT Research Stipend Scholarships.

#### AUTHOR DECLARATIONS

##### Conflict of Interest

The authors have no conflicts to disclose.

##### Author Contributions

**Rabia Jamil:** Conceptualization (lead); Writing – original draft (lead); Writing – review & editing (lead). **Suraj Loomba:** Data curation (equal); Software (equal); Writing – original draft (supporting); Writing – review & editing (supporting). **Mega Kar:** Data curation (equal); Formal analysis (equal); Writing – original draft (supporting); Writing – review & editing (equal). **Gavin E. Collis:** Formal analysis (supporting); Validation (supporting); Writing – review & editing (supporting). **Debbie S. Silvester:** Conceptualization (supporting); Formal analysis (supporting); Funding acquisition (lead); Supervision (lead); Validation (equal); Writing – original draft (supporting); Writing – review & editing (supporting). **Nasir Mahmood:** Conceptualization (equal); Formal analysis (equal); Supervision (equal); Validation (equal); Writing – original draft (supporting); Writing – review & editing (equal).

##### DATA AVAILABILITY

Data sharing is not applicable to this article as no new data were created or analyzed in this study.

##### NOMENCLATURE

[EMIM][(HF) <sub>2,3</sub> F]	1-ethyl-3-methylimidazolium oligofluorohydrogenate
[N <sub>07</sub> ][TFSI]	N,N,N-tri-(2-(2-methoxyethoxy)ethyl)-N-(2-methoxyethyl)ammonium bis(trifluoromethylsulfonyl) imide

$[N_{2(2O2O1)3}]^+$	N-ethyl-N,N,N-tris(2-(2-methoxyethoxy)ethyl)ammonium	TTE	1,1,2,2-tetrafluoroethyl propyl ether	2,2,3,3-tetrafluoro-propyl ether
AFM	Atomic Force Microscopy	Zn(OAc) <sub>2</sub>	Zinc acetate	
AIBs	Aluminum-ion batteries	ZnF <sub>2</sub>	Zinc flouride	
Al <sub>2</sub> O <sub>3</sub>	Alumina or Aluminum oxide	ZnO	Zinc oxide	
AlCl <sub>3</sub>	Aluminum chloride			
AlCl <sub>4</sub> <sup>-</sup>	Tetrachloroaluminate anion			
BH <sub>4</sub> <sup>-</sup>	Borohydride anion			
Ca(BH <sub>4</sub> ) <sub>2</sub>	Calcium borohydride			
CaH <sub>2</sub>	Calcium hydride			
DEC	Diethyl carbonate			
DEG	Diglyme			
DES	Deep eutectic solvent			
DFT	Density functional theory			
DMSO	Dimethyl sulfoxide			
EC	Ethylene carbonate			
EDL	Electrical double layer			
EG	Ethylene glycol			
Et <sub>3</sub> NHCl	Triethylamine hydrochloride			
EtAlCl <sub>2</sub>	Ethylaluminium dichloride			
[FAP] <sup>-</sup>	Tris(perfluoroalkyl)trifluorophosphate anion			
FEC	Fluorinated ethylene carbonate			
[FTFSI] <sup>-</sup>	(Fluorosulfonyl)(trifluoromethanesulfonyl) imide amide anion			
HAADF STEM	High-angle annular dark-field scanning transmission electron microscopy			
ILs	Ionic Liquids			
LIBs	Lithium-ion batteries			
LiCoO <sub>2</sub>	Lithium cobalt oxide			
MAS-NMR	Magic angle spinning nuclear magnetic resonance			
MD simulation	Molecular dynamics simulation			
Na[DCA]	Sodium dicyanamide			
Na <sub>2</sub> O	Sodium oxide			
Na <sub>2</sub> SO <sub>4</sub>	Sodium sulfate			
NaBF <sub>4</sub>	Sodium tetrafluoroborate			
NaClO <sub>4</sub>	Sodium perchlorate			
NaF	Sodium flouride			
NaFePO <sub>4</sub>	Sodium iron phosphate			
NaPF <sub>6</sub>	Sodium hexafluorophosphate			
NVP	Sodium vanadium phosphate			
NVPF	Sodium vanadium phosphate fluoride			
OCP	Open circuit potential			
PC	Propylene carbonate			
RABs	Rechargeable aluminum batteries			
rGO	Reduced graphene oxide			
RTILs	Room temperature ionic liquids			
SEI	Solid electrolyte interphase			
SEM	Scanning electron microscopy			
SHE	Standard hydrogen electrode			
SIBs	Sodium-ion batteries			
SMBs	Sodium metal batteries			
TBAH <sub>2</sub> F <sub>3</sub>	Tetrabutylammonium dihydrogen trifluoride			
TEM	Transmission electron microscopy			
TGA	Thermogravimetric analysis			
THF	Tetrahydrofuran			
TMAHCl	Trimethylamine hydrochloride			

## REFERENCES

- <sup>1</sup>K. Matsumoto, J. Hwang, S. Kaushik, C.-Y. Chen, and R. Hagiwara, *Energy Environ. Sci.* **12**(11), 3247–3287 (2019).
- <sup>2</sup>M. Li, J. Lu, X. Ji, Y. Li, Y. Shao, Z. Chen, C. Zhong, and K. Amine, *Nat. Rev. Mater.* **5**(4), 276–294 (2020).
- <sup>3</sup>T. Schoetz, C. P. de Leon, M. Ueda, and A. Bund, *J. Electrochem. Soc.* **164**(14), A3499–A3502 (2017).
- <sup>4</sup>R. Attias, M. Salama, B. Hirsch, Y. Goffer, and D. Aurbach, *Joule* **3**(1), 27–52 (2019).
- <sup>5</sup>X. Zhang, J. Meng, X. Wang, Z. Xiao, P. Wu, and L. Mai, *Energy Storage Mater.* **38**, 30–49 (2021).
- <sup>6</sup>R. J. Gummow, G. Vamvounis, M. B. Kannan, and Y. He, *Adv. Mater.* **30**(39), 1801702 (2018).
- <sup>7</sup>Z. Yi, G. Chen, F. Hou, L. Wang, and J. Liang, *Adv. Energy Mater.* **11**(1), 2003065 (2021).
- <sup>8</sup>M. Yousaf, U. Naseer, Y. Li, Z. Ali, N. Mahmood, L. Wang, P. Gao, and S. Guo, *Energy Environ. Sci.* **14**(5), 2670–2707 (2021).
- <sup>9</sup>Z. Liang and C. Ban, *Angew. Chem., Int. Ed.* **60**(20), 11036–11047 (2021).
- <sup>10</sup>T. Dong, K. L. Ng, Y. Wang, O. Voznyy, and G. Azimi, *Adv. Energy Mater.* **11**(20), 2100077 (2021).
- <sup>11</sup>J. Tu, W.-L. Song, H. Lei, Z. Yu, L.-L. Chen, M. Wang, and S. Jiao, *Chem. Rev.* **121**(8), 4903–4961 (2021).
- <sup>12</sup>L. Ma, M. A. Schroeder, O. Borodin, T. P. Pollard, M. S. Ding, C. Wang, and K. Xu, *Nat. Energy* **5**(10), 743–749 (2020).
- <sup>13</sup>S. Wei, S. Choudhury, Z. Tu, K. Zhang, and L. A. Archer, *Acc. Chem. Res.* **51**(1), 80–88 (2018).
- <sup>14</sup>A. Mahmood, Z. Yuan, X. Sui, M. A. Riaz, Z. Yu, C. Liu, J. Chen, C. Wang, S. Zhao, N. Mahmood, Z. Pei, L. Wei, and Y. Chen, *Energy Storage Mater.* **41**, 395–403 (2021).
- <sup>15</sup>A. K. Tareen, K. Khan, M. Iqbal, Y. Zhang, J. Long, A. Mahmood, N. Mahmood, Z. Xie, C. Li, and H. Zhang, *Energy Storage Mater.* **53**, 783–826 (2022).
- <sup>16</sup>X.-B. Cheng, R. Zhang, C.-Z. Zhao, and Q. Zhang, *Chem. Rev.* **117**(15), 10403–10473 (2017).
- <sup>17</sup>C. Bao, B. Wang, P. Liu, H. Wu, Y. Zhou, D. Wang, H. Liu, and S. Dou, *Adv. Funct. Mater.* **30**(52), 2004891 (2020).
- <sup>18</sup>H. Wang, J. Ryu, Y. Shao, V. Murugesan, K. Persson, K. Zavadil, K. T. Mueller, and J. Liu, *ChemElectroChem* **8**(16), 3013–3029 (2021).
- <sup>19</sup>M. Jiang, C. Fu, P. Meng, J. Ren, J. Wang, J. Bu, A. Dong, J. Zhang, W. Xiao, and B. Sun, *Adv. Mater.* **34**(2), 2102026 (2022).
- <sup>20</sup>Y. Zhao, K. R. Adair, and X. Sun, *Energy Environ. Sci.* **11**(10), 2673–2695 (2018).
- <sup>21</sup>Y. Li, M. Liu, X. Feng, Y. Li, F. Wu, Y. Bai, and C. Wu, *ACS Energy Lett.* **6**(9), 3307–3320 (2021).
- <sup>22</sup>M. Wang, F. Zhang, C.-S. Lee, and Y. Tang, *Adv. Energy Mater.* **7**(23), 1700536 (2017).
- <sup>23</sup>S. Gbadamasi, M. Mohiuddin, V. Krishnamurthi, R. Verma, M. W. Khan, S. Pathak, K. Kalantar-Zadeh, and N. Mahmood, *Chem. Soc. Rev.* **50**(7), 4684–4729 (2021).
- <sup>24</sup>N. Mahmood, T. Tang, and Y. Hou, *Adv. Energy Mater.* **6**(17), 1600374 (2016).
- <sup>25</sup>J. Xu, C. Ding, P. Chen, L. Tan, C. Chen, and J. Fu, *Appl. Phys. Rev.* **7**(3), 031304 (2020).
- <sup>26</sup>G. G. Eshetu, G. A. Elia, M. Armand, M. Forsyth, S. Komaba, T. Rojo, and S. Passerini, *Adv. Energy Mater.* **10**(20), 2000093 (2020).
- <sup>27</sup>S. Liu, R. Zhang, J. Mao, J. Yuwono, C. Wang, K. Davey, and Z. Guo, *Appl. Phys. Rev.* **10**(2), 021304 (2023).

- <sup>28</sup>R. Hagiwara, K. Matsumoto, J. Hwang, and T. Nohira, *Chem. Rec.* **19**(4), 758–770 (2019).
- <sup>29</sup>A. Basile, M. Hilder, F. Makhlooghiazad, C. Pozo-Gonzalo, D. R. MacFarlane, P. C. Howlett, and M. Forsyth, *Adv. Energy Mater.* **8**(17), 1703491 (2018).
- <sup>30</sup>D. R. MacFarlane, M. Forsyth, P. C. Howlett, M. Kar, S. Passerini, J. M. Pringle, H. Ohno, M. Watanabe, F. Yan, W. Zheng, S. Zhang, and J. Zhang, *Nat. Rev. Mater.* **1**(2), 15005 (2016).
- <sup>31</sup>M. Belotti, X. Lyu, L. Xu, P. Halat, N. Darwish, D. S. Silvester, C. Goh, E. I. Izgorodina, M. L. Coote, and S. Ciampi, *J. Am. Chem. Soc.* **143**(42), 17431–17440 (2021).
- <sup>32</sup>Q. Yang, Z. Zhang, X.-G. Sun, Y.-S. Hu, H. Xing, and S. Dai, *Chem. Soc. Rev.* **47**(6), 2020–2064 (2018).
- <sup>33</sup>A. Eftekhari, Y. Liu, and P. Chen, *J. Power Sources* **334**, 221–239 (2016).
- <sup>34</sup>E. Jónsson, *Energy Storage Mater.* **25**, 827–835 (2020).
- <sup>35</sup>J. Muldoon, C. B. Bucur, and T. Gregory, *Chem. Rev.* **114**(23), 11683–11720 (2014).
- <sup>36</sup>B. Craig, T. Schoetz, A. Cruden, and C. Ponce de Leon, *Renewable Sustainable Energy Rev.* **133**, 110100 (2020).
- <sup>37</sup>A. Manthiram, *Nat. Commun.* **11**(1), 1550 (2020).
- <sup>38</sup>Y. Liu, G. He, H. Jiang, I. P. Parkin, P. R. Shearing, and D. J. L. Brett, *Adv. Funct. Mater.* **31**(13), 2010445 (2021).
- <sup>39</sup>Y. Jin, H. Yu, and X. Liang, *Appl. Phys. Rev.* **8**(3), 031301 (2021).
- <sup>40</sup>A. Grant and C. O'Dwyer, *Appl. Phys. Rev.* **10**(1), 011312 (2023).
- <sup>41</sup>Y. Zeng, J. Liang, J. Zheng, Z. Huang, X. Zhang, G. Zhu, Z. Wang, H. Liang, and Y.-Z. Zhang, *Appl. Phys. Rev.* **9**(2), 021304 (2022).
- <sup>42</sup>T. Rütther, A. I. Bhatt, A. S. Best, K. R. Harris, and A. F. Hollenkamp, *Batteries Supercaps* **3**(9), 793–827 (2020).
- <sup>43</sup>G. A. Giffin, *J. Mater. Chem. A* **4**(35), 13378–13389 (2016).
- <sup>44</sup>Y. Zheng, D. Wang, S. Kaushik, S. Zhang, T. Wada, J. Hwang, K. Matsumoto, and R. Hagiwara, *EnergyChem* **4**(3), 100075 (2022).
- <sup>45</sup>W. Zhou, M. Zhang, X. Kong, W. Huang, and Q. Zhang, *Adv. Sci.* **8**(13), 2004490 (2021).
- <sup>46</sup>D. Fouchard and J. B. Taylor, *J. Power Sources* **21**(3), 195–205 (1987).
- <sup>47</sup>S. Jiao, J. Zheng, Q. Li, X. Li, M. H. Engelhard, R. Cao, J.-G. Zhang, and W. Xu, *Joule* **2**(1), 110–124 (2018).
- <sup>48</sup>J. Zheng, D. C. Bock, T. Tang, Q. Zhao, J. Yin, K. R. Tallman, G. Wheeler, X. Liu, Y. Deng, S. Jin, A. C. Marschilok, E. S. Takeuchi, K. J. Takeuchi, and L. A. Archer, *Nat. Energy* **6**(4), 398–406 (2021).
- <sup>49</sup>A. Aryanfar, D. J. Brooks, A. J. Colussi, B. V. Merinov, W. A. Goddard Iii, and M. R. Hoffmann, *Phys. Chem. Chem. Phys.* **17**(12), 8000–8005 (2015).
- <sup>50</sup>Y. Long, H. Li, M. Ye, Z. Chen, Z. Wang, Y. Tao, Z. Weng, S.-Z. Qiao, and Q.-H. Yang, *Energy Storage Mater.* **34**, 194–202 (2021).
- <sup>51</sup>C. Ling, D. Banerjee, and M. Matsui, *Electrochim. Acta* **76**, 270–274 (2012).
- <sup>52</sup>H. Chen, H. Xu, B. Zheng, S. Wang, T. Huang, F. Guo, W. Gao, and C. Gao, *ACS Appl. Mater. Interfaces* **9**(27), 22628–22634 (2017).
- <sup>53</sup>D.-M. She, W.-L. Song, J. He, N. Li, H. Chen, S. Jiao, and D. Fang, *J. Electrochem. Soc.* **167**(13), 130530 (2020).
- <sup>54</sup>M. S. Ding, T. Diemant, R. J. Behm, S. Passerini, and G. A. Giffin, *J. Electrochem. Soc.* **165**(10), A1983 (2018).
- <sup>55</sup>S. Hebié, H. P. K. Ngo, J.-C. Leprêtre, C. Iojoiu, L. Cointeaux, R. Berthelot, and F. Alloin, *ACS Appl. Mater. Interfaces* **9**(34), 28377–28385 (2017).
- <sup>56</sup>S. Hebié, F. Alloin, C. Iojoiu, R. Berthelot, and J.-C. Leprêtre, *ACS Appl. Mater. Interfaces* **10**(6), 5527–5533 (2018).
- <sup>57</sup>T. Jiang, M. J. Chollier Brym, G. Dubé, A. Lasia, and G. M. Brisard, *Surf. Coat. Technol.* **201**(1), 1–9 (2006).
- <sup>58</sup>H. A. Hjuler, S. von Winbush, R. W. Berg, and N. J. Bjerrum, *J. Electrochem. Soc.* **136**(4), 901 (1989).
- <sup>59</sup>D. Lloyd, T. Vainikka, and K. Kontturi, *Electrochim. Acta* **100**, 18–23 (2013).
- <sup>60</sup>F. Wu, Y.-X. Yuan, X.-B. Cheng, Y. Bai, Y. Li, C. Wu, and Q. Zhang, *Energy Storage Mater.* **15**, 148–170 (2018).
- <sup>61</sup>Y. Deng, J. Zheng, A. Warren, J. Yin, S. Choudhury, P. Biswal, D. Zhang, and L. A. Archer, *Adv. Energy Mater.* **9**(39), 1901651 (2019).
- <sup>62</sup>S. A. Ferdousi, L. A. O'Dell, M. Hilder, A. J. Barlow, M. Armand, M. Forsyth, and P. C. Howlett, *ACS Appl. Mater. Interfaces* **13**(4), 5706–5720 (2021).
- <sup>63</sup>S. A. Ferdousi, M. Hilder, A. Basile, H. Zhu, L. A. O'Dell, D. Saurel, T. Rojo, M. Armand, M. Forsyth, and P. C. Howlett, *ChemSusChem* **12**(8), 1700–1711 (2019).
- <sup>64</sup>G. Pagot, K. Vezzù, S. G. Greenbaum, and V. Di Noto, *J. Power Sources* **493**, 229681 (2021).
- <sup>65</sup>X.-C. Hu, S.-Y. Lang, Y. Shi, R. Wen, and L.-J. Wan, *J. Electroanal. Chem.* **896**, 115301 (2021).
- <sup>66</sup>F. A. Soto, P. Yan, M. H. Engelhard, A. Marzouk, C. Wang, G. Xu, Z. Chen, K. Amine, J. Liu, V. L. Sprenkle, F. El-Mellouhi, P. B. Balbuena, and X. Li, *Adv. Mater.* **29**(18), 1606860 (2017).
- <sup>67</sup>H. Yildirim, A. Kinaci, M. K. Y. Chan, and J. P. Greeley, *ACS Appl. Mater. Interfaces* **7**(34), 18985–18996 (2015).
- <sup>68</sup>F. A. Soto, A. Marzouk, F. El-Mellouhi, and P. B. Balbuena, *Chem. Mater.* **30**(10), 3315–3322 (2018).
- <sup>69</sup>M. Moshkovich, Y. Gofar, and D. Aurbach, *J. Electrochem. Soc.* **148**(4), E155 (2001).
- <sup>70</sup>S. Tröger-Müller and C. Liedel, *Batteries Supercaps* **2**(3), 223–228 (2019).
- <sup>71</sup>G. Bieker, V. Küpers, M. Kolek, and M. Winter, *Commun. Mater.* **2**(1), 37 (2021).
- <sup>72</sup>N. Zhu, K. Zhang, F. Wu, Y. Bai, and C. Wu, *Energy Mater. Adv.* **2021**, 9204217.
- <sup>73</sup>O. M. Leung, T. Schoetz, T. Prodromakis, and C. Ponce de Leon, *J. Electrochem. Soc.* **168**(5), 056509 (2021).
- <sup>74</sup>Q. Zhao, M. J. Zachman, W. I. Al Sadat, J. Zheng, L. F. Kourkoutis, and L. Archer, *Sci. Adv.* **4**(11), eaau8131 (2018).
- <sup>75</sup>E. Zhang, W. Cao, B. Wang, X. Yu, L. Wang, Z. Xu, and B. Lu, *Energy Storage Mater.* **11**, 91–99 (2018).
- <sup>76</sup>C.-Y. Chen, T. Tsuda, and S. Kuwabata, *Chem. Commun.* **56**(97), 15297–15300 (2020).
- <sup>77</sup>E. L. Smith, A. P. Abbott, and K. S. Ryder, *Chem. Rev.* **114**(21), 11060–11082 (2014).
- <sup>78</sup>M. Angell, C.-J. Pan, Y. Rong, C. Yuan, M.-C. Lin, B.-J. Hwang, and H. Dai, *Proc. Natl. Acad. Sci.* **114**(5), 834–839 (2017).
- <sup>79</sup>N. Bogolowski and J.-F. Drillet, *Electrochim. Acta* **274**, 353–358 (2018).
- <sup>80</sup>M. Angell, G. Zhu, M.-C. Lin, Y. Rong, and H. Dai, *Adv. Funct. Mater.* **30**(4), 1901928 (2020).
- <sup>81</sup>E. Emanuele, A. Li Bassi, A. Macrelli, C. Mele, J. Strada, and B. Bozzini, *Molecules* **28**, 957 (2023).
- <sup>82</sup>H. Qiu, X. Du, J. Zhao, Y. Wang, J. Ju, Z. Chen, Z. Hu, D. Yan, X. Zhou, and G. Cui, *Nat. Commun.* **10**(1), 5374 (2019).
- <sup>83</sup>Y. Guo, F. Zhang, J. Yang, F. Wang, Y. NuLi, and S. Hirano, *Energy Environ. Sci.* **5**(10), 9100–9106 (2012).
- <sup>84</sup>A. Baskin and D. Prendergast, *J. Phys. Chem. C* **120**(7), 3583–3594 (2016).
- <sup>85</sup>X. Wang, M. Salari, D. Jiang, J. C. Varela, B. Anasori, D. J. Wesolowski, S. Dai, M. W. Grinstaff, and Y. Gogotsi, *Nat. Rev. Mater.* **5**, 787–808 (2020).
- <sup>86</sup>S. S. Manna, P. Bhauriyal, and B. Pathak, *Mater. Adv.* **1**(5), 1354–1363 (2020).
- <sup>87</sup>Q. Wang, Q. Zhang, X. Lu, and S. Zhang, *Ionics* **23**(9), 2449–2455 (2017).
- <sup>88</sup>K. Xu, S. Zhang, T. R. Jow, W. Xu, and C. A. Angell, *Electrochem. Solid-State Lett.* **5**(1), A26 (2002).
- <sup>89</sup>K. Xu, S. S. Zhang, U. Lee, J. L. Allen, and T. R. Jow, *J. Power Sources* **146**(1), 79–85 (2005).
- <sup>90</sup>J. Chen, Z. Huang, C. Wang, S. Porter, B. Wang, W. Lie, and H. K. Liu, *Chem. Commun.* **51**(48), 9809–9812 (2015).
- <sup>91</sup>R. Mogensen, S. Colbin, A. S. Menon, E. Björklund, and R. Younesi, *ACS Appl. Energy Mater.* **3**(5), 4974–4982 (2020).
- <sup>92</sup>G. G. Eshetu, M. Martínez-Ibañez, E. Sánchez-Diez, I. Gracia, C. Li, L. M. Rodríguez-Martínez, T. Rojo, H. Zhang, and M. Armand, *Chemistry* **13**(19), 2770–2780 (2018).
- <sup>93</sup>I. A. Shkrob, T. W. Marin, Y. Zhu, and D. P. Abraham, *J. Phys. Chem. C* **118**(34), 19661–19671 (2014).
- <sup>94</sup>T. Hosokawa, K. Matsumoto, T. Nohira, R. Hagiwara, A. Fukunaga, S. Sakai, and K. Nitta, *J. Phys. Chem. C* **120**(18), 9628–9636 (2016).
- <sup>95</sup>C. Ding, T. Nohira, K. Kuroda, R. Hagiwara, A. Fukunaga, S. Sakai, K. Nitta, and S. Inazawa, *J. Power Sources* **238**, 296–300 (2013).
- <sup>96</sup>H.-B. Han, S.-S. Zhou, D.-J. Zhang, S.-W. Feng, L.-F. Li, K. Liu, W.-F. Feng, J. Nie, H. Li, X.-J. Huang, M. Armand, and Z.-B. Zhou, *J. Power Sources* **196**(7), 3623–3632 (2011).
- <sup>97</sup>C. Luo, Y. Li, W. Sun, P. Xiao, S. Liu, D. Wang, and C. Zheng, *Electrochim. Acta* **419**, 140353 (2022).
- <sup>98</sup>H. Matsumoto, H. Sakaebae, K. Tatsumi, M. Kikuta, E. Ishiko, and M. Kono, *J. Power Sources* **160**(2), 1308–1313 (2006).

- <sup>99</sup>R. Wibowo, L. Aldous, E. I. Rogers, S. E. Ward Jones, and R. G. Compton, *J. Phys. Chem. C* **114**(8), 3618–3626 (2010).
- <sup>100</sup>X. Gao, A. Mariani, S. Jeong, X. Liu, X. Dou, M. Ding, A. Moretti, and S. Passerini, *J. Power Sources* **423**, 52–59 (2019).
- <sup>101</sup>N. N. Rajput, X. Qu, N. Sa, A. K. Burrell, and K. A. Persson, *J. Am. Chem. Soc.* **137**(9), 3411–3420 (2015).
- <sup>102</sup>X. Gao, X. Liu, A. Mariani, G. A. Elia, M. Lechner, C. Streb, and S. Passerini, *Energy Environ. Sci.* **13**(8), 2559–2569 (2020).
- <sup>103</sup>M. Forsyth, M. Hilder, Y. Zhang, F. Chen, L. Carre, D. A. Rakov, M. Armand, D. R. MacFarlane, C. Pozo-Gonzalo, and P. C. Howlett, *ACS Appl. Mater. Interfaces* **11**(46), 43093–43106 (2019).
- <sup>104</sup>K. Doi, Y. Yamada, M. Okoshi, J. Ono, C.-P. Chou, H. Nakai, and A. Yamada, *Angew. Chem., Int. Ed.* **58**(24), 8024–8028 (2019).
- <sup>105</sup>A. Basile, H. Yoon, D. R. MacFarlane, M. Forsyth, and P. C. Howlett, *Electrochem. Commun.* **71**, 48–51 (2016).
- <sup>106</sup>T. J. Simons, A. A. J. Torriero, P. C. Howlett, D. R. MacFarlane, and M. Forsyth, *Electrochem. Commun.* **18**, 119–122 (2012).
- <sup>107</sup>T. J. Simons, P. C. Howlett, A. A. J. Torriero, D. R. MacFarlane, and M. Forsyth, *J. Phys. Chem. C* **117**(6), 2662–2669 (2013).
- <sup>108</sup>T. J. Simons, D. R. MacFarlane, M. Forsyth, and P. C. Howlett, *ChemElectroChem* **1**(10), 1688–1697 (2014).
- <sup>109</sup>M. S. Ghazvini, G. Pulletikurthi, A. Lahiri, and F. Endres, *ChemElectroChem* **3**(4), 598–604 (2016).
- <sup>110</sup>T. J. Simons, M. Salsamendi, P. C. Howlett, M. Forsyth, D. R. MacFarlane, and C. Pozo-Gonzalo, *ChemElectroChem* **2**(12), 2071–2078 (2015).
- <sup>111</sup>S. Begić, H. Li, R. Atkin, A. F. Hollenkamp, and P. C. Howlett, *Phys. Chem. Chem. Phys.* **18**(42), 29337–29347 (2016).
- <sup>112</sup>T. Khoo, P. C. Howlett, M. Tsagouria, D. R. MacFarlane, and M. Forsyth, *Electrochim. Acta* **58**, 583–588 (2011).
- <sup>113</sup>M. Hilder, M. Gras, C. R. Pope, M. Kar, D. R. MacFarlane, M. Forsyth, and L. A. O'Dell, *Phys. Chem. Chem. Phys.* **19**(26), 17461–17468 (2017).
- <sup>114</sup>C. R. Pope, M. Kar, D. R. MacFarlane, M. Armand, M. Forsyth, and L. A. O'Dell, *ChemPhysChem* **17**(20), 3187–3195 (2016).
- <sup>115</sup>M. Kerner, N. Plylahan, J. Scheers, and P. Johansson, *Phys. Chem. Chem. Phys.* **17**(29), 19569–19581 (2015).
- <sup>116</sup>N. Wongtharom, C.-H. Wang, Y.-C. Wang, C.-H. Yang, and J.-K. Chang, *ACS Appl. Mater. Interfaces* **6**(20), 17564–17570 (2014).
- <sup>117</sup>M. P. Do, N. Bucher, A. Nagasubramanian, I. Markovits, T. Bingbing, P. J. Fischer, K. P. Loh, F. E. Kühn, and M. Srinivasan, *ACS Appl. Mater. Interfaces* **11**(27), 23972–23981 (2019).
- <sup>118</sup>S. A. Mohd Noor, P. C. Howlett, D. R. MacFarlane, and M. Forsyth, *Electrochim. Acta* **114**, 766–771 (2013).
- <sup>119</sup>K. Liu, Z. Wang, L. Shi, S. Jungstuiwong, and S. Yuan, *J. Energy Chem.* **59**, 320–333 (2021).
- <sup>120</sup>M. Hilder, P. C. Howlett, D. Saurel, E. Gonzalo, M. Armand, T. Rojo, D. R. MacFarlane, and M. Forsyth, *J. Power Sources* **349**, 45–51 (2017).
- <sup>121</sup>M. Hilder, P. C. Howlett, D. Saurel, H. Anne, M. Casas-Cabanas, M. Armand, T. Rojo, D. R. MacFarlane, and M. Forsyth, *J. Power Sources* **406**, 70–80 (2018).
- <sup>122</sup>L. Su, X. Gao, A. Mariani, X. Liu, S. Passerini, Y. Gao, and L. Zheng, *J. Phys. Chem. Lett.* **13**(1), 105–111 (2022).
- <sup>123</sup>M. Kar, Z. Ma, L. M. Azofra, K. Chen, M. Forsyth, and D. R. MacFarlane, *Chem. Commun.* **52**(21), 4033–4036 (2016).
- <sup>124</sup>B. Park, H. O. Ford, L. C. Merrill, J. Liu, L. P. Murphy, and J. L. Schaefer, *ACS Appl. Polym. Mater.* **1**(11), 2907–2913 (2019).
- <sup>125</sup>D. Kurchavov, M. Haddad, V. Lair, and P. Volovitch, *Corros. Sci.* **200**, 110178 (2022).
- <sup>126</sup>M. Kar, B. Winther-Jensen, M. Forsyth, and D. R. MacFarlane, *Phys. Chem. Chem. Phys.* **15**(19), 7191–7197 (2013).
- <sup>127</sup>M. Kar, B. Winther-Jensen, M. Armand, T. J. Simons, O. Winther-Jensen, M. Forsyth, and D. R. MacFarlane, *Electrochim. Acta* **188**, 461–471 (2016).
- <sup>128</sup>G. Zhu, M. Angell, C.-J. Pan, M.-C. Lin, H. Chen, C.-J. Huang, J. Lin, A. J. Achazi, P. Kaghazchi, B.-J. Hwang, and H. Dai, *RSC Adv.* **9**(20), 11322–11330 (2019).
- <sup>129</sup>H. Wang, S. Gu, Y. Bai, S. Chen, N. Zhu, C. Wu, and F. Wu, *J. Mater. Chem. A* **3**(45), 22677–22686 (2015).
- <sup>130</sup>Y.-C. Wang, T.-C. Lee, J.-Y. Lin, J.-K. Chang, and C.-M. Tseng, *Corros. Sci.* **78**, 81–88 (2014).
- <sup>131</sup>Y. Park, D. Lee, J. Kim, G. Lee, and Y. Tak, *Phys. Chem. Chem. Phys.* **22**(47), 27525–27528 (2020).
- <sup>132</sup>C. Yang, S. Wang, X. Zhang, Q. Zhang, W. Ma, S. Yu, and G. Sun, *J. Phys. Chem. C* **123**(18), 11522–11528 (2019).
- <sup>133</sup>N. R. Levy, S. Lifshits, E. Yohanan, and Y. Ein-Eli, *ACS Appl. Energy Mater.* **3**(3), 2585–2592 (2020).
- <sup>134</sup>S. Xia, X.-M. Zhang, K. Huang, Y.-L. Chen, and Y.-T. Wu, *J. Electroanal. Chem.* **757**, 167–175 (2015).
- <sup>135</sup>H. Sun, G. Zhu, X. Xu, M. Liao, Y.-Y. Li, M. Angell, M. Gu, Y. Zhu, W. H. Hung, J. Li, Y. Kuang, Y. Meng, M.-C. Lin, H. Peng, and H. Dai, *Nat. Commun.* **10**(1), 3302 (2019).
- <sup>136</sup>S. Komaba, T. Ishikawa, N. Yabuuchi, W. Murata, A. Ito, and Y. Ohsawa, *ACS Appl. Mater. Interfaces* **3**(11), 4165–4168 (2011).
- <sup>137</sup>X. Yu, M. J. Boyer, G. S. Hwang, and A. Manthiram, *Chem* **4**(3), 586–598 (2018).
- <sup>138</sup>I. Weber, J. Ingenmey, J. Schnaidt, B. Kirchner, and R. J. Behm, *ChemElectroChem* **8**(2), 390–402 (2021).
- <sup>139</sup>T. Khoo, A. Somers, A. A. J. Torriero, D. R. MacFarlane, P. C. Howlett, and M. Forsyth, *Electrochim. Acta* **87**, 701–708 (2013).
- <sup>140</sup>Y. Yan, D. Gunzelmann, C. Pozo-Gonzalo, A. F. Hollenkamp, P. C. Howlett, D. R. MacFarlane, and M. Forsyth, *Electrochim. Acta* **235**, 270–279 (2017).
- <sup>141</sup>Y. Yan, T. Khoo, C. Pozo-Gonzalo, A. F. Hollenkamp, P. C. Howlett, D. R. MacFarlane, and M. Forsyth, *J. Electrochem. Soc.* **161**(6), A974–A980 (2014).
- <sup>142</sup>F. Mizuno, T. S. Arthur, and K. Takechi, *ACS Energy Lett.* **1**(3), 542–547 (2016).
- <sup>143</sup>D. S. Silvester, R. Jamil, S. Doblinger, Y. Zhang, R. Atkin, and H. Li, *J. Phys. Chem. C* **125**(25), 13707–13720 (2021).
- <sup>144</sup>S. Doblinger, T. J. Donati, and D. S. Silvester, *J. Phys. Chem. C* **124**(37), 20309–20319 (2020).
- <sup>145</sup>R. Kerr, N. Singh, T. S. Arthur, T. Pathirana, F. Mizuno, K. Takechi, M. Forsyth, and P. C. Howlett, *Sustainable Energy Fuels* **2**(10), 2276–2283 (2018).
- <sup>146</sup>H. Yoon, G. H. Lane, Y. Shekibi, P. C. Howlett, M. Forsyth, A. S. Best, and D. R. MacFarlane, *Energy Environ. Sci.* **6**(3), 979–986 (2013).
- <sup>147</sup>A. Basile, S. A. Ferdousi, F. Makhlooghiazad, R. Yunis, M. Hilder, M. Forsyth, and P. C. Howlett, *J. Power Sources* **379**, 344–349 (2018).
- <sup>148</sup>G. M. A. Girard, M. Hilder, N. Dupre, D. Guyomard, D. Nucciarone, K. Whitbread, S. Zavorina, M. Moser, M. Forsyth, D. R. MacFarlane, and P. C. Howlett, *ACS Appl. Mater. Interfaces* **10**(7), 6719–6729 (2018).
- <sup>149</sup>H. Yoon, P. C. Howlett, A. S. Best, M. Forsyth, and D. R. MacFarlane, *J. Electrochem. Soc.* **160**(10), A1629 (2013).
- <sup>150</sup>H. Yoon, A. S. Best, M. Forsyth, D. R. MacFarlane, and P. C. Howlett, *Phys. Chem. Chem. Phys.* **17**(6), 4656–4663 (2015).
- <sup>151</sup>T. J. Simons, P. M. Bayley, Z. Zhang, P. C. Howlett, D. R. MacFarlane, L. A. Madsen, and M. Forsyth, *J. Phys. Chem. B* **118**(18), 4895–4905 (2014).
- <sup>152</sup>D. Alwast, J. Schnaidt, Z. Jusys, and R. J. Behm, *J. Electrochem. Soc.* **167**(7), 070505 (2020).
- <sup>153</sup>M. S. Ghazvini, G. Pulletikurthi, T. Cui, C. Kuhl, and F. Endres, *J. Electrochem. Soc.* **165**(9), D354–D363 (2018).
- <sup>154</sup>K. Periyapperuma, C. Pozo-Gonzalo, D. R. MacFarlane, M. Forsyth, and P. C. Howlett, *ACS Appl. Energy Mater.* **1**(9), 4580–4590 (2018).
- <sup>155</sup>S. Begić, F. Chen, E. Jónsson, and M. Forsyth, *Phys. Rev. Mater.* **4**(4), 045801 (2020).
- <sup>156</sup>D. A. Rakov, F. Chen, S. A. Ferdousi, H. Li, T. Pathirana, A. N. Simonov, P. C. Howlett, R. Atkin, and M. Forsyth, *Nat. Mater.* **19**(10), 1096–1101 (2020).
- <sup>157</sup>J. Sun, L. A. O'Dell, M. Armand, P. C. Howlett, and M. Forsyth, *ACS Energy Lett.* **6**(7), 2481–2490 (2021).
- <sup>158</sup>H. Yang, J. Hwang, Y. Wang, K. Matsumoto, and R. Hagiwara, *J. Phys. Chem. C* **123**(36), 22018–22026 (2019).
- <sup>159</sup>K. Matsumoto, C. Y. Chen, T. Kiko, J. Hwang, T. Hosokawa, T. Nohira, and R. Hagiwara, *ECS Trans.* **75**(15), 139–145 (2016).
- <sup>160</sup>M. Forsyth, G. M. A. Girard, A. Basile, M. Hilder, D. R. MacFarlane, F. Chen, and P. C. Howlett, *Electrochim. Acta* **220**, 609–617 (2016).
- <sup>161</sup>M. Hilder, P. C. Howlett, D. Saurel, E. Gonzalo, A. Basile, M. Armand, T. Rojo, M. Kar, D. R. MacFarlane, and M. Forsyth, *Electrochim. Acta* **268**, 94–100 (2018).

- <sup>162</sup>A. Basile, F. Makhlooghiyazad, R. Yunis, D. R. MacFarlane, M. Forsyth, and P. C. Howlett, *ChemElectroChem* **4**(5), 986–991 (2017).
- <sup>163</sup>N. Takenaka, T. Fujie, A. Bouibes, Y. Yamada, A. Yamada, and M. Nagaoka, *J. Phys. Chem. C* **122**(5), 2564–2571 (2018).
- <sup>164</sup>S. Lee, K. Park, B. Koo, C. Park, M. Jang, H. Lee, and H. Lee, *Adv. Funct. Mater.* **30**(35), 2003132 (2020).
- <sup>165</sup>S. Lee, B. Koo, S. Kang, H. Lee, and H. Lee, *Chem. Eng. J.* **425**, 130612 (2021).
- <sup>166</sup>T. Tsuda, G. R. Stafford, and C. L. Hussey, *J. Electrochem. Soc.* **164**(8), H5007 (2017).
- <sup>167</sup>K. L. Ng, T. Dong, J. Anawati, and G. Azimi, *Adv. Sustainable Syst.* **4**(8), 2000074 (2020).
- <sup>168</sup>C. Xu, S. Zhao, Y. Du, Z. Wang, and J. Zhang, *Mater. Lett.* **275**, 128040 (2020).
- <sup>169</sup>Y. Peng, P. S. Shinde, and R. G. Reddy, *J. Electroanal. Chem.* **895**, 115363 (2021).
- <sup>170</sup>T. Schoetz, B. Craig, C. Ponce de Leon, A. Bund, M. Ueda, and C. T. J. Low, *J. Energy Storage* **28**, 101176 (2020).
- <sup>171</sup>K. V. Kravchik, C. Seno, and M. V. Kovalenko, *ACS Energy Lett.* **5**(2), 545–549 (2020).
- <sup>172</sup>C. Ferrara, V. Dall'Asta, V. Berbenni, E. Quartarone, and P. Mustarelli, *J. Phys. Chem. C* **121**(48), 26607–26614 (2017).
- <sup>173</sup>C. Welch, A. K. Mohammad, N. S. Hosmane, L. Zhang, and K. T. Cho, *Energies* **13**(8), 2014 (2020).
- <sup>174</sup>X.-G. Sun, Y. Fang, X. Jiang, K. Yoshii, T. Tsuda, and S. Dai, *Chem. Commun.* **52**(2), 292–295 (2016).
- <sup>175</sup>T. Schoetz, O. Leung, C. P. de Leon, C. Zaleski, and I. Efimov, *J. Electrochem. Soc.* **167**(4), 040516 (2020).
- <sup>176</sup>N. M. Rocher, E. I. Izgorodina, T. Rütther, M. Forsyth, D. R. MacFarlane, T. Rodopoulos, M. D. Horne, and A. M. Bond, *Chemistry* **15**(14), 3435–3447 (2009).
- <sup>177</sup>S. Zein El Abedin, E. M. Moustafa, R. Hempelmann, H. Natter, and F. Endres, *ChemPhysChem* **7**(7), 1535–1543 (2006).
- <sup>178</sup>P. Eiden, Q. Liu, S. Zein El Abedin, F. Endres, and I. Krossing, *Chemistry* **15**(14), 3426–3434 (2009).
- <sup>179</sup>T. Welton, *Chem. Rev.* **99**(8), 2071–2084 (1999).
- <sup>180</sup>C. Li, J. Patra, J. Li, P. C. Rath, M.-H. Lin, and J.-K. Chang, *Adv. Funct. Mater.* **30**(12), 1909565 (2020).
- <sup>181</sup>H. Wang, S. Gu, Y. Bai, S. Chen, F. Wu, and C. Wu, *ACS Appl. Mater. Interfaces* **8**(41), 27444–27448 (2016).
- <sup>182</sup>M. Hog, B. Burgenmeister, K. Bromberger, M. Schuster, S. Riedel, and I. Krossing, *ChemElectroChem* **4**(11), 2934–2942 (2017).
- <sup>183</sup>H. Xu, T. Bai, H. Chen, F. Guo, J. Xi, T. Huang, S. Cai, X. Chu, J. Ling, W. Gao, Z. Xu, and C. Gao, *Energy Storage Mater.* **17**, 38–45 (2019).
- <sup>184</sup>F. Gan, K. Chen, N. Li, Y. Wang, Y. Shuai, and X. He, *Ionics* **25**(9), 4243–4249 (2019).
- <sup>185</sup>Y. Fang, K. Yoshii, X. Jiang, X.-G. Sun, T. Tsuda, N. Mehio, and S. Dai, *Electrochim. Acta* **160**, 82–88 (2015).
- <sup>186</sup>H. Yang, F. Wu, Y. Bai, and C. Wu, *J. Energy Chem.* **45**, 98–102 (2020).
- <sup>187</sup>S. Choi, H. Go, G. Lee, and Y. Tak, *Phys. Chem. Chem. Phys.* **19**(13), 8653–8656 (2017).
- <sup>188</sup>M.-C. Lin, M. Gong, B. Lu, Y. Wu, D.-Y. Wang, M. Guan, M. Angell, C. Chen, J. Yang, B.-J. Hwang, and H. Dai, *Nature* **520**(7547), 324–328 (2015).
- <sup>189</sup>H. Sun, W. Wang, Z. Yu, Y. Yuan, S. Wang, and S. Jiao, *Chem. Commun.* **51**(59), 11892–11895 (2015).
- <sup>190</sup>H. Jiao, S. Jiao, W.-L. Song, H. Chen, M. Wang, J. Tu, and D. Fang, *J. Electrochem. Soc.* **166**(15), A3539–A3545 (2019).
- <sup>191</sup>Y. Jiang, L. Fang, L. Luo, S. Wang, and X. Wang, *J. Appl. Electrochem.* **48**(7), 827–834 (2018).
- <sup>192</sup>J. Li, K. S. Hui, S. Ji, C. Zha, C. Yuan, S. Wu, F. Bin, X. Fan, F. Chen, Z. Shao, and K. N. Hui, *Carbon Energy* **4**(2), 155–169 (2022).
- <sup>193</sup>Y. Tang, L. Lu, H. W. Roesky, L. Wang, and B. Huang, *J. Power Sources* **138**(1), 313–318 (2004).
- <sup>194</sup>C. Yan, C. Lv, L. Wang, W. Cui, L. Zhang, K. N. Dinh, H. Tan, C. Wu, T. Wu, Y. Ren, J. Chen, Z. Liu, M. Srinivasan, X. Rui, Q. Yan, and G. Yu, *J. Am. Chem. Soc.* **142**(36), 15295–15304 (2020).
- <sup>195</sup>J. Wang, H. Jiao, W.-L. Song, M. Wang, J. Tu, Z. Tang, and H. Zhu, *ACS Appl. Mater. Interfaces* **12**(13), 15063–15070 (2020).
- <sup>196</sup>X. Shen, T. Sun, L. Yang, A. Krasnoslobodtsev, R. Sabirianov, M. Sealy, W.-N. Mei, Z. Wu, and L. Tan, *Nat. Commun.* **12**(1), 820 (2021).
- <sup>197</sup>D. Lee, G. Lee, and Y. Tak, *Nanotechnology* **29**(36), 36LT01 (2018).
- <sup>198</sup>B. Shvartsev, D. Gelman, D. Amram, and Y. Ein-Eli, *Langmuir* **31**(51), 13860–13866 (2015).
- <sup>199</sup>D. Gelman, B. Shvartsev, and Y. Ein-Eli, *J. Mater. Chem. A* **2**(47), 20237–20242 (2014).
- <sup>200</sup>D. Gelman, B. Shvartsev, I. Wallwater, S. Kozokaro, V. Fidelsky, A. Sagy, A. Oz, S. Baltianski, Y. Tsur, and Y. Ein-Eli, *J. Power Sources* **364**, 110–120 (2017).
- <sup>201</sup>F. Wu, N. Zhu, Y. Bai, Y. Gao, and C. Wu, *Green Energy Environ.* **3**(1), 71–77 (2018).
- <sup>202</sup>R. Bai, J. Yang, G. Li, J. Luo, and W. Tang, *Energy Storage Mater.* **41**, 41–50 (2021).
- <sup>203</sup>Y. Cai, S. Kumar, R. Chua, V. Verma, D. Yuan, Z. Kou, H. Ren, H. Arora, and M. Srinivasan, *J. Mater. Chem. A* **8**(25), 12716–12722 (2020).
- <sup>204</sup>S. He, J. Wang, X. Zhang, J. Chen, Z. Wang, T. Yang, Z. Liu, Y. Liang, B. Wang, S. Liu, L. Zhang, J. Huang, J. Huang, L. A. O'Dell, and H. Yu, *Adv. Funct. Mater.* **29**(45), 1905228 (2019).
- <sup>205</sup>O. Tutusaus, R. Mohtadi, N. Singh, T. S. Arthur, and F. Mizuno, *ACS Energy Lett.* **2**(1), 224–229 (2017).
- <sup>206</sup>J. O. Besenhard and M. Winter, *Chemphyschem* **3**(2), 155–159 (2002).
- <sup>207</sup>C. Holc, K. Dimogiannis, E. Hopkinson, and L. R. Johnson, *ACS Appl. Mater. Interfaces* **13**(25), 29708–29713 (2021).
- <sup>208</sup>V. Küpers, D. Weintz, C. Mück-Lichtenfeld, P. Bieker, M. Winter, and M. Kolek, *J. Electrochem. Soc.* **167**(16), 160505 (2020).
- <sup>209</sup>Y. NuLi, J. Yang, and R. Wu, *Electrochem. Commun.* **7**(11), 1105–1110 (2005).
- <sup>210</sup>Y. NuLi, J. Yang, J. Wang, J. Xu, and P. Wang, *Electrochem. Solid-State Lett.* **8**(11), C166 (2005).
- <sup>211</sup>P. Wang, Y. NuLi, J. Yang, and Z. Feng, *Surf. Coat. Technol.* **201**(6), 3783–3787 (2006).
- <sup>212</sup>M. Forsyth, P. C. Howlett, S. K. Tan, D. R. MacFarlane, and N. Birbilis, *Electrochem. Solid-State Lett.* **9**(11), B52 (2006).
- <sup>213</sup>P. C. Howlett, W. Neil, T. Khoo, J. Sun, M. Forsyth, and D. R. MacFarlane, *Isr. J. Chem.* **48**(3–4), 313–318 (2008).
- <sup>214</sup>P. C. Howlett, T. Khoo, G. Mooketsi, J. Efthimiadis, D. R. MacFarlane, and M. Forsyth, *Electrochim. Acta* **55**(7), 2377–2383 (2010).
- <sup>215</sup>Z. Ma, M. Forsyth, D. R. MacFarlane, and M. Kar, *Green Energy Environ.* **4**(2), 146–153 (2019).
- <sup>216</sup>Z. Ma, M. Kar, C. Xiao, M. Forsyth, and D. R. MacFarlane, *Electrochem. Commun.* **78**, 29–32 (2017).
- <sup>217</sup>T. Mandai, K. Tatesaka, K. Soh, H. Masu, A. Choudhary, Y. Tateyama, R. Ise, H. Imai, T. Takeguchi, and K. Kanamura, *Phys. Chem. Chem. Phys.* **21**(23), 12100–12111 (2019).
- <sup>218</sup>P. Novák and J. Desilvestro, *J. Electrochem. Soc.* **140**(1), 140 (1993).
- <sup>219</sup>L. Jiao, H. Yuan, Y. Wang, J. Cao, and Y. Wang, *Electrochem. Commun.* **7**(4), 431–436 (2005).
- <sup>220</sup>Y. Bi, S. He, C. Fan, J. Luo, B. Yuan, and T. L. Liu, *J. Mater. Chem. A* **8**(25), 12301–12305 (2020).
- <sup>221</sup>L. K. Chellappan, J. Kvello, J. R. Tolchard, P. I. Dahl, S. M. Hanetho, R. Berthelot, A. Fiksdahl, and K. Jayasayee, *ACS Appl. Energy Mater.* **3**(10), 9585–9593 (2020).
- <sup>222</sup>W. Ren, D. Wu, Y. NuLi, X. Zhang, J. Yang, and J. Wang, *ACS Appl. Mater. Interfaces* **13**(28), 32957–32967 (2021).
- <sup>223</sup>A. Kitada, Y. Kang, K. Matsumoto, K. Fukami, R. Hagiwara, and K. Murase, *J. Electrochem. Soc.* **162**(8), D389 (2015).
- <sup>224</sup>A. Kitada, Y. Kang, Y. Uchimoto, and K. Murase, *J. Electrochem. Soc.* **161**(3), D102 (2014).